To the Graduate Council:

I am submitting herewith a thesis written by Alan E. Johnston entitled "Analysis of Wind Measurement Techniques and Atmospheric Stability Modeling for the Catapault Launched Fuel-Air Explosive Land Mine Countermeasure System". I have examined the final copy of this thesis for form and content and recommend that it be accepted in partial fulfillment of the requirements for the degree of Master of Science, with a major in Engineering Science.

Walter Frost, Major Professor

We have read this thesis and recommend its acceptance:

Accepted for the Council:

Vice Provost and Dean
of the Graduate School

ANALYSIS OF WIND MEASUREMENT TECHNIQUES AND ATMOSPHERIC STABILITY MODELING FOR THE CATAPULT LAUNCHED FUEL-AIR EXPLOSIVE LAND MINE COUNTERMEASURE SYSTEM

A Thesis
Presented for the
Master of Science
Degree
The University of Tennessee, Knoxville

Alan E. Johnston

December 1990

ACKNOWLEDGEMENTS

A lot of work goes into writing a thesis, and it is inevitable that the help of others will be sought. This thesis is no different. For his help and guidance with each and every step along the way, I would like to thank Dr. Walter Frost. Without his wisdom and confident support, this thesis would not have been possible. Thanks go out to the other members of my committee as well; Dr. Robert E. Turner and Dr. Kenneth Kimble. I would also like to thank Steve Fitzgibbon and Phil Sexton of the Naval Coastal Systems Center in Panama City, Florida. This thesis was funded in part by Contract Number N61331-89-M-7185 with the Naval Coastal Systems Center, and it is the results of this analysis which is reported here.

I wish to extend warm thanks to Robert Suttles, Martha Craddock, and Loretta Crowe for their help in doing such a fine job with the figures, typing the thesis, and tabulating all of the data of Appendix A, respectively, and to Jimmy Steele for helping me with the computer. Thanks everyone.

ABSTRACT

This thesis reveals that the current CATFAE wind sensor falls short of delivering the necessary wind information for successful CATFAE operation. Several potential difficulties are addressed, such as misleading local variations in the wind and inability of the sensor to see decoupled wind shear aloft. Several alternative wind sensing systems are reviewed for applicability to CATFAE, and such systems as the Laser True Airspeed System (LATAS), the Lasergage Laser Rangefinder, and a mm-wave balloon-borne transponder system are recommended as viable alternatives.

This thesis also presents an empirically based stable atmosphere wind model to enhance the predictive capabilities of the CATFAE System Effectiveness Model (SEM). The model is presented in the form of an interpolative Table Look-up scheme which utilizes extensive wind measurement data reported in the literature. The computer subroutines are given in the appendices.

TABLE OF CONTENTS

TABLE OF CONTENTS, continued

LIST OF FIGURES

LIST OF TABLES

NOMENCLATURE

A	Area
a	Acceleration
C_D	Drag coefficient
F	Force
f	Coriolis parameter
L	Monin-Obukhov stability length parameter
M, m	Mass
R	Range
RR	Range rate
R_o	Rossby number
t	Time
u	Velocity
u_*	Friction velocity
W_x	x-component wind velocity
W_y	y-component wind velocity
$\widehat{W}_x$	Non-dimensional x-component wind velocity
$\widehat{W}_y$	Non-dimensional y-component wind velocity
z	Altitude
z_o	Surface roughness length
$\widehat{z}$	Non-dimensional altitude
α	Elevation angle
κ	von Karman constant
μ	Stability parameter
ρ	Density
σ	Standard of deviation
τ	Average time
θ	Azimuthal angle

1.0 INTRODUCTION

The Catapult Launched Fuel-Air Explosive Land Mine Countermeasure System (CATFAE) is designed to meet the Marine Corps requirement for clearing a path through an enemy minefield during an amphibious assault. The system clears a path on the beach above the high watermark by launching up to 21 rounds which detonate over the surface creating the necessary overpressure and impulse to neutralize the mines. The rounds are launched from an amphibious assault vehicle as it approaches the beach. Launched with a muzzle velocity of approximately 84 m/s (275 ft/s), the rounds can achieve a maximum altitude of 259 m (850 ft). In order to control the projectile ranges, parachutes are deployed from the rounds in a preprogrammed time sequence, thus allowing an overlapping pattern of detonations which provide a continuous cleared path through the minefield.

The CATFAE system is controlled by a two stage software run scheme. The first stage calculates the form of a generalized equation which contains parameterized coefficients. In the second stage, vehicle motion and wind data are entered which allow the values of the coefficients to be calculated. With the coefficients defined, the generalized equation yields the desired fuse times for the round parachutes.

The first stage of the software creates the generalized equation, and is run in advance of the military initiative which will employ the CATFAE system. A multitude of parameters are accounted for in the program, such as vehicle motion, wind variability, ballistic characteristics, proximity to target, etc. The generalized equation is a matrix type equation which formulates coefficients to account for the parameters that are unknown at the time, such as wind variability and vehicle motion. In order to accurately determine the effects of wind on the rounds as they fall, a coefficient for wind must be included in the matrix equation.

The CATFAE Fire Control System (FCS) is the algorithm comprising the second stage of the CATFAE software. The parameters which were unknown earlier are measured and given as input to the FCS, allowing the values of the coefficients to be calculated. This algorithm is executed at the time of the amphibious assault, using the generalized equation developed earlier to calculate round trajectories via parachute fuse times.

Information on the prevailing winds must be input to the FCS since variations in the wind can have a profound effect on the drift of the munitions as they fall. For this reason, the generalized equation includes a wind coefficient. It is crucial to the success of CATFAE that knowledge of the prevailing wind conditions during the assault be available, and hence, it is critical that CATFAE have an appropriate method for measuring the winds.

A computer model, called the System Effectiveness Model (SEM), was developed by the Naval Coastal Systems Center to predict the effectiveness of the CATFAE system. The model uses the generalized software program of the CATFAE system, as well as the FCS algorithm, to predict the impact point for each round, given a set of input data. A minefield model is employed that determines the location of mines of interest and whether or not they have been neutralized by the CATFAE blasts. The model simulates variabilities in the placement of markers by the rounds and the subsequent driving of the vehicle through the marked lane. Practice runs of this model have shown that changes made only in the wind input data can have a profound effect on the SEM "clearance" output [1].

The scope of this thesis is twofold. The first part addresses the issue of wind measuring techniques for the CATFAE system. Details of the current CATFAE wind sensing design are discussed, and limitations of its effectiveness are revealed. A number of alternate measurement techniques were surveyed, with comments on the applicability of the wind systems for CATFAE. From this review, recommendations of the most promising wind sensing method is made.

The second part of this thesis discusses appropriate equations relating to atmospheric stability in order to enhance the CATFAE's accountability of wind in its current wind model. Since atmospheric stability has a tremendous effect on wind motions, this thesis reviews the concepts of wind characteristics, and the effects of stability. Appropriate stability equations are reduced to a form useable for the CATFAE software.

2.0 WIND, MEASUREMENTS, AND MODELING

A brief discussion of wind and some of its characteristics, as well as a few measuring and modeling considerations, are given in this section.

Wind velocity is usually defined as a combination of a mean component and a fluctuating component. An illustration of this concept can be seen in Figure 2.1. The mean wind is found by taking several measurements at each point in space over a specified time, and then averaging the data with respect to time. This gives an average value for each point in space and, hence, an average wind profile. The fluctuating component is the value measured at an instantaneous point in time with the mean value subtracted out, and can vary with time. The instantaneous wind profile in Figure 2.1 would, in general, look different if measured at another instant in time. The fluctuating components are obtained by subtracting out the mean velocity profile from the instantaneous velocity profile. By measuring many data values over the course of time of interest, statistical calculations can be made to define a mean profile, standards of deviation, exceedence envelopes, etc.

Careful interpretation must be made when averaging wind data over time. Figure 2.2 gives an example of how time averaging can effect the outcome of a measurement. An important consideration in a wind sensing system is the time scale of interest. Measuring wind in the wrong time scale can adversely influence the validity of the measurement.

Several elements that can affect the shape of the vertical wind profile must also be considered. No matter what the wind looks like aloft, whether a smooth constant breeze, or a strongly gusting wind including shear, the lower portion of the profile will always be affected by the surface over which it passes. In this boundary layer portion of the profile, near the earth's surface, the wind will be influenced by any obstructions present such as trees, buildings, grass fields, or open sea. As any fluid flows over a surface, the fluid in contact with the surface sticks, creating a gradient in the flow velocity which increases from zero at the surface to equal

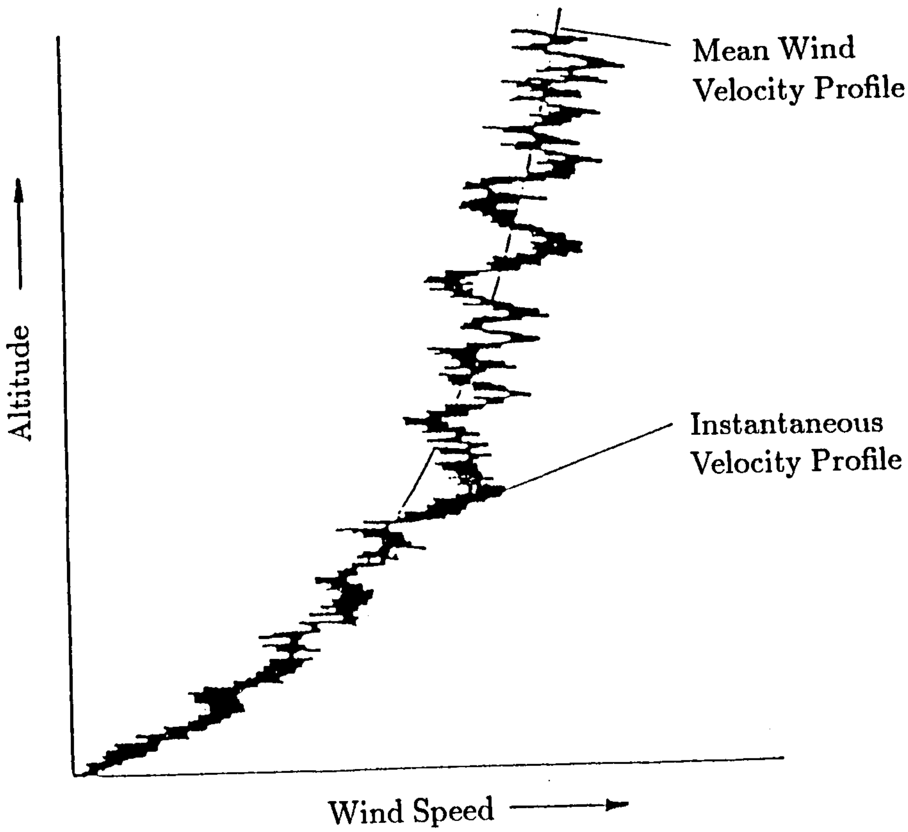

Figure 2.1 Wind is defined as a mean plus a fluctuating component.

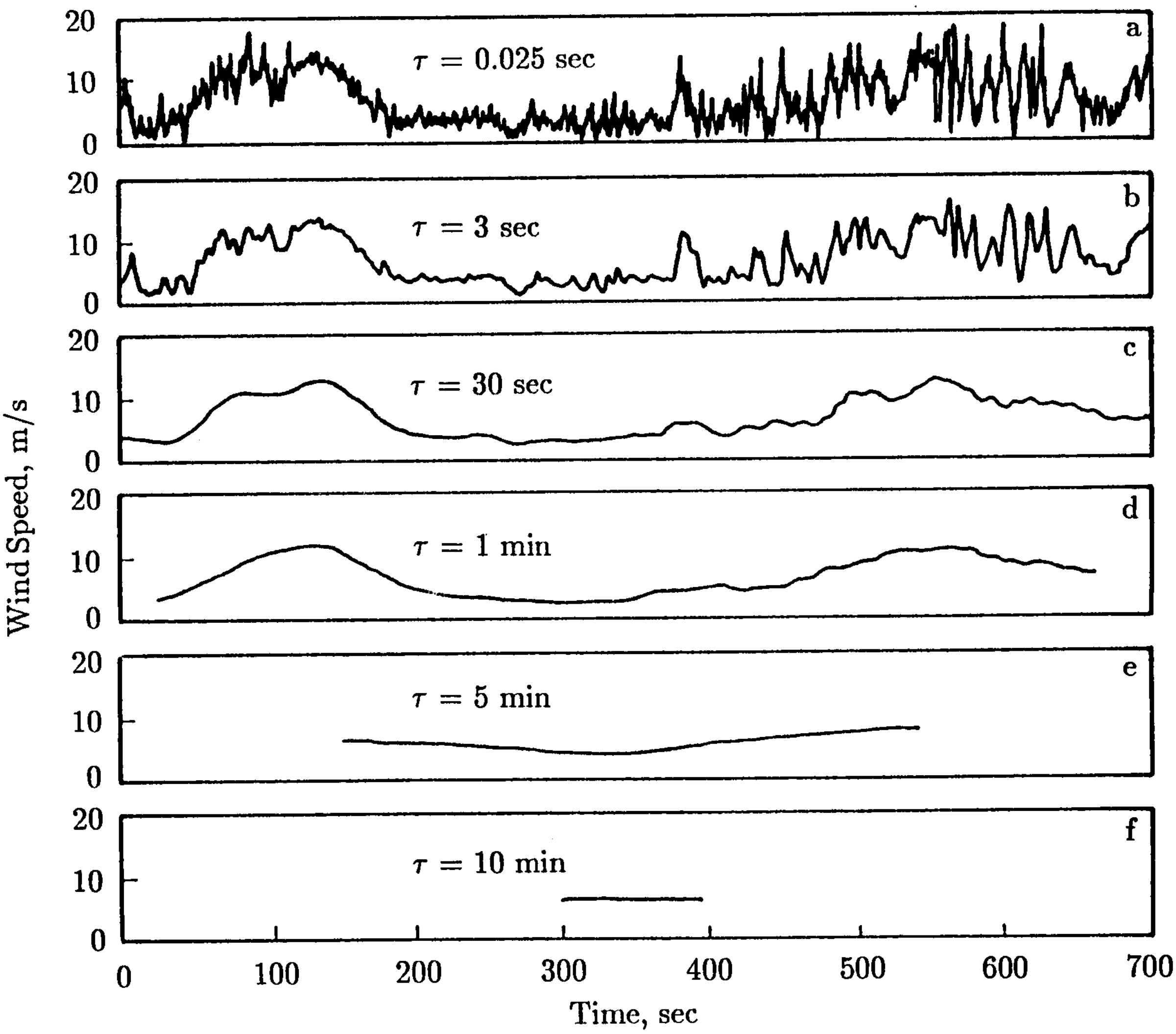

Figure 2.2 Effect of averaging time (τ average time).

to the free stream velocity at a distance from the surface. The wind behaves in a similar fashion, whereby the planetary boundary layer slows the wind near the surface, and diminishes its influence at higher altitudes. The expanse of its influence is greatly dependant on the nature of the surface. Figure 2.3 suggests the level of influence of various surfaces. For instance, the open sea is shown to have a surface roughness on the order of 0.001 meters. The illustrated profiles show that this open sea influence is quite significant in the lowest part of the profile, and less significant in the higher part. When taking measurements very near the surface as does the CATFAE system, it becomes very important to recognize the influence of surface roughness, as well as the influence of the height at which the measurement is taken.

One of the most commonly used simple wind profile models is the logarithmic profile. The wind profile is a logarithm function of altitude nondimensionalized by the roughness factor. Table 2.1 shows the equation with the parameters involved. The friction velocity is an empirically determined velocity which is a measure of the shear stress near the surface. The von Karman constant is an empirically determined constant which is about 0.40 for the atmosphere. Along with the surface roughness parameter, the logarithm equation is also a function of atmospheric stability. This stability function is based on the Monin-Obukhov length parameter, L. It is a length parameter derived from dimensional analysis which approximates the height where bouyancy energy production is equal to mechanical shear energy production.

The atmosphere can be characterized as stable, unstable, or neutrally stable. Figure 2.4 illustrates the mechanism of atmospheric stability. During the day, the sun heats the surface of the earth with its radiation. The warm earth, in turn, heats the air near the ground. The temperature gradient of the air therefore begins at the surface as warm air, cools off with altitude to a low point, then begins to become warmer again as the sun's radiation heats the upper atmosphere directly. The height at which the temperature gradient turns from cooling toward heating is called the inversion height. Below the inversion height, the atmosphere is unstable. If a parcel of air is displaced by some mechanical means, such as being lifted by the

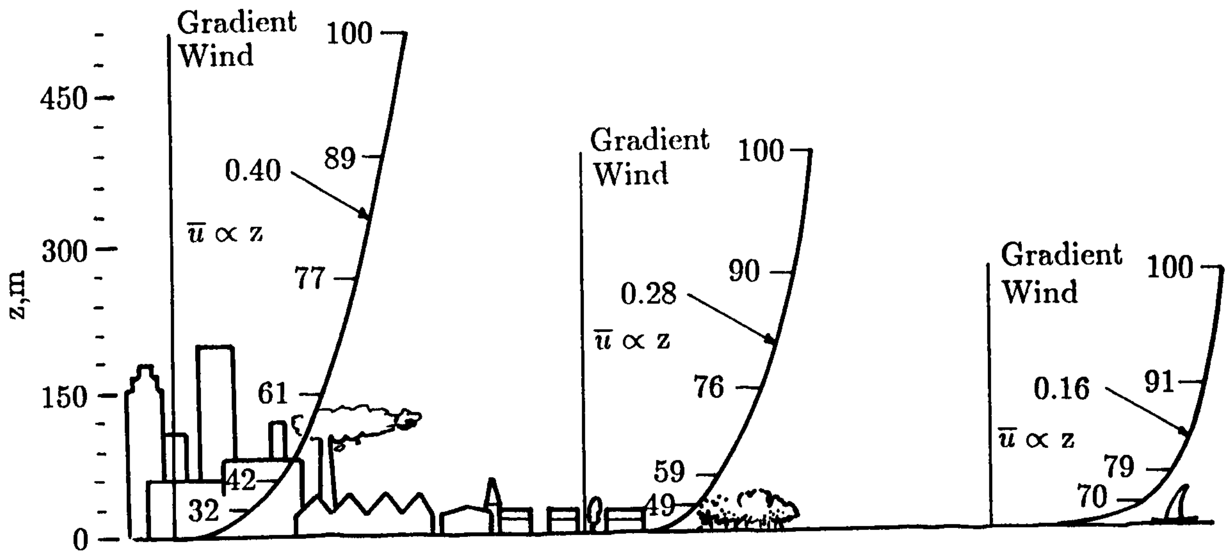

Empirical power laws over different terrain; after [2].

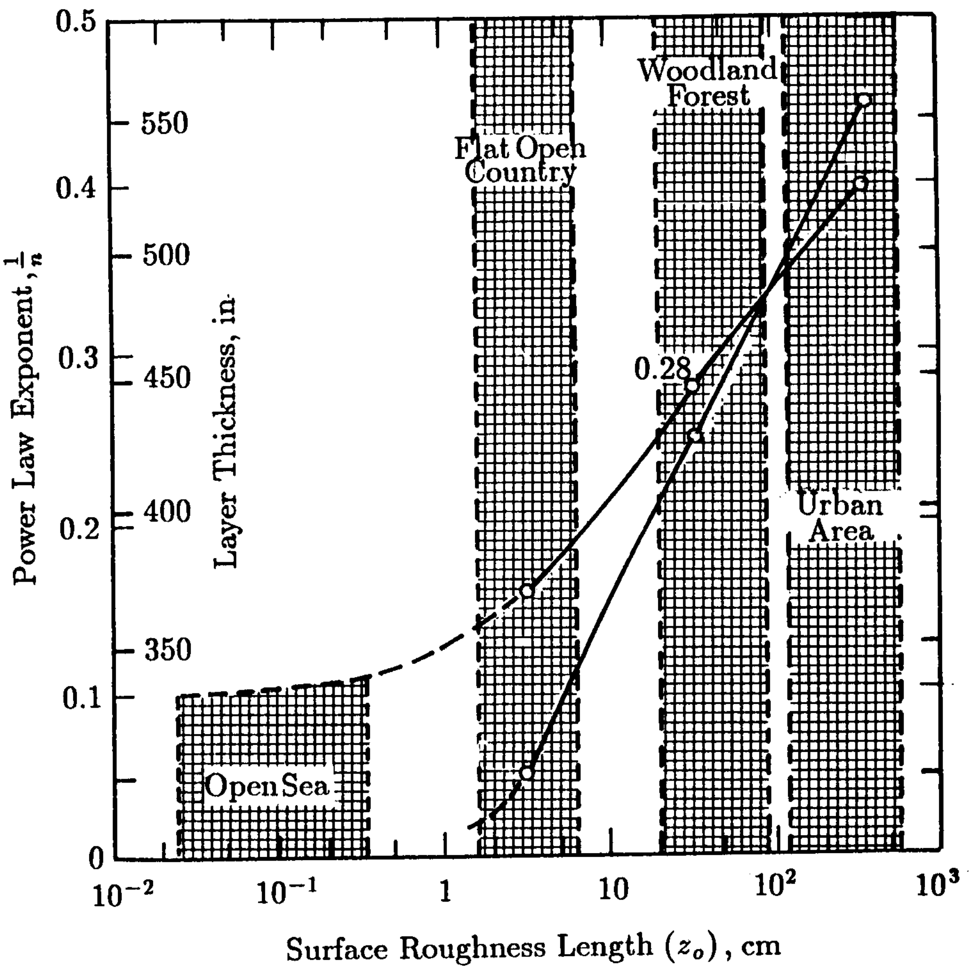

The exponent in the power law and the height of the boundary layer as functions of the roughness length and the type of terrain, from [2].

Figure 2.3 Surface roughness effects.

Table 2.1 Models.

Wind Profile with Height

- $\hat{W}(z) = \frac{u_*}{\kappa}(ln\frac{z+z_o}{z_o} + \Psi(\frac{z}{L}))$

u_* - Friction Velocity
κ - von Karman's Constant
z_o - Surface Roughness
$\Psi(\frac{z}{L})$ - Function of Atmospheric Stability

- $\hat{W}(z) = \hat{W}_{ref}(z/z_{ref})$

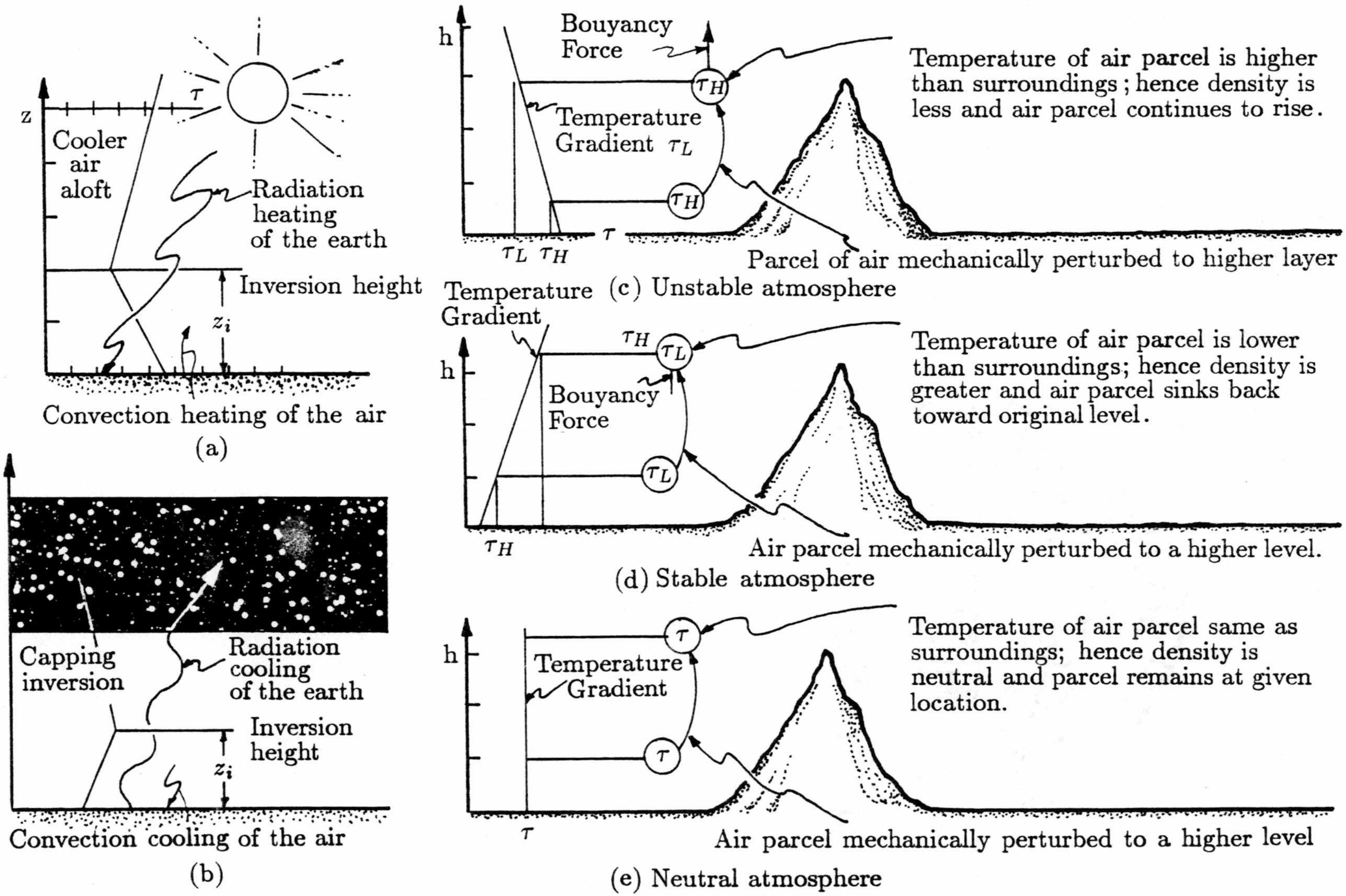

Figure 2.4 Illustration of mechanism of atmospheric stability [3].

slope of a mountain as in the figure, the displaced air parcel is suddenly warmer and lighter in density than its surroundings. If the parcel is unable to equilibrate with its new surroundings, it will remain warmer and hence will continue to rise. This divergent nature is defined as unstable.

In a stable atmosphere, the temperature gradient is positive from the surface up to the inversion height. That is, the ground cools at night by radiating its heat to cold space. Since the ground is cool, it absorbs heat from the air above it. Since the warm air above the surface is being cooled below , the air aloft is warmer than the air near the surface. The temperature gradient of the air then begins as cool at the surface, warms with altitude to a certain point, then begins to cool again by direct radiation of its heat to cold space. Below the inversion layer, the air warms with altitude. If a parcel of air is displaced by a mechanical mechanism, such as the mountain slope shown again in the figure, the perturbed parcel of air that is lifted is cooler and denser than its surroundings, thus causing it to sink back to its original position. This, by definition, is stability.

In some circumstances, the atmospheric temperature gradient can be near zero, thus allowing somewhat of a constant temperature with height to prevail. If this is so, the displaced parcel of air will be nearly the same temperature and density as its new environment, and hence will simply remain where it is placed. This is called neutrally stable, since the air parcel does not diverge from or converge with its former position. However, any change in the temperature gradient will cause the atmosphere to become either stable or unstable.

An important consequence of atmospheric stability is the influence it has on wind flow. In an unstable atmosphere, convective circulation invariably sets in, which drives the atmosphere in large scale convective eddies. The eddies in this situation are very large, and when limited to the area of interest to CATFAE, the flow of an unstable atmosphere becomes fairly straight forward. Since the wind is driven by large scale circulation, the low altitude winds being measured by CATFAE are very well represented by the simple logarithmic model shown earlier. It is when the atmosphere is stable that the wind profile can become somewhat problematic. Since a CATFAE operation is likely to occur in the middle of the night or in an early morning time frame, the atmosphere is likely to be stable. It is important therefore, for CATFAE to understand the possible consequences of a stable atmosphere. Since perturbations can occur which tend to return to their original positions, activities can occur at various altitudes without affecting the wind at other altitudes. The significance of this decoupling condition is best illustrated by Figure 2.5. In this figure, a stable atmosphere has allowed the wind to be driven in one direction near the surface, thus blowing the smoke from the lower stack in one direction, while some driving mechanism has caused the wind at a higher altitude to be driven in a completely opposite direction, blowing the smoke from the higher stack in the other direction. The decoupled nature of the stable atmosphere permits this kind of sheared wind profile. A shear layer exists between the two independent wind profiles. When considering the needs of the CATFAE program, it becomes clear that this type of situation could dramatically affect the placement of the explosive rounds. It is unquestionable that CATFAE must have a means to measure whether this type of condition is present during operation. The currently designed wind sensor has no way of detecting a decoupled wind shear profile.

Section 6.0 of this thesis discusses in detail a model for the stable boundary layer. This model does not, however, consider external forcing mechanisms which could cause the decoupling shear as in Figure 2.5. The model defines unperturbed stable wind profiles. Section 4.0 will discuss possible wind sensors for CATFAE that would measure profiles accurately, including detection of the decoupled shear layer.

One last discussion for this section is the particular phenomenon known as sea breeze. This is a wind circulation which occurs in coastal environments, or in fact, wherever a significant body of water comes into contact with a land mass. Depicted simply in Figure 2.6, this flow phenomenon is basically a circulation of the air in a large convective eddy due to the differences in temperature of the land and the water. During the earlier portion of the day, while the land is warm and the water

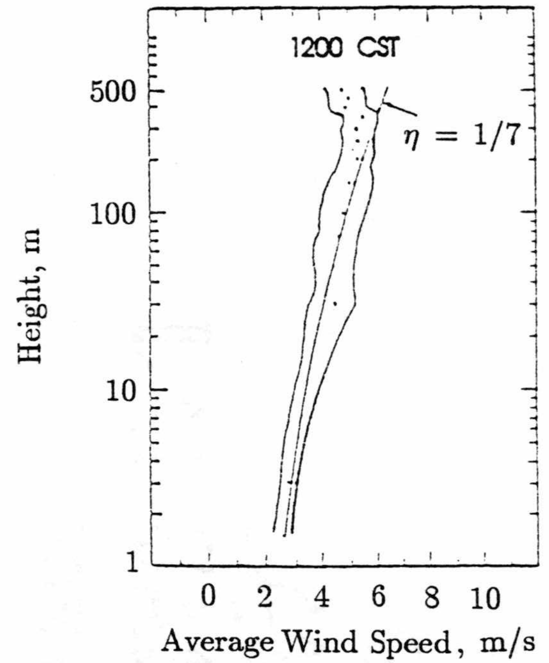

(a) Average wind profile observed in well-mixed conditions at 1200 CST (16 days, 1975; not normalized)[4]

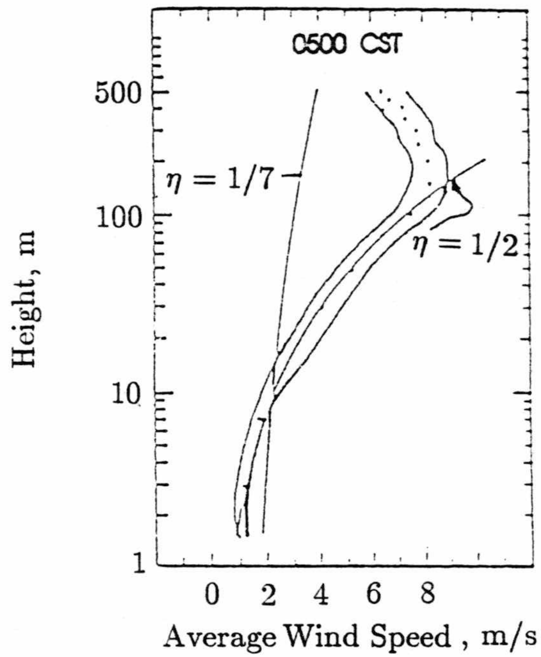

(b) Average wind profile observed in decoupled conditions at 0500CST(16 days,1975;not normalized)[4]

Stable flow visually illustrated by smoke plume [5]

Decoupling of wind layer visually illustrated by smoke plumes [6]

Figure 2.5 Effects of a stable atmosphere.

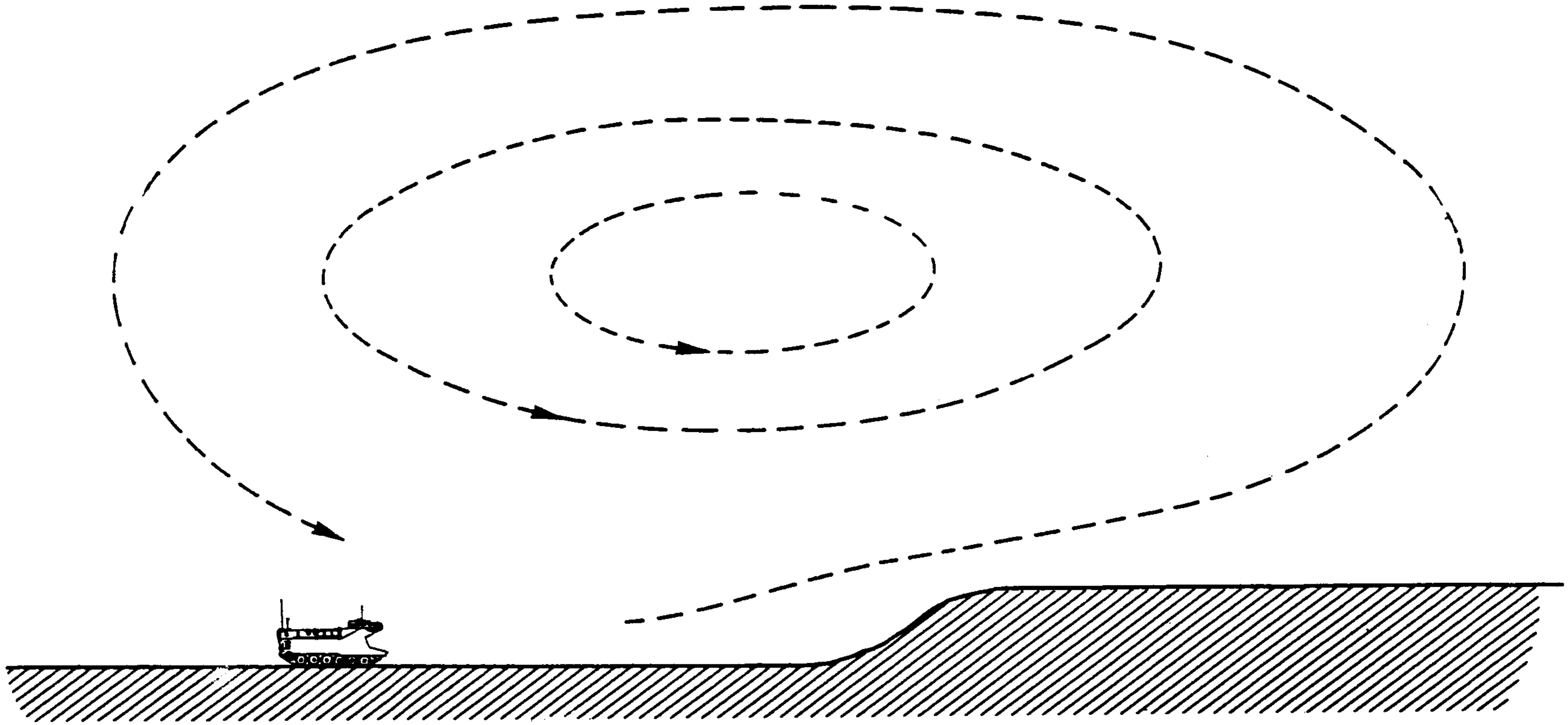

Figure 2.6 Schematic of sea breeze.

is cooler, the air above the land is warmer and lighter than the air above the sea. The cooler air from the sea moves inland and displaces the warmer air upward. The air above the cool air moving inland sinks to replace the vacated space, and then follows the path of the air it replaced. The warm air being forced upward above the land is cooled at the higher altitude, and moves out over the sea to replace the air sinking downward. This air, now cooler, falls into the circulation pattern. This is called a sea breeze because the lower layer of air blows from sea to land. After sunset, this pattern can reverse. Since the land cools off rapidly at night, while the water, having been heating all day, takes its time in giving off its heat, the land becomes cooler than the sea. Suddenly, the situation from the early part of the day has been reversed, and the circulation pattern begins to flow the other way. This night time breeze is called a land breeze since the lower air layer blows from land to sea. During times between these breezes, late at night to early morning and in the evening just before sunset, the temperature of land and sea becomes nearly equal, allowing a stable atmosphere to prevail.

Land and sea breeze is a large scale flow. Figure 2.7 shows examples of some sea breeze modeling output [7]. The emphasis on this figure is the spacial scale. It can be seen that the flow circulation is spread over several kilometers in the horizontal direction, and several hundred meters in the vertical scale. This illustrates the fact that a measurement of the wind at a distance of a few kilometers from the shore would be closely representative of the wind at the shore. Although the land and sea breeze phenomenon is a large scale flow similar to that of the unstable atmosphere, at night and early morning times when the CATFAE is likely to be in operation, the breeze is not predominant, in fact, a stable atmosphere is often the predominant condition. In the early morning, the onset of a sea breeze emerging from a stable atmosphere would generally lead to a fairly uniform horizontal flow for a long distance, but with the very real possibility of a decoupled shear layer aloft.

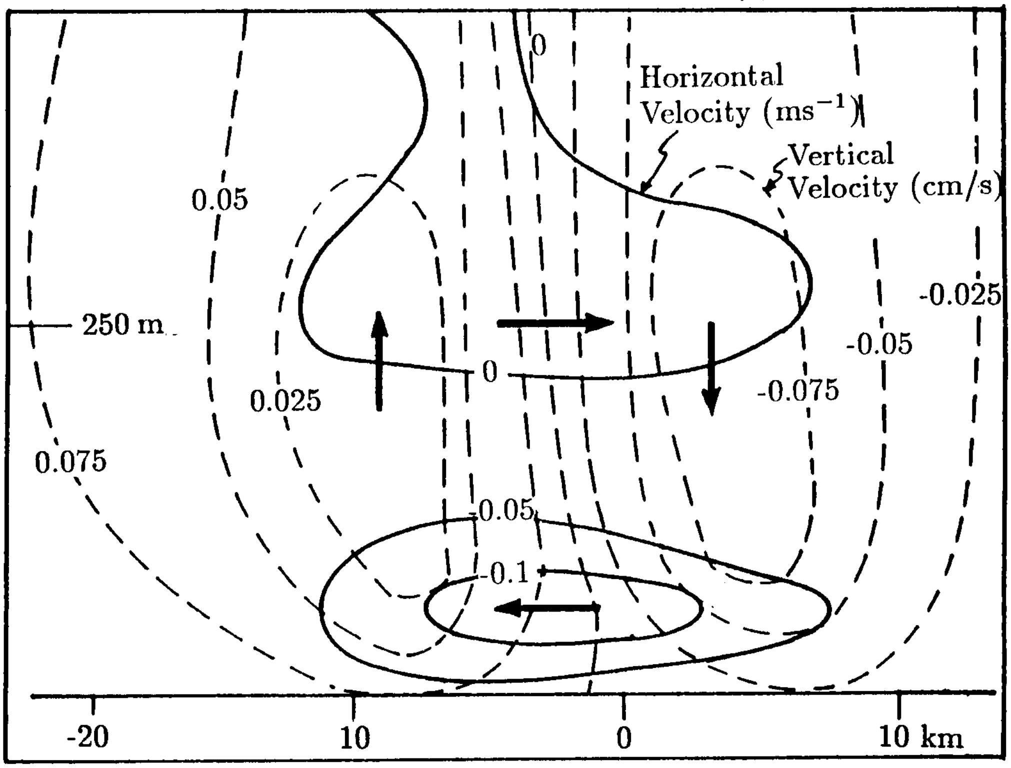

1 hour after onset of heating

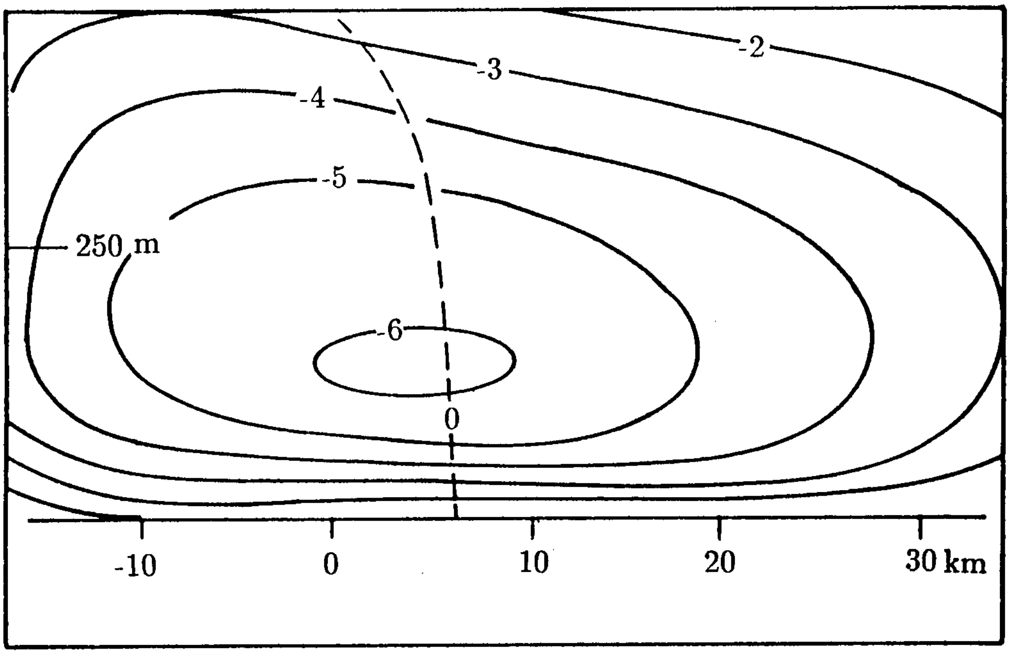

9 hours after onset of heating

Figure 2.7 Sea breeze modeling output [7].

3.0 WIND MEASUREMENT INSTRUMENTATION SURVEY

There are several constraints to which the wind sensing system must conform to be appropriate for the CATFAE system. First of all, the maximum altitude of the rounds is around 250 m, so the instrument must be capable of measuring very low altitude winds with meaningful volume resolution. The instrument must also be portable for autonomy, which means that it is constrained by size. In an assault situation , time can be a critical commodity, so quick profiling of the wind for input into the FCS is also a requirement. The environment during an assault will be rough, and the wind sensing system must be rugged enough to withstand such dynamic treatment. A table of operating environment tests is given in Table 3.1 [8]. Visibility could also be a constraint. That is, a wind profile must be able to be taken even in situations of low visibility, such as fog or battle field obscurants. Lastly, the instrument must be able to compensate for motion as its carrier vehicle moves with the waves. A discussion of motion compensation will be deferred until a later section.

3.1 Current CATFAE Wind Sensor Design

The current CATFAE wind sensor design is an omni-directional device which is attached at the rear of the top hull plate of the amphibious assault vehicle. The sensor is attached at the top of a 61 cm (24") stand pipe. Figure 3.1a shows a sketch of the wind sensor and Figure 3.1b shows the amphibious assault vehicle with the sensor attached [8]. Limited operational testing of this sensor arrangement has found strong disagreement between winds measured with the sensor on the CATFAE vehicle and with those measured at a 15 m height above ground from a stationary tower [1]. During this testing, the difference between the CATFAE measured wind and the tower measured wind was found to significantly influence the prediction of the CATFAE SEM computational algorithm. Better methods of measuring the winds for input to the FCS are therefore required.

Table 3.1 CATFAE operating environment tests.

1. Operating temperature;	-26^o C to 60^o c (-15^o to 140^oF)
2. Humidity; 810-507.1 Procedure IV	Consists of 5 -24 Hr cycles 95% Humidity 16 Hrs at 60°C (140^oF) 8 Hrs at 30^oC (86^oF)
3. Vibration; 810-514.2 Procedure	Sinusoidal cycling 3 Hrs/Axis VIII Sweeptime 15 minutes 5-500-5Hz Curve - 1.5G from 5 to 30 Hz 4.2G from 50 to 500 Hz
4. Shock 810- 516.2 Procedure I	3 Hits each axis each direction (18 shocks) 40 g's peak 11 ms duration sawtooth wave 30 g's peak 11 ms duration sine wave
810-516.2 Procedure II	Transmit Drop Test (48 drops) Drop 1.2 m (48") on each face, edge, and corner
5. Salt Fog; 810-510.1 Procedure I	Salt Fog for 48 Hrs at 35°C (95^oF)
6. Dust; 810-510.1 Procedure I	Air Velocity 8.9 m/s (1750 ft/min) at 23^oC (73^oF) for 6 Hrs Repeat at 63^oC (145^oF)
7. Rain; 810-516.1 Procedure II	5 cm (2") of rain for 2 Hrs total Orientations; perpendicular to normal horizontal plane, tilted 45^o to normal horizontal plane, so all sides are exposed. (5 orientations)

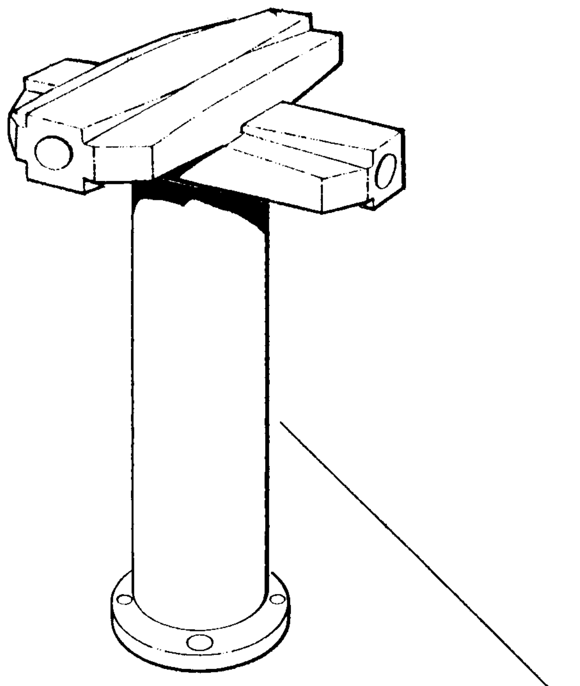

(a) CATFAE wind sensor

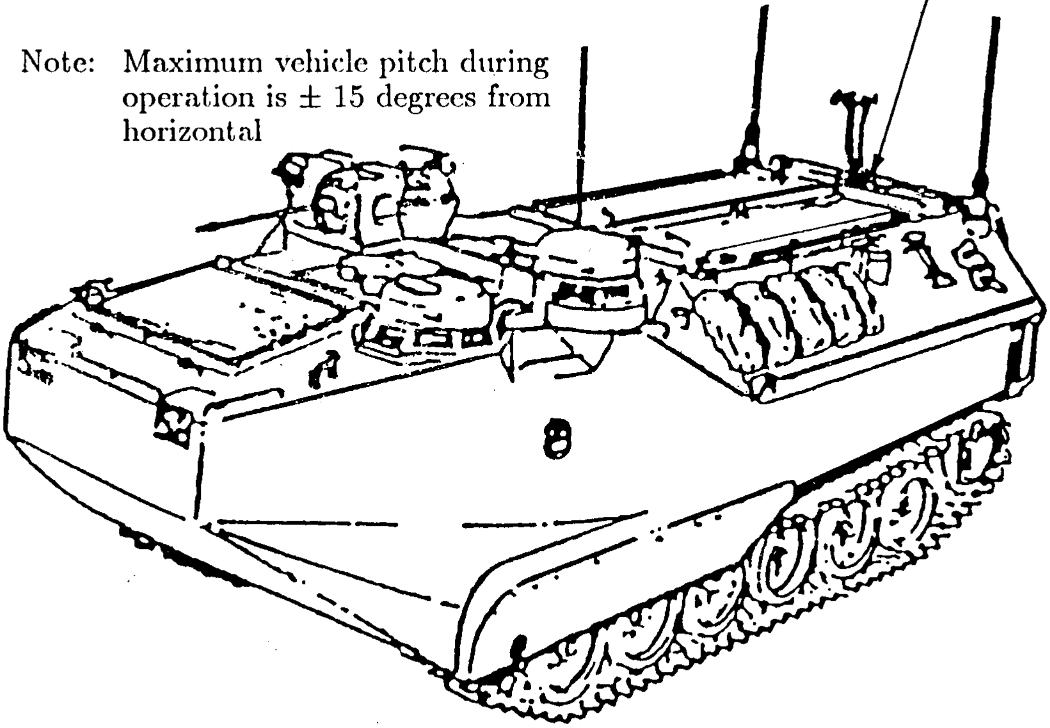

(b) CATFAE wind sensor mounting location

Figure 3.1 CATFAE wind sensor and mounting location[8].

There are a number of factors which could lead to significant errors in the representation of the wind profile. As the CATFAE assault vehicle bobs up and down, rolls, pitches, and yaws as it crashes through the waves upon approaching the shore, the wind sensor is slung chaotically about, creating unpredictable relative motions between the sensor and the actual wind attempting to be measured. Although the vehicle's motion is monitored and mathematically accounted for, it is difficult to fully appreciate the chaotic fluctuations in the calculations accurately.

The height of the sensor is an important factor, as well. Only two-thirds of a meter above the vehicle, the sensor is within the influence of the wake of the vehicle hull. Figure 3.2 illustrates this concept. The vehicle's hull sheds vortices which can create a velocity defect in the wind as seen by the sensor.

The height of the sensor is important in another respect. The wind measured by such a low sensor is deep within the surface boundary layer. Taking a measurement so near the surface and then attempting to generate a log profile by backing out of the equation, one must be very cautious of one's assumption regarding the effects of surface roughness. It was shown earlier in this report how differences in this parameter alone can affect the profile. The uncertainty of the surface effects actually experienced by CATFAE at the time of measurement brings into question the accuracy of the calculated wind profile. The eddies shed by the waves as they swell and fall, and as the vehicle crashes through them varies rather dynamically, making an assumed surface roughness somewhat questionable.

The boundary layer portion of a logarithmic wind profile is very sensitive to height. As the vehicle and its sensor bob up and down, the sensor could be taking data at any height from zero meters to three or four meters above the water's surface. With an FCS algorithm assumption of, say, 2 or 3 meters height for the data, and a particular surface roughness of some z_0, the friction velocity derived empirically could be dramatically tainted. For example, Figure 3.3 shows the difference between two log profiles influenced only by the height at which a "true" log profile was measured. Curve (a) is the "true" log profile. Curve (b) was generated by measuring

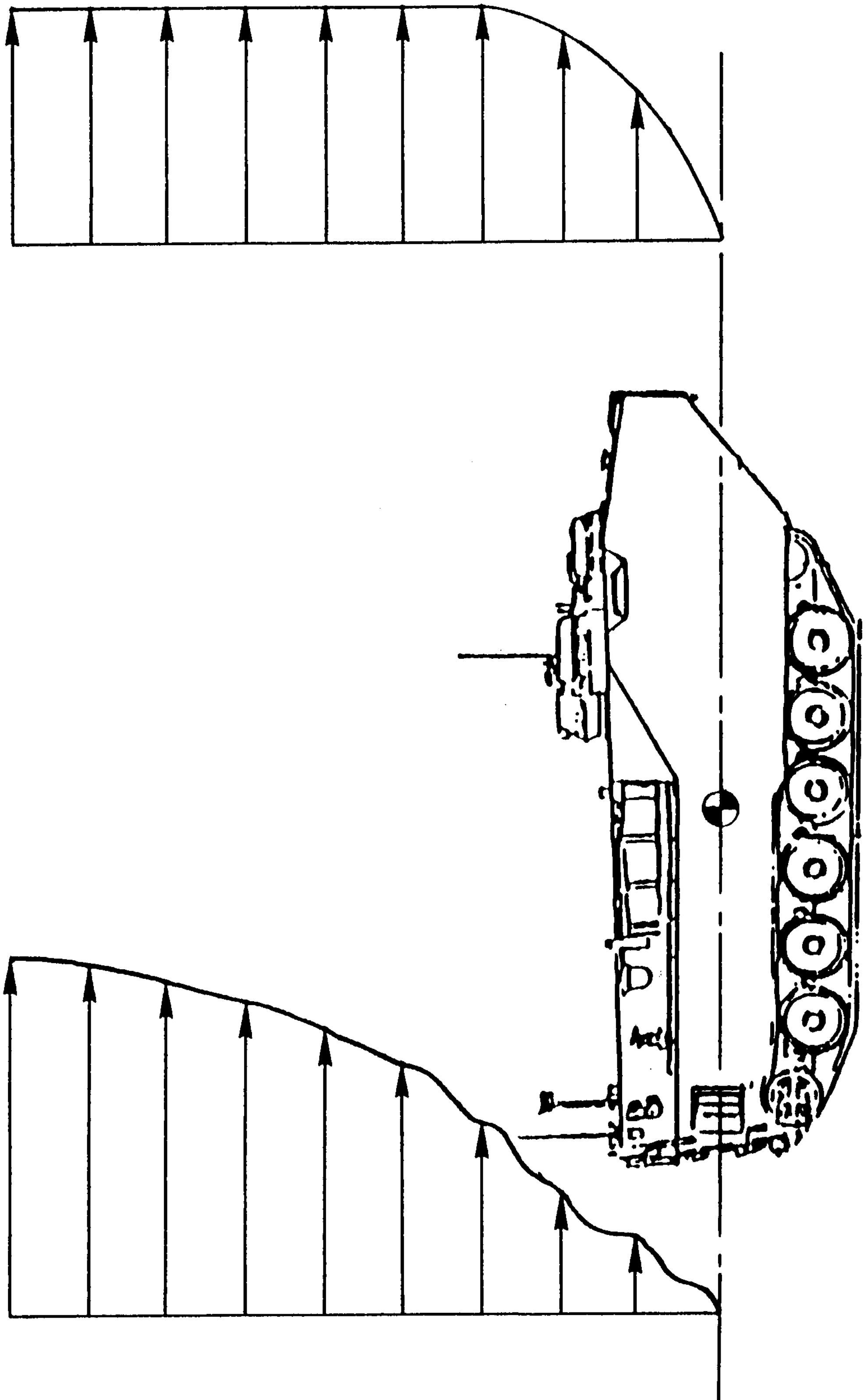

Figure 3.2 Induced hull effects on wind profile.

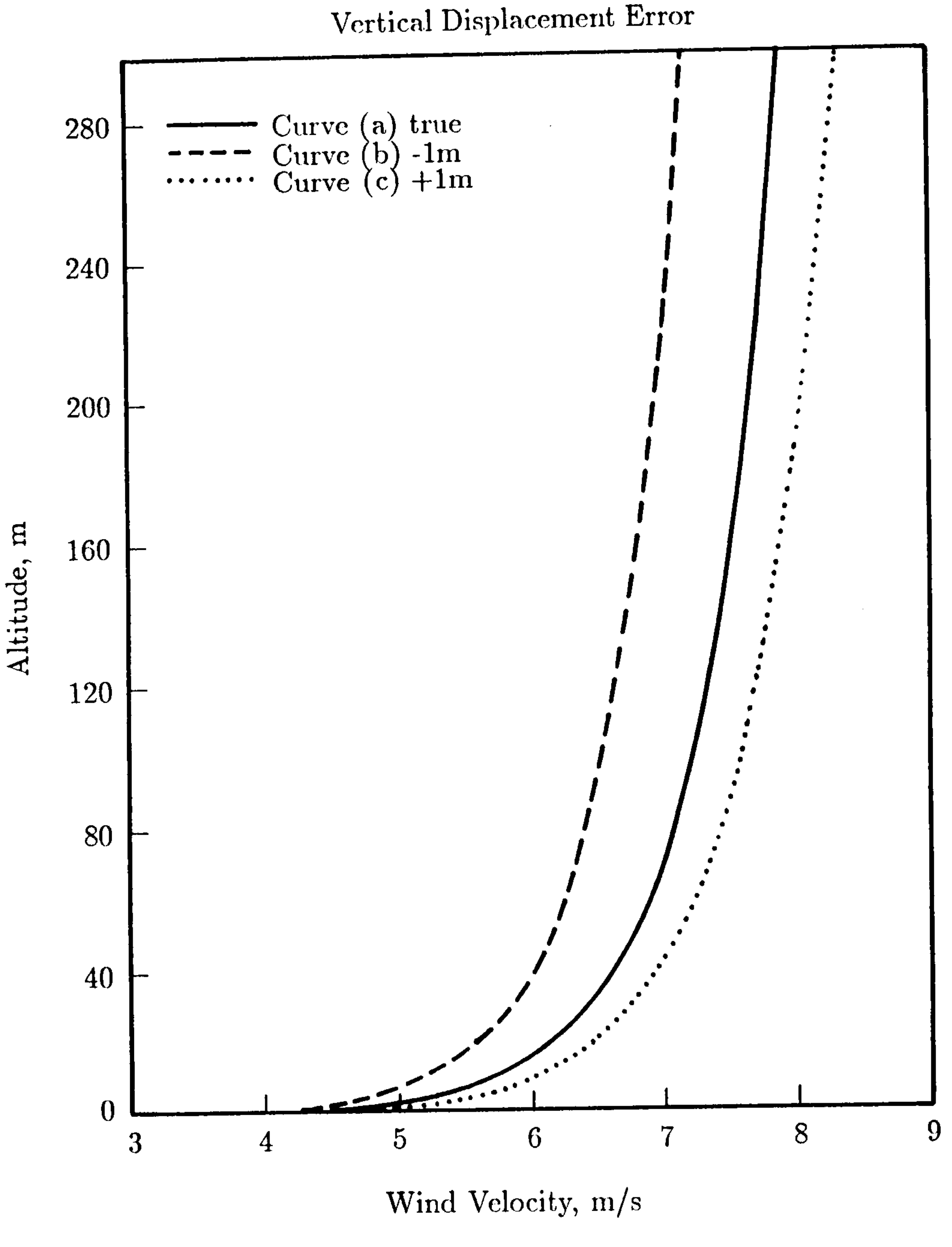

Figure 3.3 CATFAE measured log profiles.

the value of the true profile at 1 m and assuming it to have been measured at 2 m. Curve (c) is the profile from having read the value of the true profile at 3 m and assuming it to have been measured at 2 m. The differences in these profiles, as a result of this displacement error alone, is about +5% to −10%.

One last important factor concerning the CATFAE sensor design, and perhaps the most significant, is that this sensor has no idea what the wind is doing above it. As shown in Section 2.0, atmospheric stability can have a profound effect on the flow pattern of wind. Referring back to Figure 2.5, it is stressed that the wind aloft could actually be blowing in the opposite direction as the surface layer wind. With a CATFAE sensor unable to see this occurring, and assuming a simple log profile instead, the FCS fuse time calculations, and hence round dispersement pattern, could be dramatically impacted. Figure 3.4a shows an example of a wind shear profile compared to the log profile CATFAE would see. Figure 3.4b shows the drift pattern and impact point of a single round, based on approximated drag characteristics and a fall of 250 meters, subject to each wind profile. Appendix C details the calculation method used to approximate the CATFAE round drag characteristics and drift distance.

A last concern to be considered is time. If CATFAE takes only a few sample readings over a very short time frame, the measurements could actually be taken too quickly. It may read a gust or stall in the wind, failing to realize the true mean wind velocity. A slow rising balloon ranged at several altitude intervals would damp out the small scale gusts.

3.2 Acoustic Sounders (SODAR)

The technique of sodar wind measurement is based on the backscattering of sonic waves by inhomogeneities in the refractive index of the air. This technique has proven to be quite successful in low altitude profiling, including measurements of coastal sea breeze [9,10,11]. Sodar systems have excellent vertical resolution on the order of 30 m, and can take soundings from near the surface up to altitudes well above interest to CATFAE (approximately 1000 m) [12,13]. A sodar instrument would be

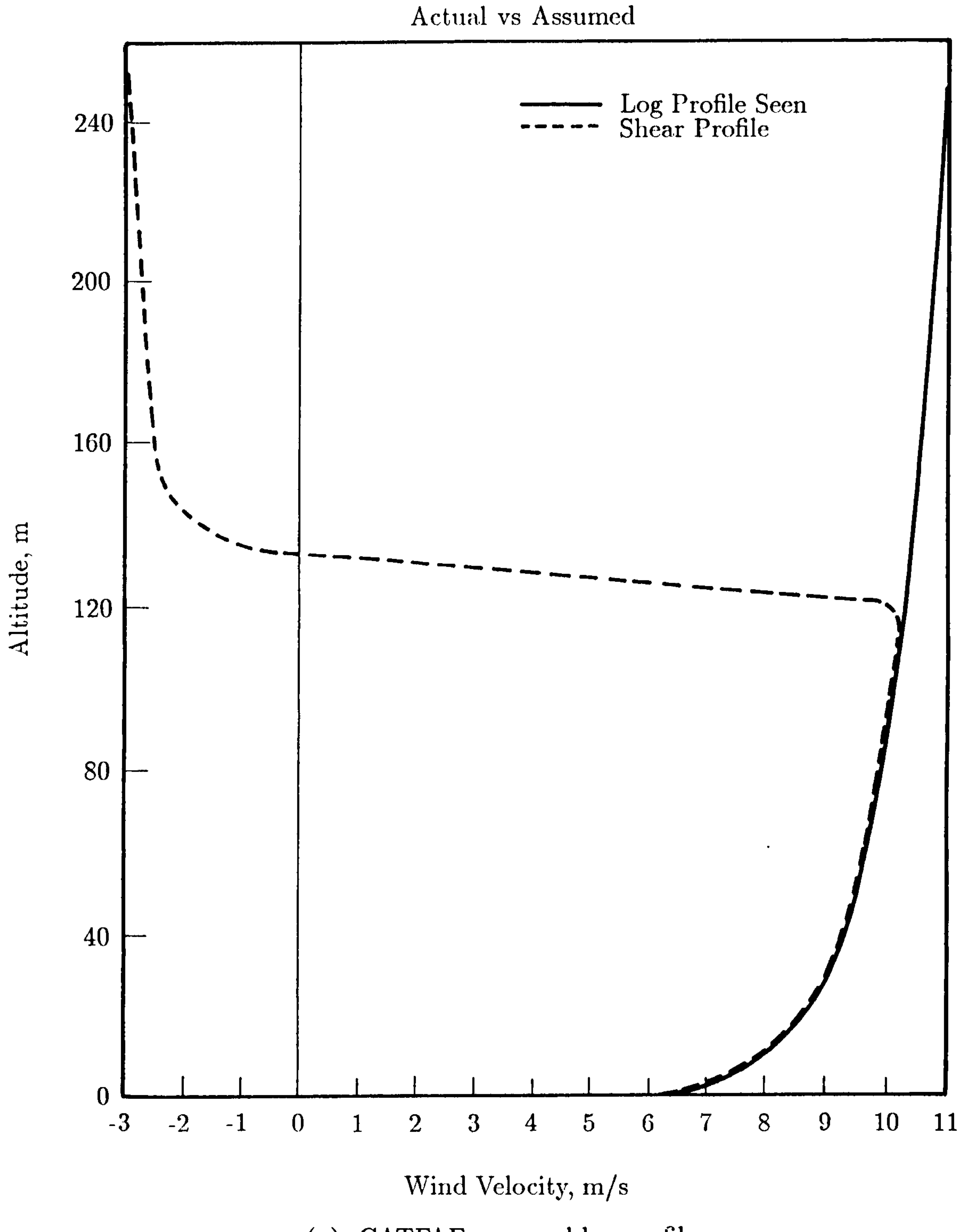

(a) CATFAE assumed log profile

Figure 3.4 CATFAE asumed log profile and round drift.

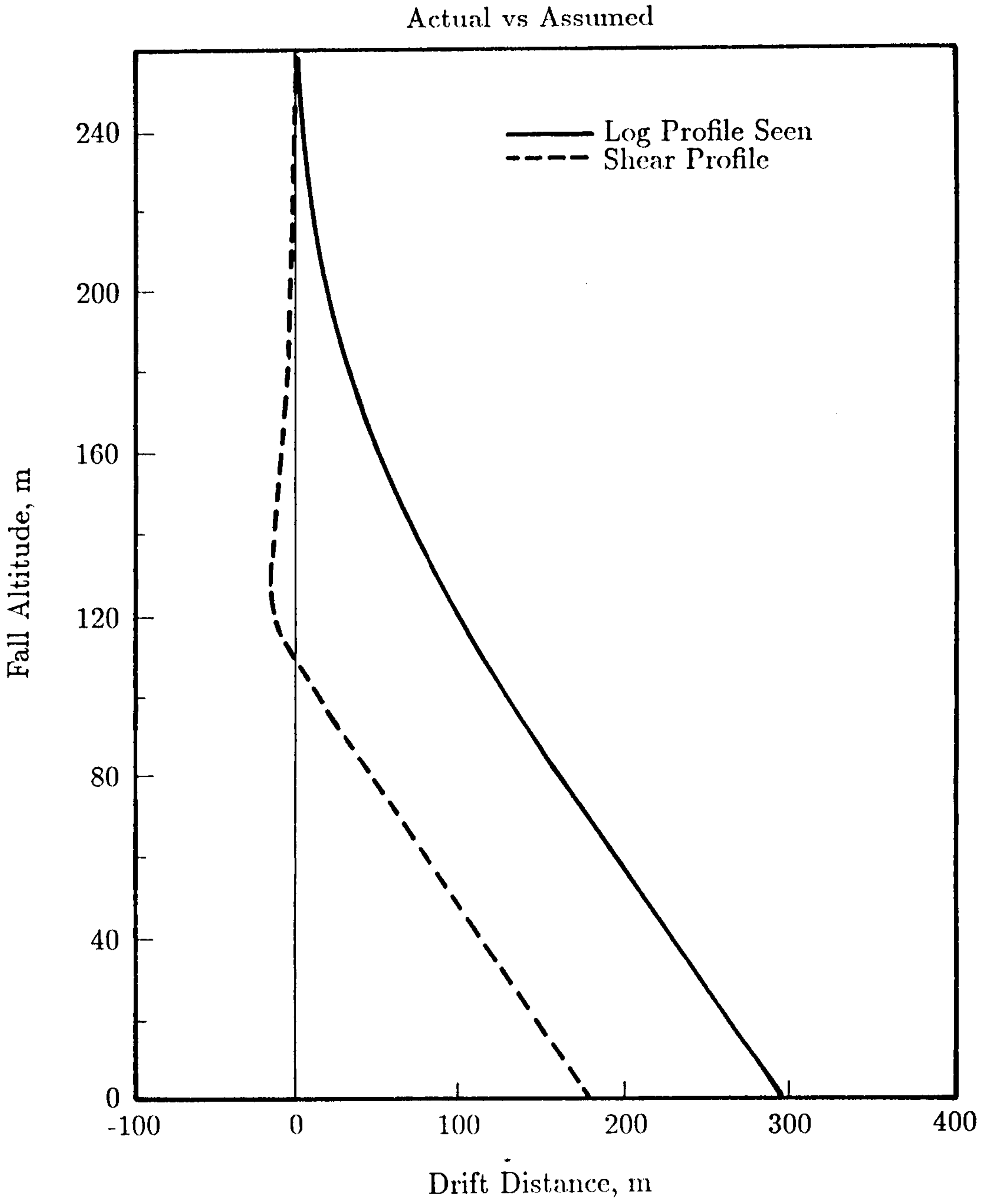

(b) CATFAE round drift

Figure 3.4 (continued).

able to take several data points within the 250 m height to derive a very good, high resolution profile for input to the FCS. Also, time would not be a constraint, since taking acoustic soundings is fast. Sodar systems can make data soundings in a matter of a few seconds, thus requiring only one or two minutes to measure a profile. Unfortunately, some of the other constraints imposed by the CATFAE system limit the usefulness of sodar instruments. A parabolic transmit/receive dish of some 1 or 2 m in diameter is required. To get clear soundings, acoustic shielding is also required, which involves something like a polyurethane foam lined cuff of some 2 m or more height surrounding the dish. Size and encumbrance is obviously a limiting constraint here. Also, even with the acoustic cuff to damp out ground clutter, vehicle generated noise would probably prove prohibitive. The visibility could also be a problem. Sodar signals may be tainted or even entirely reflected by the fog or obscurations. Lastly, the requirement that the system be rugged would probably be violated. The parabolic dish my be able to withstand some of the dynamic environment such as temperature and some water spray, but the drop and impact testing described in Table 3.1 would undoubtedly cause serious damage to the dish.

3.3 Radar

Radar systems work in a manner similar to the acoustic sounders. High frequency signals are transmitted and reflected signals are received from particulate matter in the air. Although typical radar wind sensing systems are not low altitude, high resolution systems, a few are being developed for this type of application. For instance, the University of Oklahoma has recently developed a portable radar system for tracking thunderstorms, and the National Oceanic and Atmospheric Administration (NOAA) has developed what is called a Boundary Layer (BL) radar [14,15]. The NOAA BL radar is a system which was reviewed as a potential candidate for the CATFAE system. It is a small, portable 915 MHz doppler radar system which provides high resolution clear air profiles from near the ground to 2-3 km or more. The system will soon be PC based, reducing cost and allowing faster pulses, sampling, and processing. The system will be able to profile the wind from as low as 100 m or less to well beyond the 250 m height of interest to CATFAE with a resolution as good as 30 m. Ground clutter (noise) prevents the radar from taking good data much below 100 m. The size of this system is easier to accommodate than the sodar instrument described above, but it is still a limiting constraint. The dish is composed of 91 cm × 91 cm segments which can be connected together. Since CATFAE is only interested in the lowest altitudes, one dish segment should suffice. However, as with the sodar, some sort of noise screen would be required to damp out ground clutter. Thus, size becomes limiting. Also, as with the sodar parabolic dish, the dish for this radar system would be susceptible to damage by the testing parameters specified in Table 3.1. That is, ruggedness is a difficult constraint for the BL radar to conform to. The fact that the BL radar measures clear air profiles is also a limiting factor to this system's usefulness. In the presence of fog or battlefield obscurants, the system would be crippled.

3.4 Lasers

Laser systems work much in the same way as the radar and acoustic systems, but use lasers instead of radar or acoustic frequencies. The laser optical system measures the strength of returning signals from backscattering caused by aerosols in the air. For the most part, however, laser doppler radar, or LIDAR, systems are used in meteorology to measure large scale atmospheric motions or shear by averaging over large sample volumes. Not many LIDAR wind systems have been used for low altitude, high resolution wind profiling. Recently, however, lasers have begun to be used in this type of application. There is a British system called the Laser True Airspeed System (LATAS) developed by the Royal Aircraft Establishment and commercially marketed by GEC limited of England [16,17]. It is a CO_2 continuous wave laser that has been proven to be rugged and very reliable. This instrument can be focused at different ranges from 25 m to 1 km or more. At the near focal length the sample resolution is around 30 m. This wind instrument is a very attractive candidate for the CATFAE system, because it can accommodate the constraints of CATFAE. That is, it is portable, being comprised of four hardware items no larger than 0.7 m $\times$ 0.33 m $\times$ 0.3 m each. Since LATAS is a computer controlled laser, it is very fast. Sample readings take only milliseconds, thus requiring only about 1 second to get a complete profile. LIDAR systems can profile the wind in a variety of conditions from rain and fog, to clear dry air. Also, it is a very rugged instrument. It has been flown on an airplane for over 2 years without harm to its diamond-like coating on the optical window (this includes flights through soft hail) [17]. The system should be rugged enough to withstand the tests specified in Table 3.1. Work with the LATAS is reported in [18]. In 1985 an assessment as to the potential value of this instrument as a wind shift detector for the America II yacht was carried out. The only real drawback to this system is cost. Although cost was not mentioned above as a constraint, it goes without saying that money is almost always a concern. This system is much more expensive than the other systems reviewed. Also, battlefield obscurations targeted at blocking infrared would be an impediment to successful LATAS operation.

3.5 Balloons

Another possible technique usable by the CATFAE system is to employ balloons for measuring the winds. Balloons have been used quite successfully in meteorology for many years, and, in fact, are still used in such important circumstances as launch commit criteria for the Space Shuttle program. Different ways of employing balloons exist. A balloon can be tethered to the vehicle with sensors attached to the tether at intervals; one or more balloons can be released, carrying transmitters that return signals to a receiver on the vehicle; or one or more passive balloons can be released, and the motion of the balloons relative to the vehicle tracked. Below is a brief discussion of each of these concepts.

3.6 Balloon with Tether

A balloon can be released which would rise above the altitude of interest to CATFAE. Having a tether attached between the balloon and the assault vehicle, the balloon would hold the tether taught. Sensors located at particular intervals along the tether would allow a wind profile to be measured directly. This method, however, would require over 250 meters of tether and several sensors. This could potentially be disorganizing, as well as a burden to the balloon lifting such weight. A balloon of possibly undesirable size would be required. Also, the motion of the vehicle riding the waves would jerk on the tether, causing the balloon to bounce and sway. These unpredictable motions would invariably degrade the quality of the wind measurement [19].

3.7 Balloon with Transmitter

By separating the balloon from the vehicle, the problem of jerking on the tether is eliminated. If one or more balloons were to be released which carried transmitters, signals could be sent back to the vehicle. From these signals the processor could calculate approximate locations and, hence, wind profiles. A single balloon that rises slowly at a predetermined rise rate could be tracked to give a vertical profile, or a number of neutrally buoyant balloons could drift at predetermined altitudes. This type of measuring system is a very attractive possibility for the CATFAE system. Given the right type of transponder on the balloon, an acceptably accurate wind profile could be obtain in a reasonable amount of time, say one or two minutes. Using a single, slow rising balloon would not be unwieldy, and would allow a vertical profile to be taken in a variety of environmental conditions. A very good candidate for this type of profiling is discussed in a later part of this paper. It is a mm-wave transponder which sends signals back to a small receiving dish of no more than 0.6 meter diameter.

3.8 Passive Balloon

The other possibility is to release one or more balloons by themselves and track their motion [20]. Several neutrally buoyant balloons may be employed, or one slow rising balloon. To lift to an altitude of 250 m without instrumentation, the slow rising balloon would not have to be very large (less than 1 m diameter). Also, the neutrally buoyant balloons would range from very small to no larger than 1 m. The problem here is again to find a tracking device that can be accommodated and is rugged enough to withstand the CATFAE environment. There is an excellent devise which is available for this application. It is called a Laser Rangefinder and is produced by Lasergage [21]. It uses infrared pulses and a clock to determine how far the observed target is from the user. Several variations of this apparatus are available, from hand-held units to much larger, mounted units. The device could be used to follow the balloon, taking distances at intervals of time to figure out the velocity of the balloon relative to the vehicle. Of course, weather and visibility could prove to be limiting factors for this technique of wind sensing, since visible tracking would be required. A more detailed look at this type of system is given later in this thesis.

4.0 SUGGESTED WIND SENSING TECHNIQUE

The above portion of this thesis stressed the need for CATFAE to utilize a better wind profiling system. This section will suggest three possible systems that would provide adequate measurements: the LATAS laser doppler system, the Lasergage infrared rangefinder with passive balloon, and the mm-wave transponder balloon tracking system. After presenting some details of each candidate, a recommendation will be made as to the most promising system for CATFAE.

Before the suggested systems are discussed, however, an alternative operational scheme for assessing the wind for FCS input shall be put forth here. Instead of tackling the nearly unsolvable difficulties of measuring the wind with an instrument attached to the amphibious assault vehicle, the idea of placing the instrument aboard the mother ship should be seriously considered. There are several advantages to this approach. For one, the ship would be a far more stable platform from which to operate. As mentioned earlier, the assault vehicle is tossed dynamically in the water, but the larger ship would ride more smoothly. With an INS aboard the ship, corrections can be made to the wind data to resolve the ship's motions relative to the wind, or if the ship is stable enough, its motions could be ignored. Also, convenience is a factor. To operate a wind sensing system while aboard the assault vehicle would be an extra concern to the soldiers preparing for the launch of CATFAE rounds. Operating the wind instrument aboard the mother ship would be easier, and could be performed during less chaotic moments. The fact that the wind can be measured before launch of the CATFAE vehicle would allow the FCS operator to acquire the wind data and input it into the FCS manually before or during the time that the amphibious assault vehicle motors to position. Measuring the wind from the mother ship would also allow anonymity to the assault vehicle. No wind instrumentation would have to be included on the exterior hull of the assault vehicle.

A couple of concerns may arise when considering placing the wind sensor on the mother ship. For instance, the validity of a measurement taken some several kilometers from the shore, or the tactical implications of losing the autonomy of the amphibious vehicle by being dependant upon a ship borne instrument may be questioned. These concerns can be appeased. As far as autonomy is concerned, the wind instrumentation was described earlier to be compact and light weight. It could be integrated onto its own portable carrier harness that could be placed aboard the ship along with other equipment. It could be moved onto deck and the wind tracked. Once this was accomplished, the instrumentation could be moved again. Thus, portability would afford a certain degree of autonomy. Regarding the concern of validity, the discussion in Section 2.0 addressed the concept of spatial and time scales. The scales of the synoptic sea breeze and stability phenomena were shown to be quite large. The horizontal variation in the wind profile would be small over large distances, and the variation in the wind would be small over a period of some time. A distance of 10 km and a time frame of a couple of hours would only experience marginal changes in the wind.

4.1 LATAS

The Laser True Airspeed System (LATAS) is an infrared laser transmit/receive device which measures the backscatter by aerosols in the air. This system has been shown to be capable of measuring backscatter signals in environments ranging from fog and rain to clear air with no aerosols greater than 0.5 μm [17]. The system is composed of three primary units, as well as support processors, structure, etc. The three primary units are the Optical Head, the Surface Acoustic Wave (SAW) Spectrum Analyzer, and the Video Integrator. Some of the support units are the beam transmit scanning system, the stabilization support and a cooling unit. Figure 4.1 shows the general layout of the LATAS with manufacturers listed in brackets [17].

The optics head, shown in Figure 4.2, transmits the main beam from the 3 watt Ferranti Wave Guide laser through a germanium plate and a remotely adjustable expanding lens. When the signal returns, its polarization is changed and

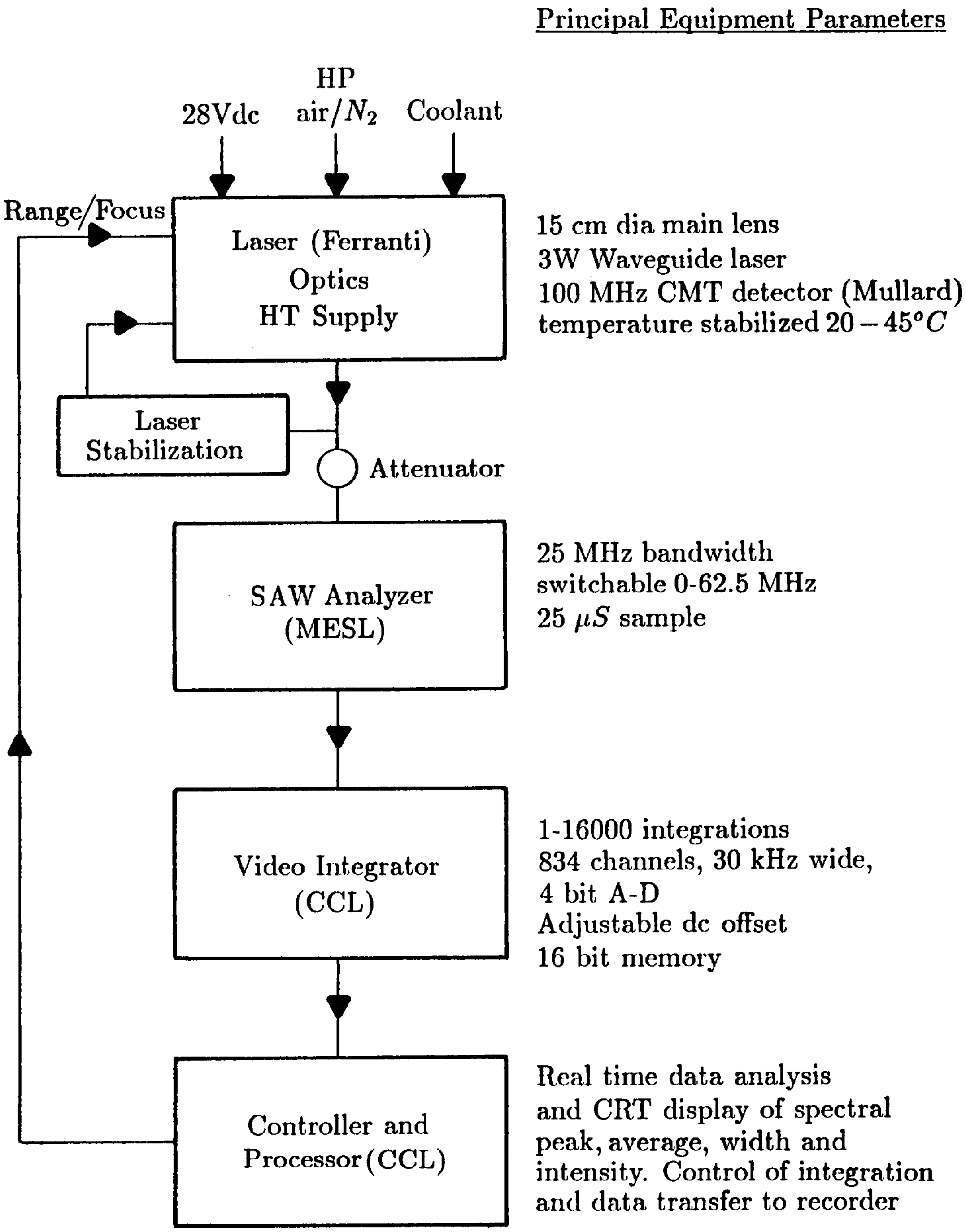

Figure 4.1 Block diagram of the Laser True Airspeed System (LATAS).

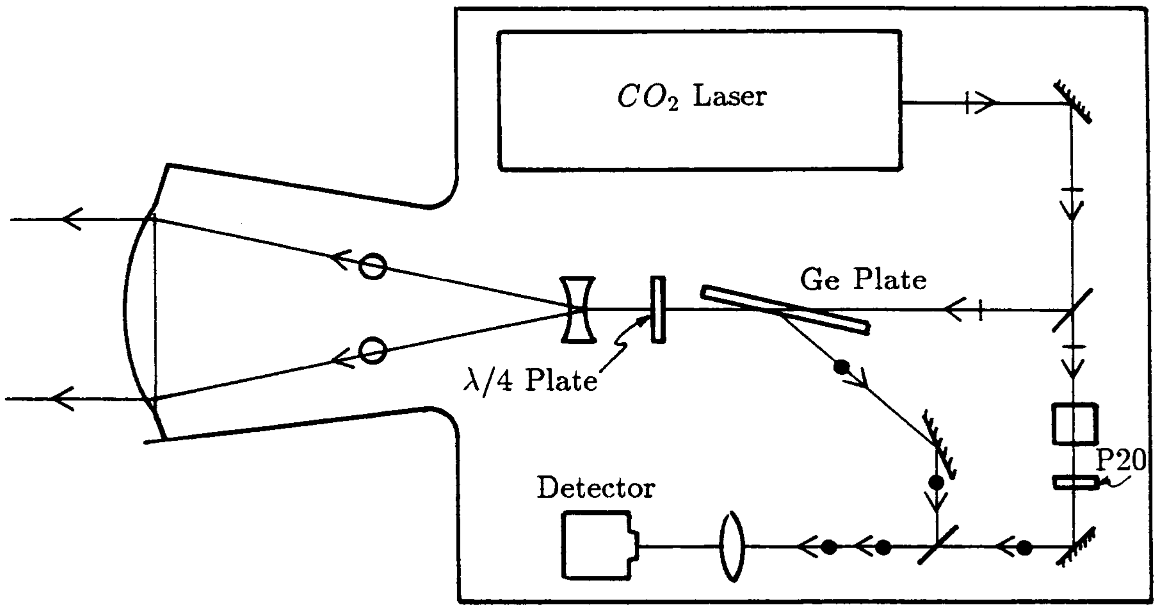

Figure 4.2 Layout of the Optics Head in the LATAS equipment [17].

it is reflected off the germanium plate toward the Mullard CMT detector, being augmented by a portion of the main beam while on its way.

From the detector, the output is transferred to the SAW spectrum Analyzer. In a matter of milliseconds the signal is transformed into the frequency plane and then transmitted to the Video Integrator. The Video Integrator collects the output spectrum from the SAW and integrates the frequency spectra over several samples to reduce the signal to noise ratio.

All of these units can be accommodated on a portable carrier. The optical head unit is 68 cm × 32 cm × 29 cm (27" × 13" × 12"), including the HT power supplies, and weighs only about 13.5 kg (30 lb). Figure 4.3 shows a mock-up of the LATAS system which was designed with a horizontally stabilized scanning periscope [18]. This gives an idea of the space required for the LATAS and its support. The SAW Spectrum Analyzer, the Video Integrator and the cooling unit can be housed within the carrier unit or attached next to the Optical Head as required by space management and access needs. The SAW is 8 cm × 24 cm × 34 cm (3.3" × 9.5" × 13.6") and weighs about 4.5 kg (10 lb), the Video Integrator is 26 cm × 48 cm × 20 cm (10.5" × 19" × 8") and weighs about 4.5 kg (10 lb), the cooling unit is 8 cm × 24 cm × 34 cm (3.3" × 9.5" × 13.6") and weighs about 4.5 kg (10 lb).

The output from the LATAS consists of either analog or digital complete spectra and the peak values associated with the spectra. The form of the signal obtained is shown in Figure 4.4. The strongest signal comes from the region where the laser beam is most narrow. This is where the beam is focused, and the illumination intensity is greatest. The velocity at the peak of the frequency spectrum is that of the air at the beam waist. The beam waist can be focused at distances from as close as 25 m to 300 m or more. At focal lengths greater than 300 m, however, the volume resolution becomes too extended to resolve wind information from a discrete height interval.

In order to get signals that have appropriate information from which wind speed and direction can be obtained, a controlled scanning motion of the transmit beam

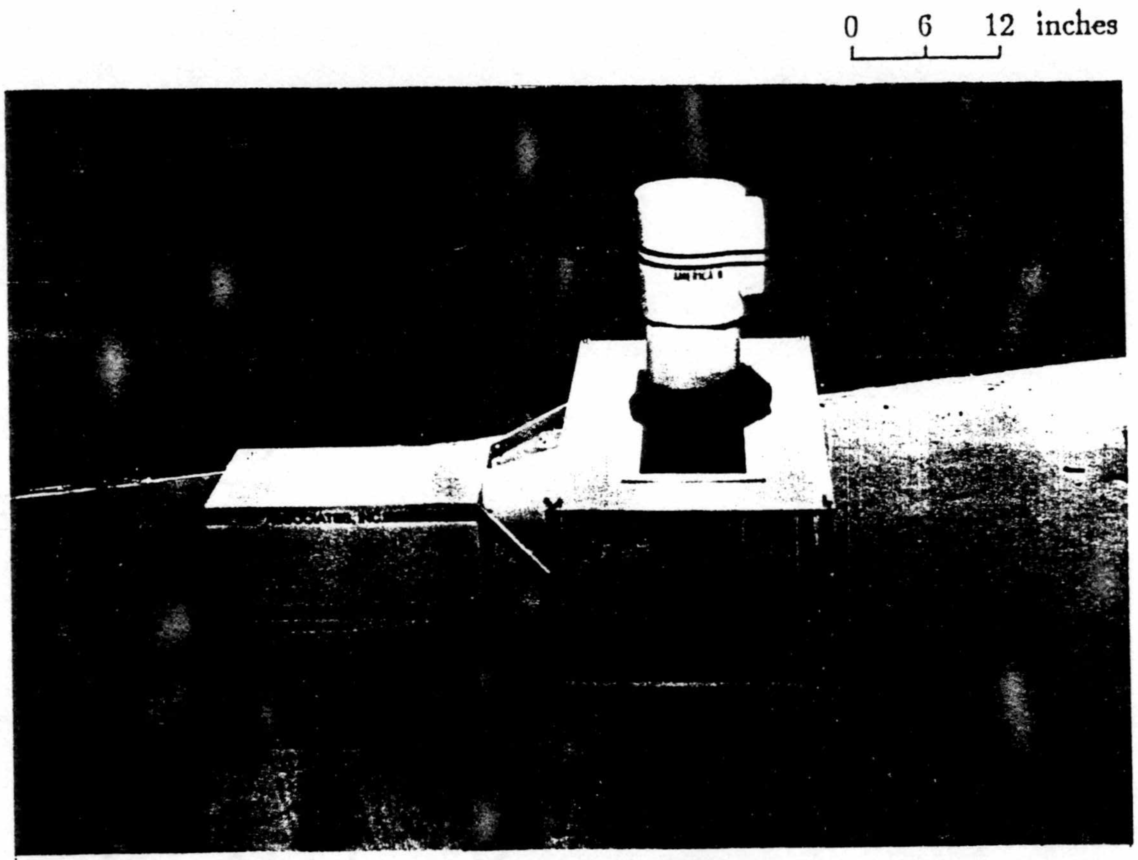

Figure 4.3 Mock-up of the LATAS system and horizontal, optical, scanning periscope[18].

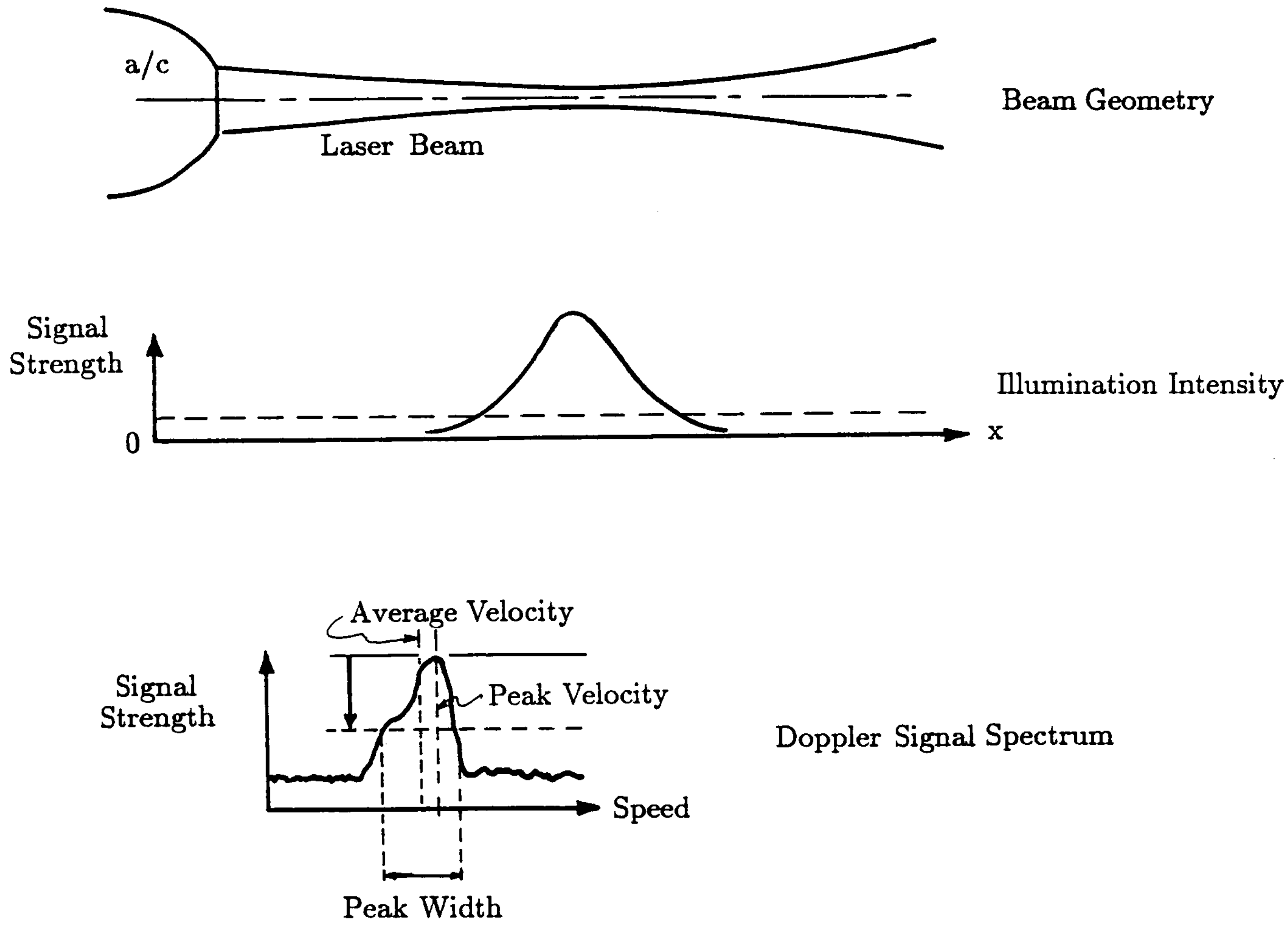

Figure 4.4 Parameters of a focused CW laser anemometer showing schematically the laser beam, the illumination, and Doppler spectrum[17].

is required. Scanning motion produces variations in the radial component measured at the focused range which yields directional information. Two scanning methods have been designed for the LATAS. In Reference [18] work with the America II yacht racers in designing a LATAS wind shift detector for their yacht is reported. Involved in this design was a forward looking horizontal scanning periscope for the optical head which scans a 90^o angle between port and starboard. Figure 4.3 has already shown a mock-up of this design. Based on sampling time and focal switching time, a 90^o horizontal scan could be completed in approximately 1 second with a 40 sample integration per data point [18].

The other scanning technique, developed by the Royal Signals and Radar Establishment (RSRE), is a vertical looking conical scanner [16]. This system takes circular scans at discrete altitudes to get vertical profiles of horizontal winds. Vertical winds can also be derived. The scanner employs one rotating and one stationary mirror to direct the transmit beam and backscatter signals in a conical pattern at 45^o or 60^o. The rate of scan for this system is about 1 cycle per second, allowing about 78 data points (256 integrations per point) for each cycle. Figure 4.5a shows the scanning setup and Figure 4.5b shows an example of a signal polar plot. In Figure 4.5b, the peak value of the two lobes is related to the magnitude of the horizontal wind speed and the main axis drawn through the lobes gives the angular direction of the horizontal component. Any vertical component of wind causes asymmetry in the two lobes.

In the work reported in [18], stabilization was also an issue addressed since the system was to be placed aboard a yacht. In the design of the optical scanner mount, the Optical Head was to be rigidly mounted under the half deck of the yacht, and the light beam was to be horizontally stabilized with a gravity balance rotating head scanning periscope (see Figure 4.6) [18]. Pitch stabilization was not planned for the America II yacht since this motion would simply give an averaging in the vertical plane. Since the RSRE conical scanning LATAS wind profiler was a ground unit, it was not stabilized against external motions. For the CATFAE system, some sort of

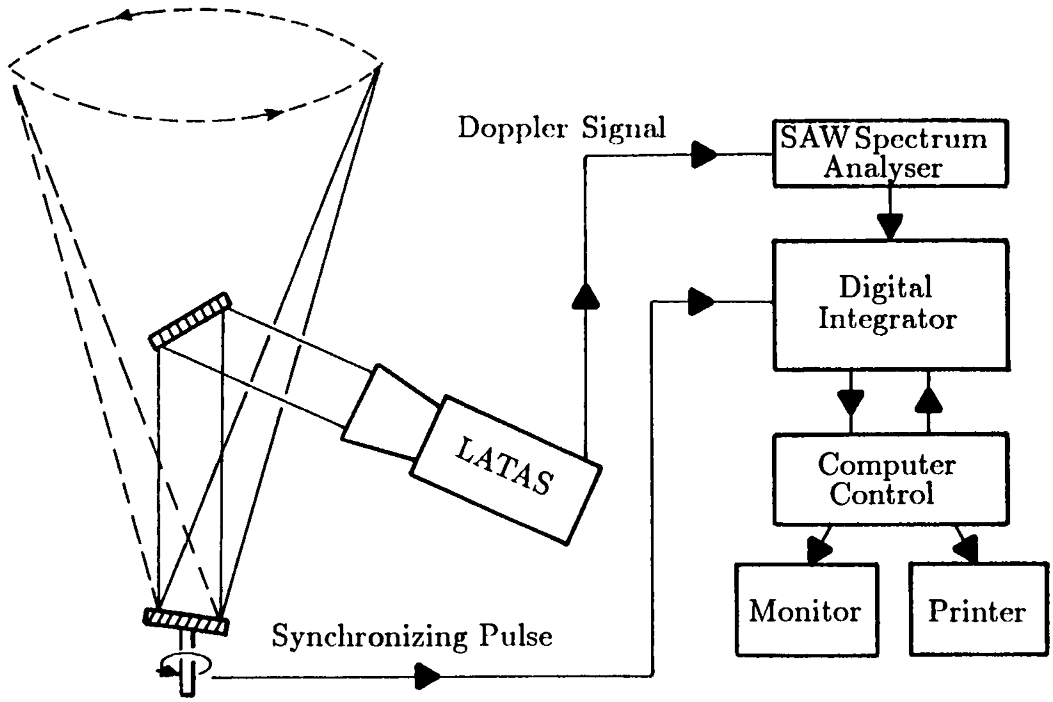

(a) Scanning setup

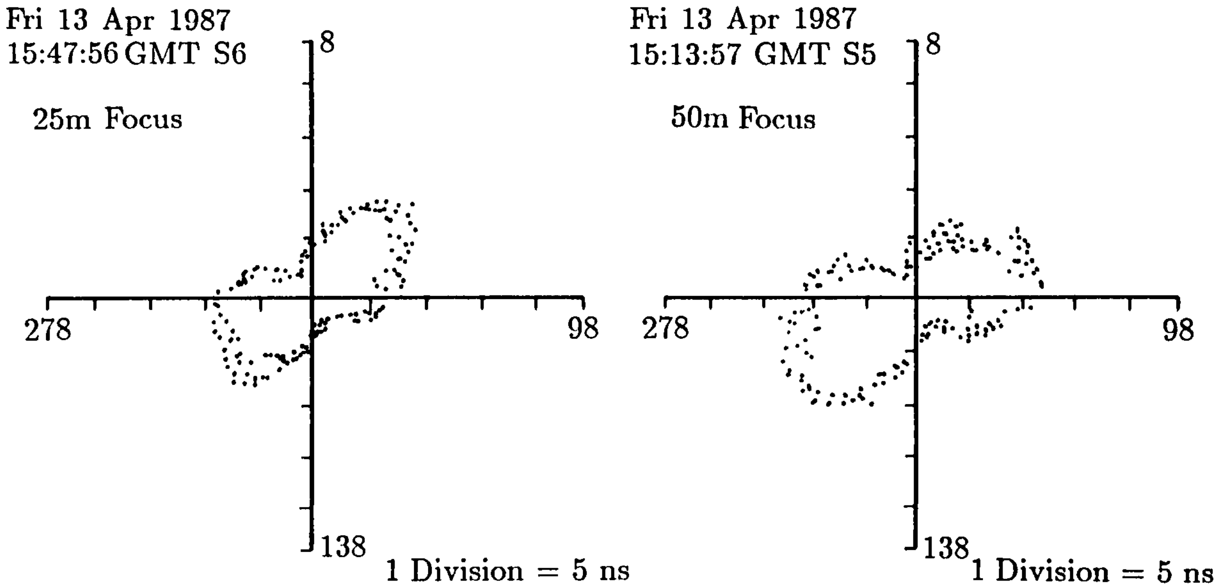

(b) Signal polar plot

Figure 4.5 **Scanning setup and signal polar plot for a vertical looking conical scanner[16].**

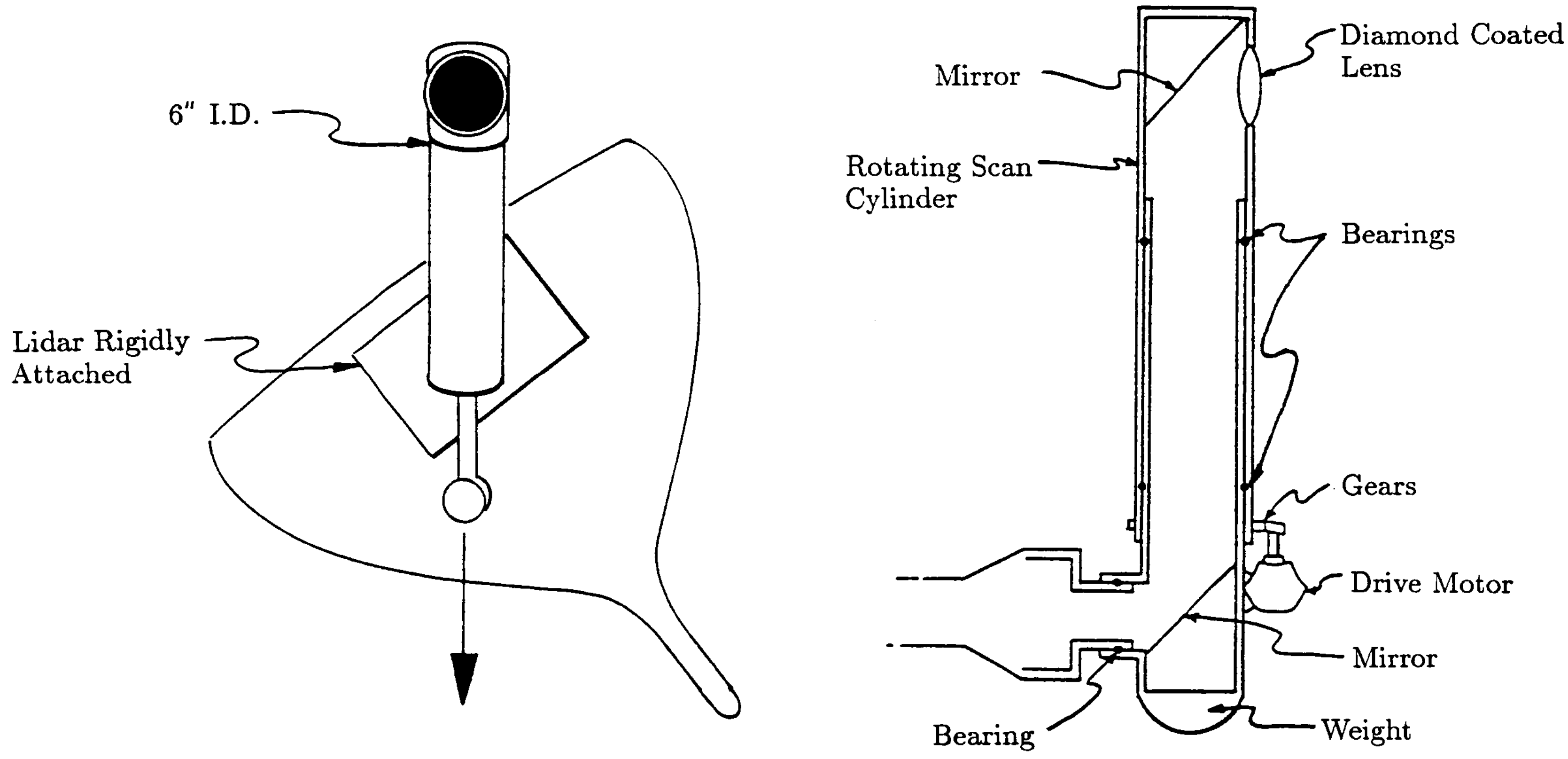

Figure 4.6 Schematic of system for horizontally stabilizing the optical beam in roll [18].

stabilizer similar to the America II system can be designed which would allow the LATAS to utilize a scanning technique which would yield the proper data required for the SEM. The scanning system would be something similar to those designed in [17] and [18]. Further studies can be pursued toward defining a scanning and stabilization design applicable to CATFAE if so warranted.

4.2 Lasergage Rangefinder

The hand-held laser rangefinder is a device which looks and feels much like an ordinary 7 × 50 field binocular when used. Figure 4.7 shows one that is marketed by Lasergage limited of England [21]. The device uses a miniaturized dye Q - switched Nd:YAG Laser transmitter of simple and reliable construction. With each push of the trigger button, a short intense pulse of infrared energy is generated for range measurement. The receiver is a photodiode optimized for the operational wavelength and includes a gain amplifier to accommodate the wide range of return signals. The circuitry also includes filters to prevent the registration of reflections from smoke and dust. Thus, the unit is capable of handling imperfect weather situations. In order to make a range measurement, the instrument is turned "on", and by viewing through the sighting telescope is "aimed" at the selected target and "fired". Ranging is initiated either when the trigger button is pressed and released with the laser firing after one second, or if the button is depressed for more than one second, the laser fires immediately on release. The display appears instantly when the ranging is made [22]. The range capabilities of this device depend on atmospheric conditions, but on clear days it has a maximum range of 9 km, and can even detect a standing man at 1.5 km [23]. When ranging is made, reflections from foreground interferences or unwanted targets can be eliminated by using the continuously adjustable minimum range control. This control can be set to eliminate targets from as close as 150 m to as far as 3 km. Figure 4.8 is an example sequence of how this minimum range control can be used [21].

For application to the CATFAE system as a wind sensing instrument, a modified version of this device can be used in conjunction with a theodolite mount to

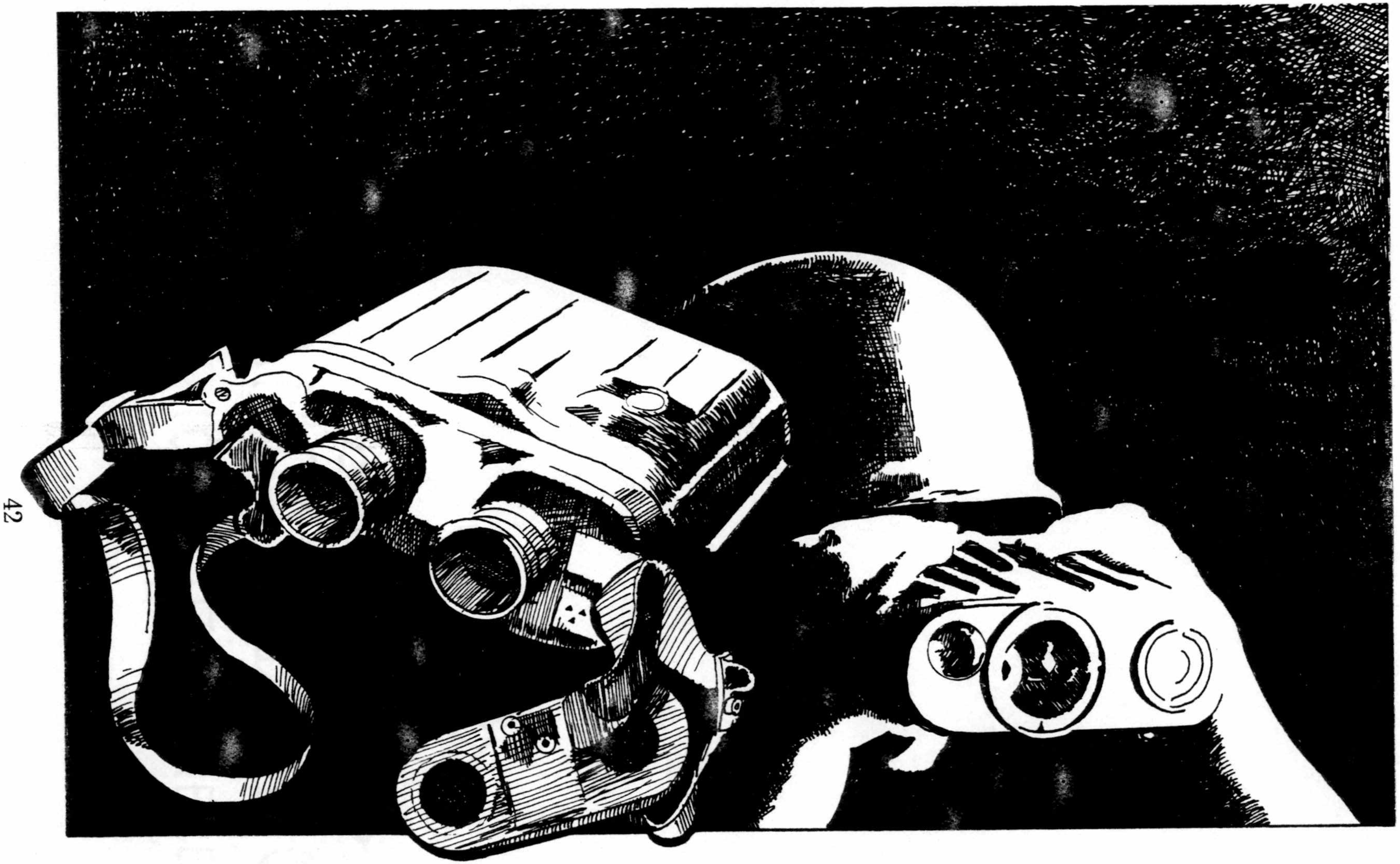

Figure 4.7 Lasergage rangefinders for military use.

The distance to a target is to be ranged as shown above. The line of sight is interferred with some obstructions which are likely to reflect laser light, e.g. a hill and a cliff behind the target.

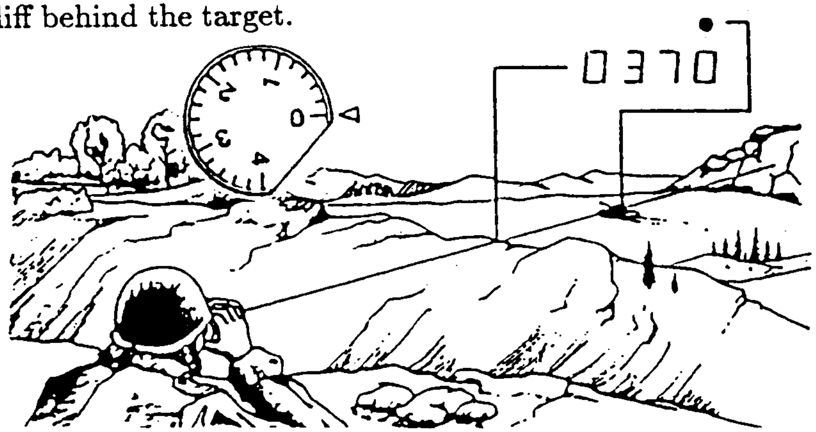

1st ranging: ranging with the mininum range set to minimum yeilds a display of the range to the hill (370 m) and indication of additional target.

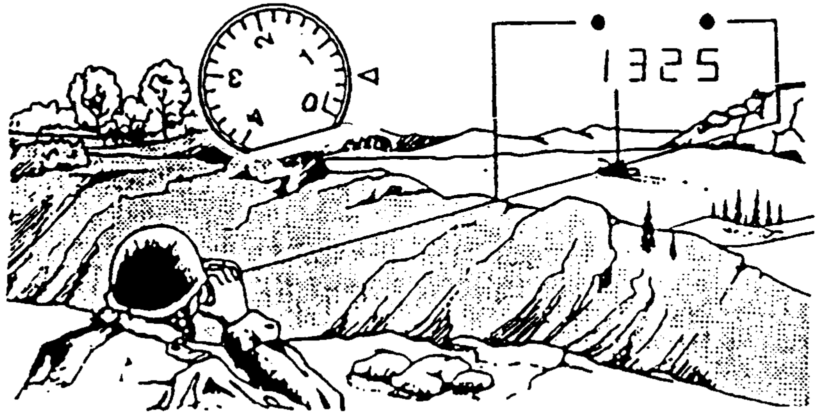

2nd ranging: ranging with the minimum range set on 0.5 km (beyond the hill) yields a display of the range to the target (1325 m), and indication of additional target. The hill is now within the minimum range and reflects the laser light, thus actuating the G-indicator.

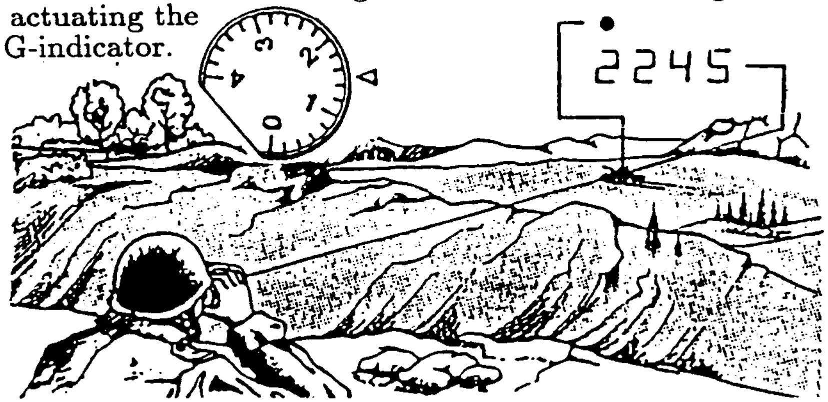

3rd ranging: to estabish that 1325 m is the true range to the target in question, the minimum range set on 1.5 km (beyond the target) will display 2245 m to the cliff, and no indication of additional targets. Both the hill and the target are now within the minimum range and reflect the laser light, actuating the G-indicator.

Figure 4.8 Diagram showing use of minimum range control with a Lasergage rangefinder[21].

track a balloon as it drifted with the wind. Figure 4.9 depicts the LP150E which would serve the purpose [24]. Either a single slow rising balloon can be followed, or a number of neutrally buoyant balloons can be ranged one after the other. As the balloons drift, the rangefinder can be used in conjunction with a theodolite to measure distances and angles over time in order to calculate the balloon/wind velocity relative to the vessel. The altitude of the balloon(s) will, of course, be known since the slow rising balloon will have a predetermined rise rate, or the neutrally buoyant balloons will have predetermined equilibrium altitudes. It is suggested that a slow rising balloon be employed for ease of use.

4.3 mm-wave Transponder

The mm-wave transponder balloon is probably the best method. The proposed system would be able to measure the horizontal winds to a maximum altitude of 330 meters with sufficient accuracy to support launch of the CATFAE weapons system. The winds would be measured by tracking a beacon carried by a balloon rising at a known rate of change in altitude (see Figure 4.10). A passive tracking system can supply sufficient information to estimate the mean horizontal wind velocity as a function of altitude. System parameters are described below in Table 4.1. The system would be able to operate at low power levels due to the short maximum range requirements. This limited power level and range of the beacon would afford an element of discreetness when operated as far offshore as the mother vessel because the signal would probably be too weak to be detected by enemy receivers on the shore. Stripline technology will allow the transmitter to be built with printed circuits to hold down cost and size. Several receiver architectures are possible including one, two and three channel designs. The operating frequency has been chosen in the atmospheric transmission window for convenience and availability of off-the-shelf components. Receiver size and weight will be reduced at millimeter wave frequencies where the antenna would only need to be 0.6 meter in diameter. A design based on this approach should provide a highly favorable system for CATFAE.

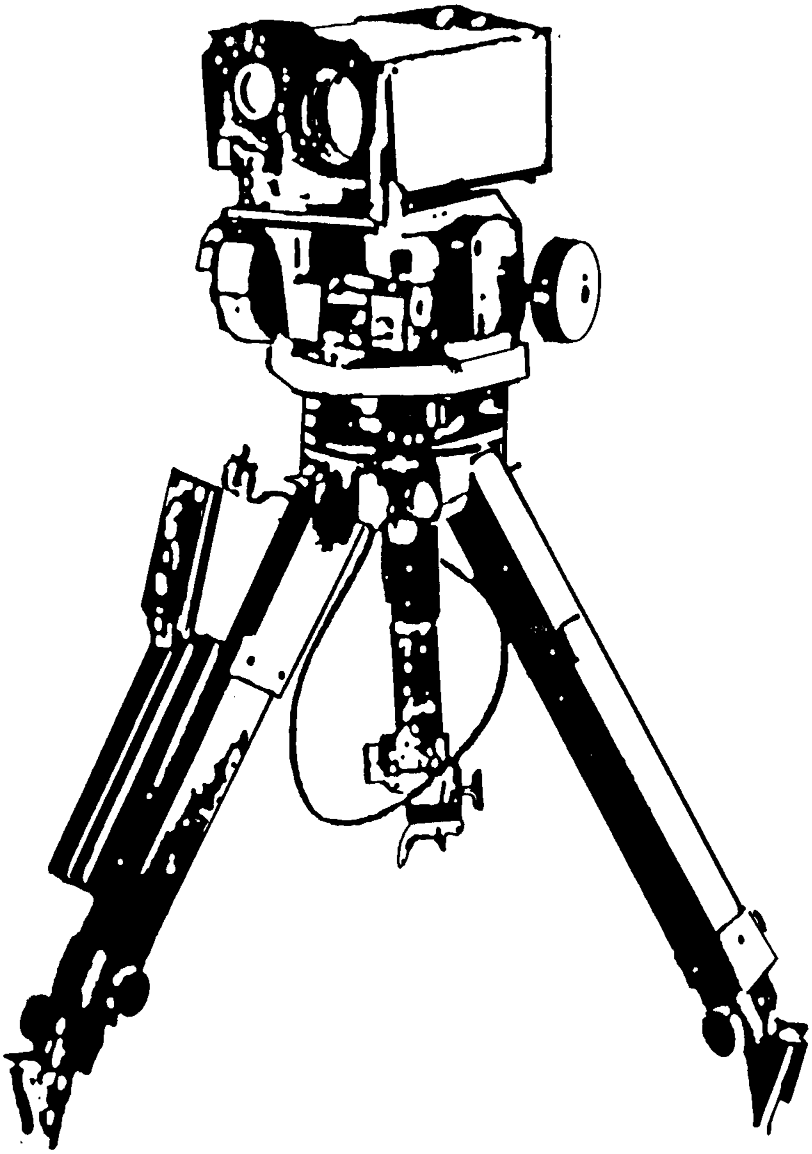

Figure 4.9 LP150E Laser Rangefinder [24].

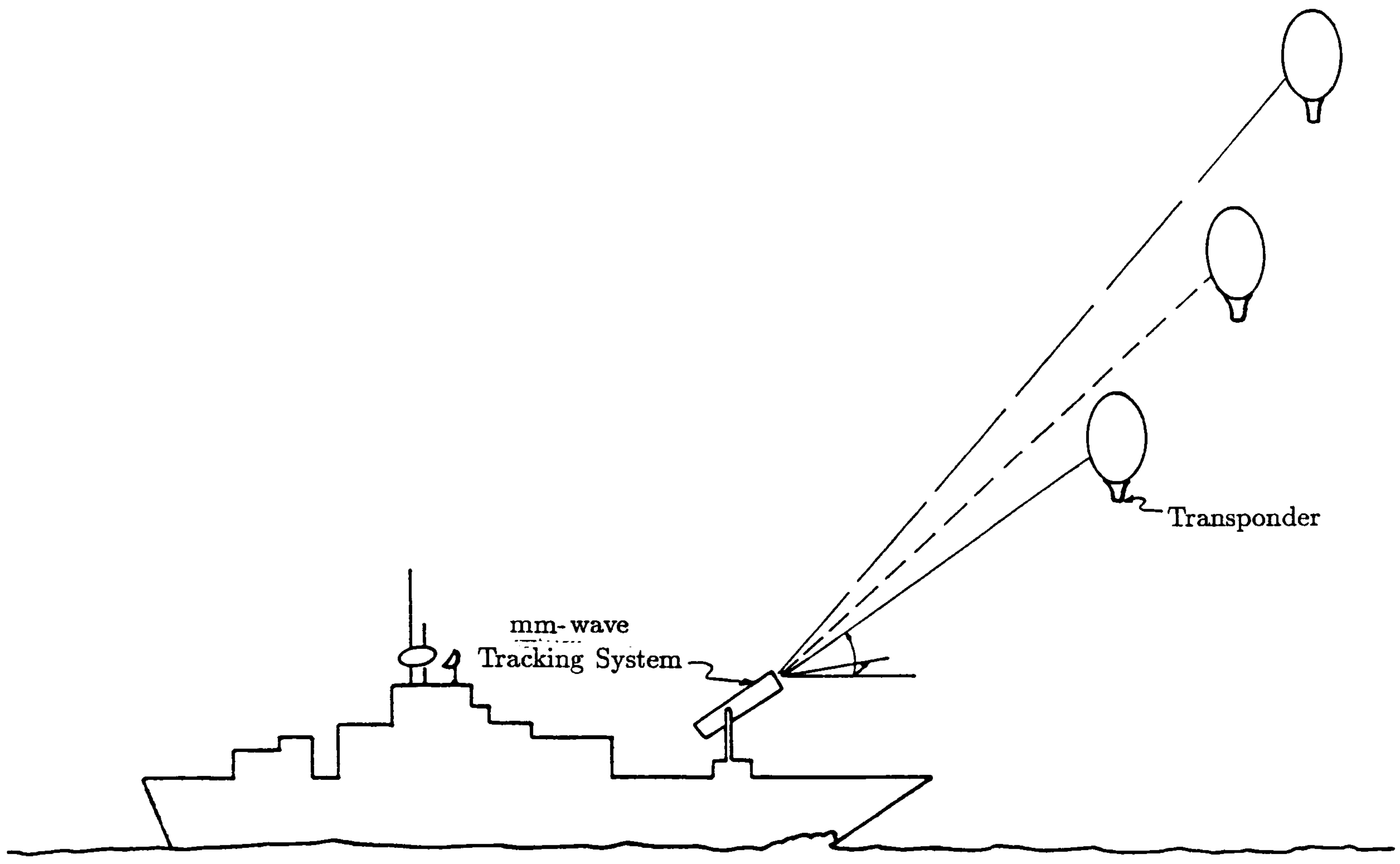

Figure 4.10 Shipboard wind profiling system.

Table 4.1 System characteristics of a mm-wave system to measure horizontal winds.

Transmitter

Frequency:	35 GHz
Power:	10 mW
Antenna Gain:	1
Transmit Losses:	< 3 dB

Receiver

Antenna Gain:	35 dB
Beamwidth:	$< 4^{o}$ az, el
Filter Bandwidth:	2 kHz
Noise Figure:	10 dB
Receiver Losses:	2 dB $\pm$ 1 dB mismatch losses

System design would depend on digital signal processing of received data to a 1 kHz sample rate to reduce the horizontal wind profile.

Proposed System Measurement Accuracies

Angular Measurements	$< \pm 0.4^{o}$
Range Rate	$< \pm 0.6$ m/s

4.4 Recommended Sensor

All three of the systems described above are viable systems for CATFAE operation. The mm-wave transponder balloon ranging system probably has the greatest advantage, however, in that it would be able to penetrate obscurations better than the others. Also, its off-the-shelf stripline technology would make it far less expensive than the LATAS, while at the same time giving it superior automation and accuracy capabilities compared to the Lasergage Rangefinder system.

The mm-wave receiver, processor and support hardware could be mounted to a carrier chassis which would allow portability. It could be placed aboard the ship in an appropriate location and secured for later use. Once the ship reached its destination, and the CATFAE vehicles were motoring or preparing for launch, the transponder balloon could be released. As it rises, the receiver would track the balloon (Figure 4.10) and calculate wind velocities. An interface with the ship's INS information would give the processor the data it would need regarding the ship's motion if warranted. Given the data, the processor could compute the balloon's motion relative to the inertial frame, and hence the wind profile. The wind data could then be provided to the FCS controller for input. The data passed to the FCS could be a complete wind profile, or a reduced downrange and crossrange data pair such that the log profile assumed in the FCS would be an adequate "effective" wind profile. Armed with this data, the CATFAE could proceed on its mission with forehand knowledge of the wind.

5.0 ERROR ANALYSIS

This section takes a look at the possible error sources when using the mm-wave transponder system, and attempts to reflect the impact of such error in the accuracy of the wind profile measurement. The error sources and their potential magnitudes are first identified, and then an example scenario is used to study the significance of the identified error.

Basically speaking, there are three places where error could manifest itself in measuring the wind profile. These are the range, the elevation angle, and the azimuthal angle measurements.

The mm-wave specifications shown in Table 4.1 show that the range rate measurement is accurate to $\pm$ 0.6 m/s, and the angular measurements are accurate to $\pm$ 0.4 degrees. This will be accepted as the maximum errors associated with each measurement.

5.1 Example Profile

This part of the section gives an example case of a wind profile generated by a simple log function in the x-direction and a simple constant in the y-direction. The example profile is arbitrary and is used here to examine the effect of the predicted error on the accuracy of wind measurements using the mm-wave transponder system. It will represent the "true" wind, or the wind which is actually being measured. The error bands will reflect the possible wind profiles which could be seen by the mm-wave system based on the assumed errors.

5.2 Case Scenario

- Mother ship speed set at 0 m/s
- Cross wind set at constant 1 m/s
- Down range log profile set at $u/u_* = (\frac{1}{\kappa})\ \ell n\ ((z + z_0)/z_0)$

  κ = von Karman constant = 0.40

  u_* = friction velocity = 0.35 m/s arbitrarily

  z_0 = surface roughness = 0.001 m for open sea

- Balloon rise rate = 5 m/s arbitrarily
- Measurement time interval = 10 sec

The equations used to derive the profiles from the scenario data are shown in Table 5.1. Table 5.2 lists some of the variables and calculated intermediate values needed to derive the wind profile from the data above. X_b and Y_b are the relative distances in the x and y directions of the balloon from the receiver, RR is the Range Rate as measured by the transponder, and α and θ are the measured elevation and azimuthal angles. Table 5.3 lists the x-component wind profile generated by the example data above. Also given are the minimum and maximum velocity values obtainable by "optimizing" the greatest possible combination of the error predictions described previously. That is, in order to predict the greatest possible velocity component for a particular time interval, the distance traveled by the balloon during the interval must be maximized. Note that by combining minimized angle errors with maximized range rate error, x is maximized, and so on.

Figure 5.1 shows the x-component generated profile plotted between the respective minimum and maximum error bands, as represented in Table 5.3. It can be seen that the percent error becomes less as altitude, or more accurately range, increases. The profile error is on the order of 5.5% at the largest range achieved in this case, whereas at the low altitude level, the error is 6.8%. This kind of accuracy is quite reasonable. Since these error profiles constitute "optimized" or maximized error, it may be of interest to see what "realistic" error may look like.

In order to demonstrate that the error bands calculated above are extreme, 20 simulated x-component profiles were generated for the wind profile defined in the example. The errors imposed on the range rate, elevation angle, and azimuthal angle were chosen randomly within the error range predicted for each data item. That is, for each range rate measurement, each elevation measurement, and each azimuth measurement, a random error of $\pm$ 0.6 m/s, $\pm 0.4^o$, and $\pm 0.4^o$ was imposed by a Microsoft BASIC randomizing program. These 20 profiles include the predicted error, but the error is no longer "optimized" for greatest composite error.

Table 5.1 Equations used to derive wind profiles.

Measured Data

$$R = \text{range from receiver to transponder}$$
$$RR = \text{Range Rate measured by transponder}$$
$$\alpha = \text{elevation angle}$$
$$\theta = \text{azimuthal angle}$$
$$t = \text{time (zeroed at balloon release)}$$

Intermediate Calculations

$$X_b = \text{distance of balloon from ship in x-direction}$$
$$= R * cos(\alpha) * cos(\theta)$$
$$Y_b = \text{distance of balloon from ship in y-direction}$$
$$= R * cos(\alpha) * sin(\theta)$$
$$X = \text{x-distance balloon traveled during interval}$$
$$= X_b(i) - X_b(i-1)$$
$$Y = \text{y-distance balloon traveled during interval}$$
$$= Y_b(i) - Y_b(i-1)$$

Profile Data

$$W_x = \text{down range velocity}$$
$$= RR * cos(\alpha) * cos(\theta)$$

Table 5.4 shows the generated "true" profile data along with the mean profile data averaged over all 20 simulations, as well as the standard deviation. This gives a representative "realistic" error bound.

Table 5.2 Example case: input values used to derive the wind profile.

TIME (sec)	HEIGHT (m)	X_b (m)	Y_b (m)	R(m)	RR (m/s)	$\alpha(^\circ)$	$\theta(^\circ)$
0	0	0	0	0	0	0	0
10	50	89	10	102.2	10.2	29.3	6.2
20	100	187	20	212.8	11.6	28.0	6.2
30	150	290	30	327.4	11.46	27.3	5.7
40	200	395	40	444.6	11.72	26.7	5.9
50	250	503	50	563.8	11.92	26.3	5.7

Table 5.3 Example case: x-component wind profile.

TIME (sec)	HEIGHT (m)	W_x (m/s)		
		MIN	MEAN	MAX
0	0	0		
10	50	8.3	8.8	9.4
20	100	9.1	9.7	10.3
30	150	9.6	10.1	10.7
40	200	9.8	10.4	11.0
50	250	10.1	10.6	11.2

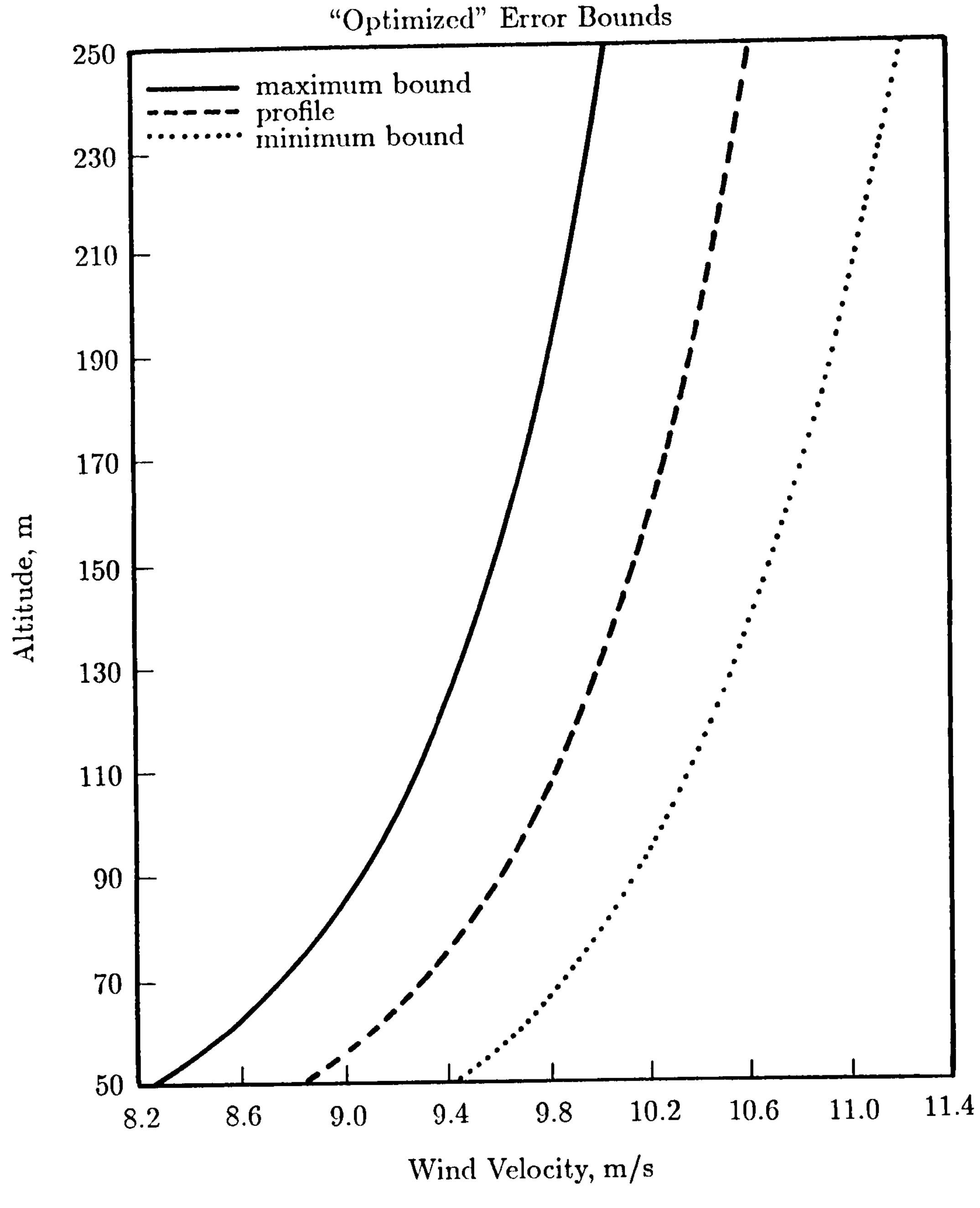

Figure 5.1 mm-wave profile error bounds.

Table 5.4 Realistic error bounds for wind profiles.

HEIGHT z (m)	ACTUAL PROFILE (m/s)	RANDOM AVG. (m/s)	σ
50	8.84	8.91	0.25
100	9.71	9.74	0.33
150	10.13	10.29	0.35
200	10.41	10.43	0.26
250	10.63	10.69	0.30

Figure 5.2 shows these profiles in a plot, with the optimized error bounds shown for comparison. It can be seen that the realistic error bounds did not even reach the optimized error bounds. The second standard deviation lies nearly upon the "optimized" bounds.

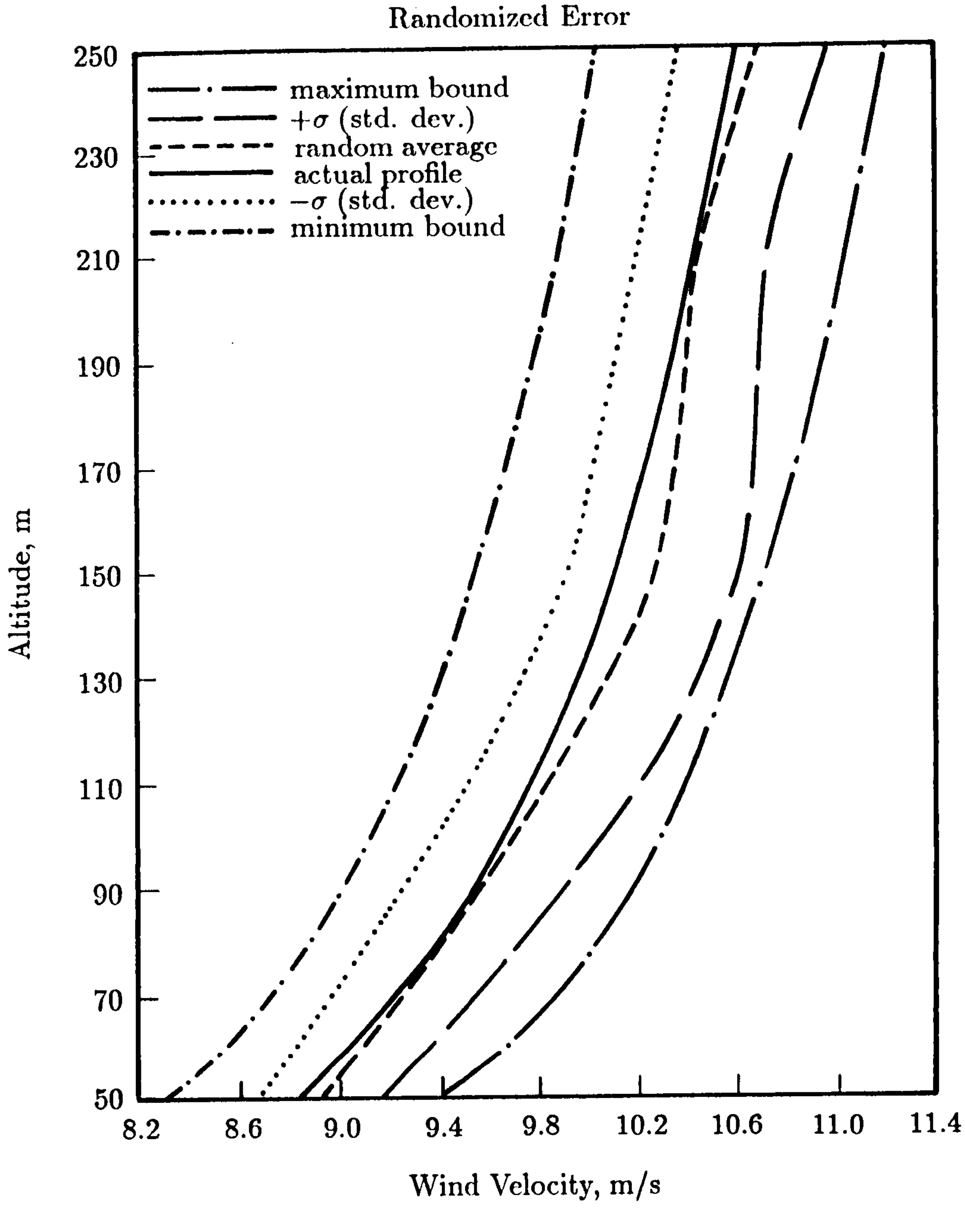

Figure 5.2 mm-wave error analysis.

6.0 STABILITY MODEL

The goal of this section is to present an adequate stable boundary layer model for simulation exercises of the CATFAE SEM. Considerable information on the behavior of the atmospheric boundary layer is available in the literature, encompassing both empirical data and numerical model simulation. Often it is useful and even wise to combine these empirical and analytical resources to enhance simulation accuracy. In this section, such a symbiotic model will be presented [25,26]. The model described below can be used as a subroutine in an existing computer program.

The data set utilized in formulating this stable wind field model relies mainly on the work of Clarke and Hess [27]. The data set is presented in Figures 6.1 and 6.2 in the form of contour maps of constant longitudinal and lateral wind speeds as a function of a nondimensional height $\hat{z}$, and the stability of the atmosphere expressed by the stability parameter μ [26]. The parameter μ is a non-dimensional stability parameter based on the stability length, L. By imposing a grid system on the contours, the wind fields were picked off and tabulated. An altered form of the data are tabulated in Appendix A [26]. These tabulated data were then coupled with a table look-up program subroutine to provide fast wind speed profile modeling. A listing of the subroutine is given in Appendix B [26].

Because of the generally recognized horizontal homogeneity of the planetary boundary layer, few mathematical models incorporate horizontal variation of the wind speed, and hence the wind model reported herein depends only on the vertical scale [26]. It should be borne in mind, however, that terrain features indigenous to each operation site, such as bluffs at the shoreline, can influence the spatial gradient of the wind speed horizontally and also introduce a possible vertical wind speed component. Fortunately, the open sea is relatively flat, and with a reasonably smooth shoreline, the wind model described in this section is expected to present a valid simulation.

Also, remember that this model does not consider mechanical forcing func-

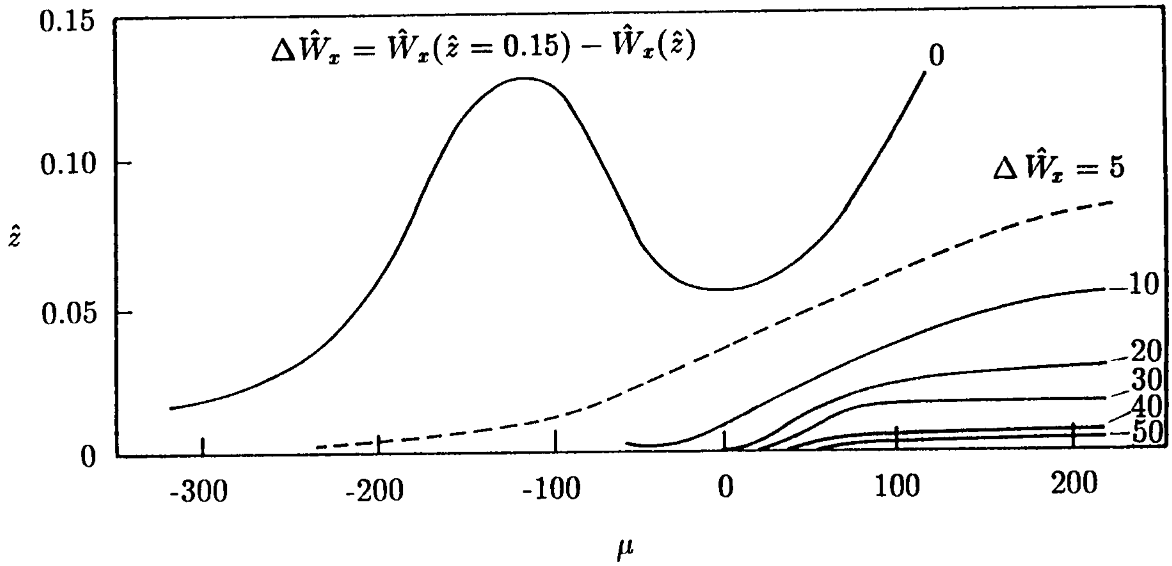

Figure 6.1 Longitudinal wind speeds [27].

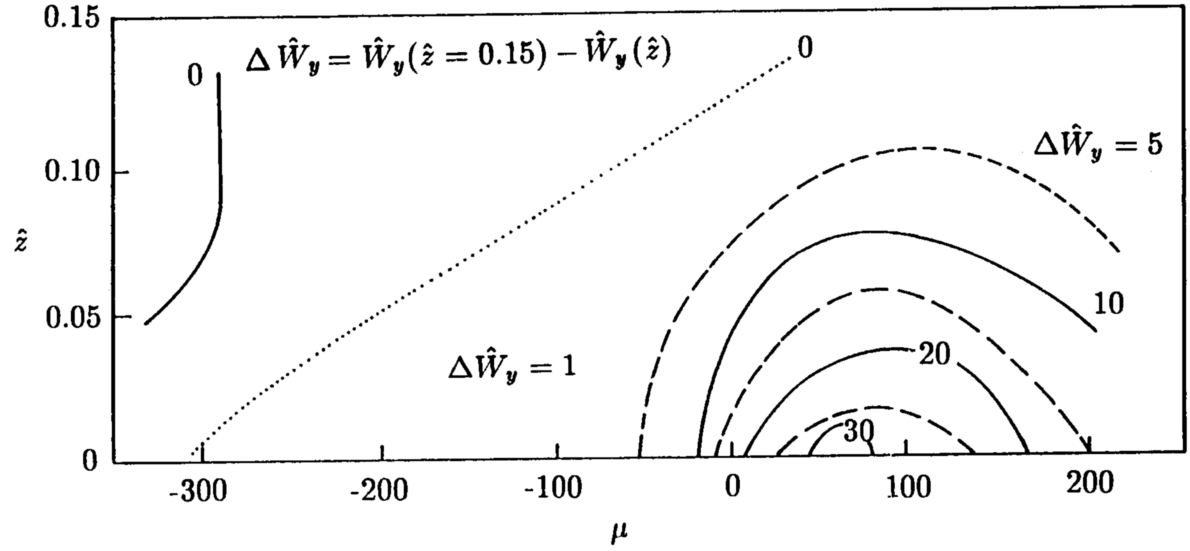

Figure 6.2 Lateral wind speeds (Clarke and Hess)[27].

tions which could drive a decoupled shear layer aloft. This model assumes that at some height $\widehat{z} = 0.15$, the wind profile reaches some sort of constant wind speed. Measuring the winds aloft is the only certain way of detecting a sheared profile.

6.1 Generation of the Data Tables

The data presented in Figures 6.1 and 6.2 are in a coordinate grid system with μ ranging from -333.34 to 216.67 in increments of $\Delta\mu = 16.67$, traversing left to right on the x-axis. The unusual increment size was chosen for convenience in extracting the data from the contour plots. Values of $\widehat{z}$ range from 0.001 to 0.15 in increments of $\Delta\widehat{z} = 0.0149$, increasing from bottom to top on the y-axis.

Because of the similarity and scaling laws used in reduction of the data, values of wind below $\widehat{z} = 0.001$ are not given. To establish the profile from $\widehat{z} = 0.0$ to $\widehat{z} = 0.001$, the log linear wind speed profile should be used (see Table 2.1). The stability parameter has been defined here [26]. For a description of the log linear profile, see reference [25]. The log profile defining the x-component of wind looks like

$$\widehat{W}_x(\widehat{z}) = \frac{1}{\kappa}[\ell n(Ro * \widehat{z} + 1) + (4.5 * \widehat{z} * \mu)/\kappa] \tag{1}$$

where $\mu \geq 0.0$.

Ro is the Rossby number and is a dimensionless measure of the relationship between inertial forces and coriolis force, indicating how important coriolis turning is to the flow. It is defined as

$$Ro = u_*/(f * z_0). \tag{2}$$

where f is the coriolis parameter which indicates the magnitude of the earth's rotational influence as a function of latitude.

Introducing the value of $\widehat{z} = 0.001$ into Equation (1),

$$\widehat{W}_x(\widehat{z} = 0.001) = \frac{1}{\kappa}[\ell n(0.001 Ro + 1) + 0.01125 * \mu] \tag{3}$$

gives the value of wind speed to which all of the tabulated longitudinal wind speeds are referenced. The value of the y-component of wind below $\widehat{z} = 0.001$ is defined as zero.

Although the Clarke and Hess curves include the range of unstable conditions, i.e. $-333.34 \leq \mu < 0.0$, strong wind shear is not normally associated with unstable boundary layers and hence no tabulated values of winds for this range of μ are given.

The tabulated longitudinal and lateral wind speeds $\widehat{W}_x(\widehat{z})$ and $\widehat{W}_y(\widehat{z})$ given in Appendix A were generated from the curve data in Figures 6.1 and 6.2 by the relationships

$$\widehat{W}_x(\widehat{z}) = \Delta\widehat{W}_x(\widehat{z} = 0.001) - \Delta\widehat{W}_x(\widehat{z}) + \widehat{W}_x(\widehat{z} = 0.001) \tag{4}$$

and

$$\widehat{W}_y(\widehat{z}) = \Delta\widehat{W}_y(\widehat{z}) - \Delta\widehat{W}_y(\widehat{z} = 0.001), \tag{5}$$

with

$$\widehat{W}_x(\widehat{z}) = W_x(\widehat{z})/u_* \tag{6}$$

and

$$\widehat{W}_y(\widehat{z}) = W_y(\widehat{z})/u_* \tag{7}$$

where $W_x(\widehat{z})$ and $W_y(\widehat{z})$ are the longitudinal and lateral wind speeds.

In tabulating the data given in Appendix A, the following methodology was used.

As mentioned before, the tabulated wind speeds are referenced to the value at $\widehat{z} = 0.001$, but the curve data are referenced to the value of the wind speed at $\widehat{z} = 0.15$. Therefore, the first step was to account for the differences in reference values. This was easily done by reading the curves to get the $\Delta\widehat{W}(\widehat{z} = 0.001)$ values. That is, the departure of the value at $\widehat{z} = 0.001$ from the value at $\widehat{z} = 0.15$.

The next step was to calculate the values of $\widehat{W}_x$ and $\widehat{W}_y$ at $\widehat{z} = 0.001$. The values were calculated for a range of $0.0 \leq \mu \leq 200$ in increments of 10. Equation (3) was used for the longitudinal calculation, and the lateral value was assumed zero as stated earlier. Note that to tabulate the data in a generic format, allowing the desired degrees of freedom in the range of input values, the range of Rossby numbers had to be accounted for in calculating $\widehat{W}_x(\widehat{z} = 0.001)$. This added another dimension to the tabular data. To encompass the desired input ranges, it was found that the Rossby number ranged from $1E+07$ order magnitude to $1E+03$ order magnitude. Therefore, five sets of x and y tables were derived, one for each Rossby number order of magnitude $(1E+07, 1E+06, 1E+05, 1E+04, 1E+03)$.

Finally, the $\Delta\widehat{W}(\widehat{z})$ values for the range of $0.001 < \widehat{z} \leq 0.15$ had to be read from the curves for x and for y. The increment of $\widehat{z}$ was chosen to be 0.01, with a couple of extra points near the lower end.

Once all of the terms of Equations (4) and (5) were determined for x and for y, the data tables of Appendix A could be generated, with the tables being a function of $\widehat{z}, \mu$, and Ro.

6.2 Description of Look-up Subroutine

In order to generate a stable boundary layer wind profile, a few variables must be specified which defines the atmospheric conditions of the scenario. These values are the friction velocity, u_*, the surface roughness, z_0, the Coriolis parameter, f, and the stability length parameter, L.

With this input, the dimensionless vertical scale, $\widehat{z}$, can be calculated for each discrete altitude of interest by the equation

$$\widehat{z} = (z * f)/u_* \tag{8}$$

and the Rossby number can be calculated by the equation

$$Ro = u_*/(f * z_0) \tag{9}$$

Also, the stability parameter, μ, can be calculated by

$$\mu = (\kappa * u_*)/(f * L) \tag{10}$$

where $\kappa = 0.4$ is the von Karman constant.

The first step of the subroutine is to choose which set of tables is to be used. The main subroutine, STB, does this. With the Rossby number known, the two sets of tables defined by the bracketing Rossby numbers are identified. For example, if $Ro = 5E + 04$, the W_x and W_y table sets for $Ro = 1E + 05$ and $Ro = 1E + 04$ are chosen. Then, subroutine INIT reads in all of the tabulated data. The next step is to run the interpolation subroutine for each set of Rossby tables selected. This subroutine is called WINDF. Interpolation is performed by an area-weighting method for the velocity at the elevation $\widehat{z}$ and for the stability condition μ. The area-weighting interpolation method is illustrated in Figure 6.3. The scheme calculates the velocity at the specified point by using the four nearest neighboring grid point values. The velocity at point $P(\widehat{z}, \mu)$ is given by

$$W_p = 1/A(A_1 * W_1 + A_2 * W_2 + A_3 * W_3 + A_4 * W_4) \tag{11}$$

where

$$A = A_1 + A_2 + A_3 + A_4 \tag{12}$$

Subroutine WINDF interpolates an x- and a y-velocity component for each $\widehat{z}$ specified, and is run twice (once for each Rossby magnitude).

Once the x and y-profiles are generated for each Ro magnitude, a linear interpolation can be carried out to resolve the two profiles into a single profile for the actual Rossby number of interest. Thus, an empirically based wind profile can be mathematically modeled for a specified atmospheric condition.

6.3 Example Profile

In an effort to clarify the use of the program, an example wind profile will be generated. The input for this example will be as follows:

Stability length, $L = 100$ m

Friction velocity, $u_* = 0.5$ m/s

Coriolis parameter, $f = 1E - 04\ s^{-1}$

Roughness factor, $z_0 = 0.1$ m

Given $\kappa = 0.4$ (von Karman constant), the Rossby number and stability parameters are first calculated, and are found to be

$$Ro = u_*/(f * z_0) = 0.5/(0.1 * 1E - 04) = 5E + 04 \tag{13}$$

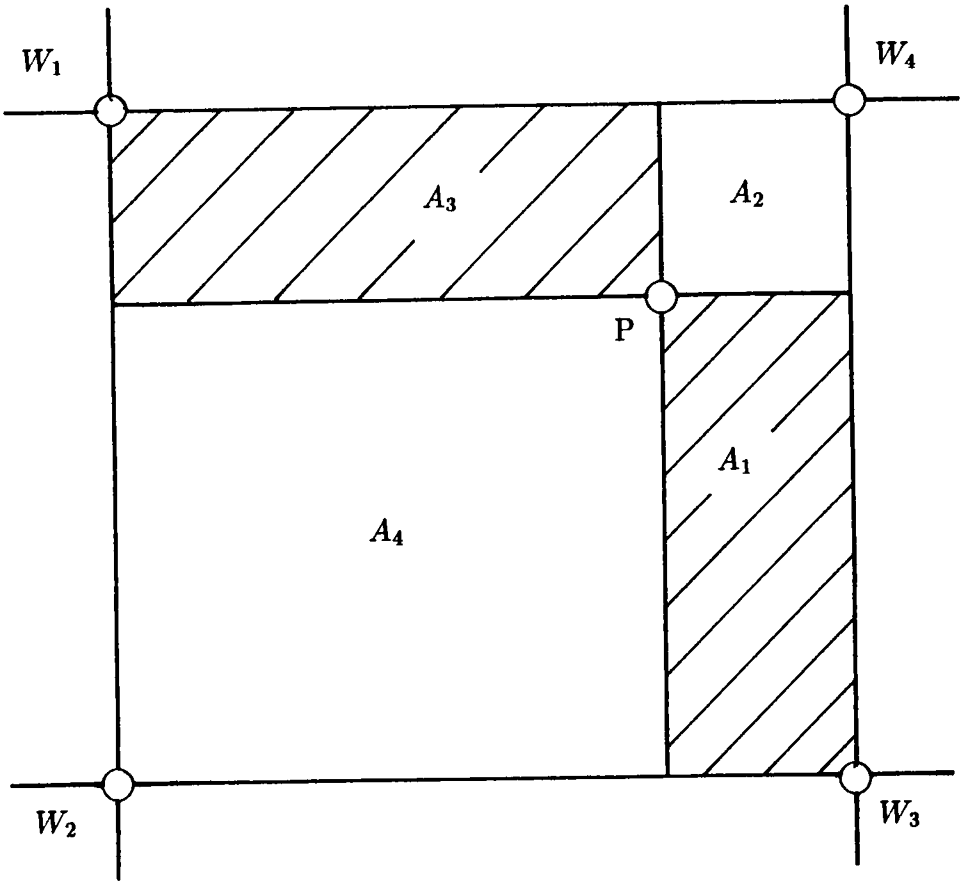

Figure 6.3 Area-weighting technique.

$$\mu = (\kappa * u_*)/(f * L) = (0.4 * 0.5)/(1E - 04 * 100) = 20 \quad (14)$$

The next step of the subroutine is to check the Ro and choose the appropriate tables. Since $Ro = 5E + 04$, Tables A.5 and A.6, and Tables A.7 and A.8 are the appropriate Tables.

Calculating $\hat{z}$ for say, $z = 100$ m, shows

$$\hat{z} = (z * f)/u_* = 100E - 04/0.5 = 0.02 \quad (15)$$

Looking up on Table A.5 under the column for $\mu = 20$ and the row for $\hat{z} = 0.02$ yields $\widehat{W}_x(\hat{z} = 0.02) = 30$. In turn,

$$W_x(z = 100 \text{ m}) = \widehat{W}_x(\hat{z} = 0.02) * u_* = 30 * 0.5 = 15 \text{ m/s} \quad (16)$$

Following this procedure for a variety of heights, and consulting Table A.6 for the y-components yields the data listed in Table 6.1 below.

Table 6.1 Example profile ($R_o = 10^5$).

HEIGHT z	HEIGHT $\hat{z}$	W_x (m/s)	W_y (m/s)
50	0.01	11.15	-1.0
100	0.02	15.0	-2.2
150	0.03	16.15	-3.6
200	0.04	17.2	-4.6
250	0.05	18.4	-5.45

Consulting the data in Tables A.7 and A.8 in the same manner as above yields the data listed in Table 6.2 below.

Table 6.2 Example profile ($R_o = 10^4$).

HEIGHT z	HEIGHT $\hat{z}$	W_x (m/s)	W_y (m/s)
50	0.01	11.15	-1.0
100	0.02	15.0	-2.2
150	0.03	16.15	-3.6
200	0.04	17.2	-4.6
250	0.05	18.4	-5.45

Finally, linearly interpolating between Table 6.1 and Table 6.2 yields the data in Table 6.3. This data is plotted in Figure 6.4.

Table 6.3 Example profile (linear interpolation).

HEIGHT z	HEIGHT $\hat{z}$	W_x (m/s)	W_y (m/s)
50	0.01	8.25	-1.0
100	0.02	12.1	-2.2
150	0.03	13.25	-3.6
200	0.04	14.3	-4.6
250	0.05	15.5	-5.45

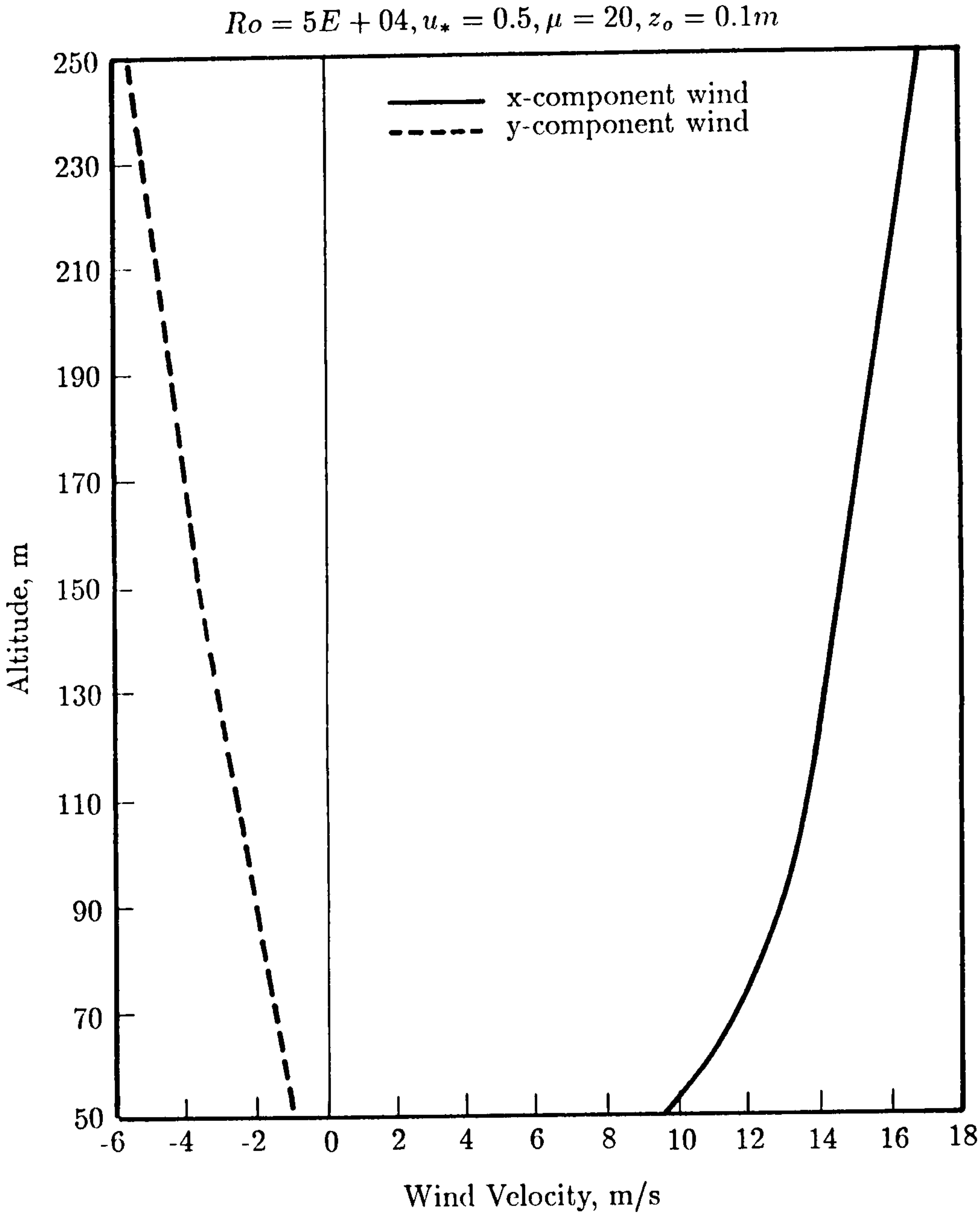

Figure 6.4 Example model generated profile.

7.0 CONCLUDING SUMMARY

The current design of the CATFAE wind sensor was shown in this thesis to be inadequate for the needs of the CATFAE program. The wind sensor obtains data in a dynamic boundary layer and uses this information to predict winds at altitude using a simple, 2-parameter, logarithmic wind model. As the amphibious assault vehicle bobs in the waves on its way toward the shore, the sensor makes measurements of an ambiguous local variation of wind in the downstream and cross-stream directions. The sensor has no way to account for windshear or inversion layers. In fact, the inferred wind profile used in the FCS algorithm could be so dramatically different from the actual wind that it could even be in the wrong direction.

For the successful operation of the CATFAE system, it is therefore necessary to measure the actual existing wind profile at the time when the CATFAE rounds are launched. Such a measurement could be taken either from the amphibious assault vehicle or aboard the mother ship prior to the CATFAE amphibious vehicle launch. Several wind measurement schemes were investigated as possible alternatives to the existing CATFAE wind measurement system. For example, it was shown that using a mm-wave transponder balloon ranging system, a sufficiently accurate profile could be available for FCS input. In an attempt to minimize FCS hardware and software impact, a true wind profile could be reduced to a CATFAE specific "effective" wind composed of a downrange and a crossrange component which, when utilized by the FCS, would yield a profile resulting in reasonable fuse time calculations. Several other wind measurement schemes were also discussed which can potentially improve the current wind measurement capabilities of the CATFAE system. It is recommended that these, and perhaps other, systems be seriously considered as potential alternates to the present wind measurement system.

Also discussed in this thesis was the advantage of using an empirically based wind model to enhance the predictive capabilities of the SEM, which does not currently employ an effective wind model. The recommended empirical model, incorporated into subroutines to be developed will take into account the effects of stability and surface roughness on wind predictions. Implementation of these subroutines into the SEM will therefore provide a better representation of wind effects than presently available models.

REFERENCES

1. Fitzgibbon, S., and P. Sexton, "Atmospheric Turbulence Effects on the Trajectory of a Low Altitude Parachute Deploying Projectile by Simulation and Testing", Presentation at AIAA 27th Aerospace Sciences Meeting, January 9-12, 1989, Reno, NV.

2. Davenport, A.G., "The Relationship of Wind Structure to Wind Loading", National Physical Laboratory, Symposium No. 16, Wind Effects on Buildings and Structures, Her Majesty's Stationery Office, London, 1965, pp. 54-102.

3. Frost, W., and C.F. Shieh, "Guidelines for Siting WECS Relative to Small/Scale Terrain Features", Final Report under Prime Contract No. EY-76-C-06-2443, U.S. Dept. of Energy, Office of Solar Power Applications, December 1981.

4. Sisterson, D.L., and P. Frenzen, "Noctural Boundary-Layer Wind Maxima and the Problem of Wind Power Assessment", Env. Sci. and Tech., 1978, 12:218.

5. Proceedings of the Fourth Symposium on Turbulence, Diffusion, and Air Pollution of the American Meteorological Society, January 15-18, 1979, Reno, NV.

6. Proceedings of the Joint Conference on Applications of Air Pollution Meteorology, sponsored by the American Meteorological Society and the Air Pollution Control Association, November 29 - December 2, 1977, Salt Lake City, UT.

7. Chang, L.P., et al., "Development of a Two Dimensional Finite-Element PBL Model and Two Preliminary Model Applications", Monthly Weather Review, Vol. 110, Dec. 1982, p. 2025-2037.

8. Martin, C. L. III, "CATFAE Fire Control System Wind Sensor Interface Specification", USMC DWG # 845029A3530, September 6, 1985 (Rev. Jan. 8, 1986).

9. Aggarwal, S.K., et al., "A Study of Atmospheric Structures Using SODAR in Relation To Land and Sea Breezes", Boundary Layer Meteorology, Vol. 18, June 1980, p. 361-371.

10. Bacci, P., et al., "Acoustic Sounding of Land and Sea Breezes", Boundary Layer Meteorology, Vol. 28, Jan-Feb. 1984, p. 187-192.

11. Jury, M, and G. Spencer-Smith, "Doppler Sounder Observations of Trade Winds and Sea Breezes Along the African West Coast Near 34^o S, 19^o E", Boundary Layer Meteorology, Vol. 44, No. 4, Sept. 1988, p. 373-405.

12. Mastrontonio, G., and G. Fiocco, "Accuracy of Wind Velocity Determinations With Doppler SODARS", Journal of Applied Meteorology, Vol. 21, June 1982, p. 823-830.

13. Finkelstein, P.L., et al., "Comparison of Wind Monitoring Systems. Part II: Doppler SODARS", Journal of Atmospheric and Oceanic Technology, Vol. 3, Dec. 1986, p. 594-604.

14. Ecklund, W., D.A. Carter, B.B. Balsley, "A UHF Wind Profiler For The Boundary Layer: Brief Description And Initial Results", Submitted to Journal of Atmospheric and Oceanic Technology, Aeronomy Laboratory, National Oceanic and Atmospheric Administration, Boulder, CO, 1988.

15. Ecklund, W.L., D.A. Carter, et al., "Recent Field Tests of a Lower Tropospheric Wind Profiler", submitted to Radio Science, Aeronomy Laboratory, National Oceanic and Atmospheric Administration, Boulder, CO, May 1989.

16. Foord, R., and J.M. Vaughan, "Wind Sensing Using A Conical Scanned CO_2 Laser Doppler System", Royal Signals and Radar Establishment, 1987.

17. Woodfield, A.A., and J.M. Vaughan, "Airspeed and Wind Shear Measurements With an Airborne CO_2 Continuous Wave Laser", Technical Report 83061, Royal Aircraft Establishment, July 1983.

18. FWG Associates, Inc., "Preliminary Assessment of America II LIDAR Wind Shift Detector", Contractor Report, Aug. 6, 1985.

19. Readings, C.J., and H.E. Butler, "The Measure of Atmospheric Turbulence From a Captive Balloon", Meteorological Magazine, Vol. 101, Oct. 1972, p. 286-298.

20. Jasperson, W.H., "The Limiting Accuracy of Wind Profiles Obtained by Tracking Rising Balloons", Journal of Applied Meteorology, Vol. 21, June 1982, p. 816-822.

21. Ground Defense International, No. 59, Dec. 1979.

22. Avimo, Ltd./Ferranti, Ltd., Hand Held Laser Rangefiner Product Information and Specification, Ferry Road, Edinburgh EH5 2XS, Scotland.

23. British Defense Equipment Catalogue, 12th ed., 1980.

24. LASERGAGE Limited, LASERGAGE Product Information, LP150 Laser Rangefinder, Croydon CRO 9XS, England.

25. Frost, W. and D.W. Camp, "Wind Shear Modeling for Aircraft Hazard Definition", Contractor Interim Report (# FAA-RD-77-36) for U.S. Department of Transportation, FAA Systems Research and Development Service, Washington, D.C. 20590, March 1977.

26. Frost, W., D. W. Camp, and S. T. Wang, "Wind Shear Modeling for Aircraft Hazard Definition", Contractor Final Report (# FAA-RD-78-3) for U.S. Department of Transportation, FAA Systems Research and Development Service, Washington, D.C. 20590, Feb. 1978.

27. Clarke, R.H. and G. G. Hess, "Geostrophic Departure and the Functions A and B of Rossby Number Similarity Theory", Boundary Layer Meteorology, 7(1974), pp. 267-287.

APPENDICES

APPENDIX A - TABULATED DATA

This appendix contains the tabulated data interpolated from the extensive measurement of wind speeds under varying conditions of stability reported by Clarke and Hess [27].

The tabulated values are the longitudinal and lateral wind speeds $\widehat{W}_x(\widehat{z}) = W_x(\widehat{z})/u_*$ and $\widehat{W}_y(\widehat{z}) = W_y(\widehat{z})/u_*$ for neutral and stable boundary layers for values of μ ranging from 0 to 200 in increments of $\Delta\mu = 10$, and for values of $\widehat{z}$ ranging from 0.001 to 0.15 in increments of 0.01. Five sets of tables are given, one for each Rossby number order of magnitude between 10^7 and 10^3, inclusively.

The data stored on disk and used in the look-up routine given in Appendix B was converted to $\widehat{W}_x$ and $\widehat{W}_y$ from the Clarke and Hess curves by using the relationships [26]

$$\widehat{W}_x(\widehat{z}) = \Delta\widehat{W}_x(\widehat{z} = 0.001) - \Delta\widehat{W}_x(\widehat{z}) + \widehat{W}_x(\widehat{z} = 0.001)$$

and

$$\widehat{W}_y(\widehat{z}) = \Delta\widehat{W}_y(\widehat{z}) - \Delta\widehat{W}_y(\widehat{z} = 0.001)$$

where

$$\widehat{W}_x(\widehat{z} = 0.001) = (1/\kappa)\ (\ell n(0.001Ro + 1) + 0.01125\mu)$$

To extend the tables to values of $\widehat{z} < 0.001$, wind speeds can be computed from

$$\widehat{W}_x(\widehat{z}) = (1/\kappa)\ (\ell n(Ro\widehat{z} + 1) + 4.5(\widehat{z}\mu)/k) \quad \mu \geq 0,\ 0 \leq \widehat{z} \leq 0.001$$

and

$$\widehat{W}_y(\widehat{z}) = 0.0$$

The data listed in this appendix is in the format of a Lotus file. To use the data in the look-up routine, it must be written into a file in the correct format. The format can be found by referring to the READ statements of the subroutine INIT shown in Appendix B.

From these tables the user can construct wind speed profiles for given values of L, u_*, z_0, and f. Note that $\hat{z} = (z * f)/u_*$, $Ro = u_* \,/\, (z_0 * f)$ and $\mu = (\kappa * u_*) \,/\, (f * L)$.

Table A.1 Longitudinal wind speed, $\widehat{W}_x$, $Ro = 1E+07$.

μ	0	10	20	30	40	50	60	70	80	90	100	110	120	130	140	150	160	170	180	190	200
$\widehat{z}$	$\widehat{W}_x$																				
0.15	42.0	46.5	51.2	56.3	60.1	63.4	66.1	68.8	71.5	73.8	75.8	77.3	78.6	79.5	80.4	81.2	81.5	81.8	82.1	82.4	82.7
0.14	42.0	46.5	51.2	56.3	60.1	63.4	66.1	68.8	71.5	73.8	75.8	77.3	78.6	79.4	80.2	81.0	81.1	81.3	81.6	81.8	82.1
0.13	42.0	46.5	51.2	56.3	60.1	63.4	66.1	68.8	71.5	73.8	75.8	77.3	78.4	79.1	79.8	80.5	80.6	80.7	81.0	81.3	81.5
0.12	42.0	46.5	51.2	56.3	60.1	63.4	66.1	68.8	71.5	73.8	75.8	77.1	78.2	78.6	79.2	79.7	79.9	80.1	80.4	80.7	80.9
0.11	42.0	46.5	51.2	56.3	60.1	63.4	66.1	68.8	71.5	73.8	75.8	76.9	77.7	78.0	78.6	79.3	79.4	79.5	79.7	79.9	80.2
0.10	42.0	46.5	51.2	56.3	60.1	63.4	66.1	68.8	71.5	73.8	75.5	76.4	77.1	77.4	78.0	78.8	78.8	78.9	78.9	79.1	79.4
0.09	42.0	46.5	51.2	56.3	60.1	63.4	66.1	68.8	71.4	73.3	74.9	75.8	76.5	76.8	77.4	78.2	78.2	78.2	78.1	78.3	78.6
0.08	42.0	46.5	51.2	56.3	60.1	63.4	65.9	68.2	70.3	72.0	73.5	74.6	75.4	75.9	76.4	77.1	77.1	77.2	77.1	77.2	77.3
0.07	42.0	46.5	51.2	56.3	59.9	62.7	65.0	67.1	69.0	70.6	72.1	73.2	74.1	74.4	75.0	75.7	75.7	75.7	75.7	75.8	75.8
0.06	41.9	46.4	51.0	56.1	59.2	61.4	63.4	65.5	67.6	69.2	70.7	71.8	72.5	72.6	73.2	74.1	73.9	73.8	73.9	74.0	74.2
0.05	39.9	43.9	48.3	53.1	56.6	59.3	61.4	63.5	65.5	67.2	68.7	69.8	70.6	70.7	71.3	72.1	71.9	71.6	71.4	71.2	71.1
0.04	37.9	41.8	45.9	50.6	54.0	56.9	59.0	60.9	62.7	64.0	65.2	66.8	66.9	66.9	67.3	68.1	68.0	67.9	67.8	67.7	67.7
0.03	35.9	39.7	43.8	48.2	51.3	53.8	55.8	57.5	58.6	59.4	60.0	60.9	61.5	61.2	61.6	62.4	62.6	62.9	63.1	63.3	63.5
0.02	33.9	37.7	41.5	45.0	46.3	46.5	46.8	47.1	47.2	48.3	50.0	51.3	52.3	52.9	53.6	54.5	54.8	55.0	55.3	55.6	55.8
0.01	29.1	31.5	33.8	35.8	36.2	35.9	35.8	35.7	35.7	36.5	37.9	38.9	39.8	40.5	41.1	41.7	42.0	42.3	42.6	42.9	43.1
0.005	25.7	27.0	28.1	29.2	29.5	29.5	29.7	29.8	29.9	30.4	31.2	31.8	32.4	32.8	33.2	33.7	34.0	34.3	34.5	34.8	35.1
0.001	23.0	23.3	23.6	23.9	24.1	24.4	24.7	25.0	25.3	25.6	25.8	26.1	26.4	26.7	27.0	27.2	27.5	27.8	28.1	28.4	28.7

Table A.2 Lateral wind speed, $\widehat{W}_y$, $Ro = 1E+07$.

μ	0	10	20	30	40	50	60	70	80	90	100	110	120	130	140	150	160	170	180	190	200
$\widehat{z}$	$\widehat{W}_y$																				
0.15	-18.0	-20.4	-22.9	-25.6	-28.7	-32.0	-31.4	-30.7	-29.8	-28.9	-28.0	-26.8	-25.8	-25.2	-24.2	-23.0	-21.8	-20.5	-19.1	-17.2	-15.0
0.14	-17.4	-19.8	-22.3	-24.9	-28.0	-31.2	-30.6	-29.8	-28.9	-27.9	-27.0	-25.8	-24.7	-24.2	-23.3	-22.2	-21.1	-19.8	-18.4	-16.5	-14.3
0.13	-17.1	-19.4	-21.7	-24.2	-27.2	-30.4	-29.7	-28.9	-28.0	-27.0	-26.1	-24.8	-23.8	-23.3	-22.4	-21.4	-20.2	-19.0	-17.6	-15.7	-13.6
0.12	-17.0	-19.1	-21.2	-23.4	-26.3	-29.5	-28.8	-28.1	-27.1	-26.1	-25.2	-23.9	-22.9	-22.4	-21.6	-20.5	-19.3	-18.0	-16.6	-14.8	-12.8
0.11	-16.3	-18.4	-20.5	-22.8	-25.3	-28.3	-27.6	-26.7	-25.6	-24.6	-23.7	-22.5	-21.5	-21.0	-20.0	-18.8	-17.9	-16.9	-15.6	-13.8	-11.8
0.10	-15.5	-17.8	-19.9	-21.8	-24.3	-27.2	-26.2	-25.2	-24.0	-23.0	-22.1	-21.0	-20.0	-19.6	-18.6	-17.3	-16.6	-15.8	-14.6	-13.0	-11.1
0.09	-14.5	-17.1	-19.4	-20.9	-23.2	-25.9	-24.7	-23.5	-22.3	-21.3	-20.4	-19.4	-18.5	-18.1	-17.1	-15.9	-15.3	-14.7	-13.8	-12.3	-10.5
0.08	-13.5	-15.5	-17.4	-18.9	-20.9	-23.2	-22.3	-21.4	-20.4	-19.6	-18.8	-17.8	-17.1	-16.7	-15.8	-14.6	-14.0	-13.3	-12.5	-11.2	-9.8
0.07	-12.1	-13.5	-15.0	-16.5	-18.6	-21.1	-20.3	-19.3	-18.0	-17.2	-16.5	-15.8	-15.3	-15.0	-14.2	-13.3	-12.7	-12.0	-11.3	-10.1	-8.7
0.06	-10.4	-11.3	-12.4	-13.9	-16.4	-19.4	-18.4	-17.2	-15.2	-14.3	-13.9	-13.5	-13.2	-13.0	-12.5	-11.9	-11.3	-10.7	-10.2	-8.9	-7.2
0.05	-8.7	-9.8	-10.9	-12.0	-14.2	-17.0	-15.9	-14.7	-13.3	-12.3	-11.5	-11.0	-10.7	-10.8	-10.5	-9.9	-9.7	-9.3	-8.6	-7.3	-5.6
0.04	-7.0	-8.1	-9.2	-10.2	-12.1	-14.5	-13.3	-12.1	-10.9	-9.9	-9.0	-8.4	-8.0	-8.1	-7.9	-7.7	-7.8	-7.6	-7.0	-5.7	-4.0
0.03	-5.3	-6.2	-7.2	-8.4	-10.0	-11.8	-10.6	-9.4	-8.2	-7.2	-6.3	-5.7	-5.2	-5.0	-5.0	-5.3	-5.6	-5.8	-5.5	-4.2	-2.4
0.02	-3.7	-3.9	-4.4	-5.4	-7.1	-9.1	-7.9	-6.8	-5.8	-4.9	-4.0	-3.1	-2.7	-3.1	-3.1	-3.0	-3.5	-3.8	-3.8	-2.8	-1.4
0.01	-1.8	-1.8	-2.0	-2.5	-3.6	-4.8	-4.1	-3.4	-2.9	-2.4	-1.8	-1.3	-1.0	-1.4	-1.4	-1.2	-1.6	-1.8	-1.9	-1.4	-0.6
0.005	-0.8	-0.8	-0.9	-1.1	-1.6	-2.1	-1.8	-1.5	-1.3	-1.0	-0.8	-0.6	-0.5	-0.6	-0.6	-0.5	-0.7	-0.8	-0.8	-0.6	-0.3
0.001	0.0	0.0	0.0	0.0	0.0	0.0	0.0	0.0	0.0	0.0	0.0	0.0	0.0	0.0	0.0	0.0	0.0	0.0	0.0	0.0	0.0

Table A.3 Longitudinal wind speed, $\widehat{W}_x$, $Ro = 1E+06$.

μ	0	10	20	30	40	50	60	70	80	90	100	110	120	130	140	150	160	170	180	190	200
$\widehat{z}$	$\widehat{W}_x$																				
0.15	36.3	40.7	45.4	50.5	54.4	57.7	60.4	63.0	65.7	68.0	70.1	71.6	72.8	73.7	74.6	75.5	75.8	76.1	76.3	76.6	76.9
0.14	36.3	40.7	45.4	50.5	54.4	57.7	60.4	63.0	65.7	68.0	70.1	71.6	72.8	73.6	74.4	75.2	75.3	75.5	75.8	76.1	76.4
0.13	36.3	40.7	45.4	50.5	54.4	57.7	60.4	63.0	65.7	68.0	70.1	71.5	72.7	73.3	74.0	74.7	74.3	74.9	75.2	75.5	75.8
0.12	36.3	40.7	45.4	50.5	54.4	57.7	60.4	63.0	65.7	68.0	70.1	71.4	72.4	72.9	73.4	74.0	74.1	74.3	74.6	74.9	75.2
0.11	36.3	40.7	45.4	50.5	54.4	57.7	60.4	63.0	65.7	68.0	70.1	71.1	71.9	72.2	72.8	73.5	73.6	73.8	73.9	74.2	74.4
0.10	36.3	40.7	45.4	50.5	54.4	57.7	60.4	63.0	65.7	67.9	69.8	70.7	71.4	71.6	72.2	73.0	73.1	73.1	73.2	73.4	73.7
0.09	36.3	40.7	45.4	50.5	54.4	57.7	60.3	63.0	65.7	67.6	69.1	70.0	70.7	71.1	71.7	72.4	72.4	72.4	72.4	72.6	72.8
0.08	36.3	40.7	45.4	50.5	54.4	57.7	60.1	62.5	64.5	66.2	67.7	68.8	69.7	70.1	70.7	71.3	71.4	71.4	71.4	71.4	71.5
0.07	36.3	40.7	45.4	50.5	54.1	57.0	59.2	61.4	63.2	64.9	66.3	67.5	68.3	68.7	69.2	69.9	69.9	69.9	70.0	70.0	70.0
0.06	36.1	40.6	45.3	50.3	53.5	55.7	57.7	59.7	61.8	63.5	65.0	66.0	66.7	66.9	67.5	68.4	68.2	68.1	68.1	68.3	68.4
0.05	34.1	38.2	42.5	47.4	50.8	53.6	55.6	57.7	59.8	61.5	62.9	64.1	64.9	65.0	65.6	66.4	66.1	65.9	65.6	65.5	65.4
0.04	32.1	36.0	40.1	44.8	48.3	51.1	53.2	55.2	56.9	58.3	59.4	60.5	61.2	61.1	61.6	62.4	62.3	62.2	62.0	62.0	61.9
0.03	30.1	34.0	38.0	42.5	45.6	48.1	50.0	51.7	52.8	53.6	54.3	55.2	55.7	55.5	55.9	56.7	56.9	57.1	57.3	57.6	57.8
0.02	28.1	32.0	35.7	39.2	40.5	40.7	41.0	41.3	41.4	42.5	44.2	45.5	46.6	47.1	47.9	48.7	49.0	49.3	49.5	49.8	50.1
0.01	23.3	25.8	28.1	30.0	30.5	30.2	30.1	30.0	29.9	30.8	32.2	33.2	34.1	34.7	35.3	36.0	38.3	36.5	36.3	37.1	37.4
0.005	20.0	23.2	22.4	23.4	23.8	23.8	23.9	24.0	24.1	24.7	25.5	26.1	26.6	27.0	27.5	27.9	28.2	28.5	28.8	29.1	29.3
0.001	17.2	17.5	17.8	18.1	18.3	18.6	18.9	19.2	19.5	19.8	20.1	20.4	20.6	20.9	21.2	21.5	21.8	22.1	22.3	22.6	22.9

Table A.4 Lateral wind speed, $\widehat{W}_y$, $Ro = 1E+06$.

μ	0	10	20	30	40	50	60	70	80	90	100	110	120	130	140	150	160	170	180	190	200
$\widehat{z}$	$\widehat{W}_y$																				
0.15	-18.0	-20.4	-22.9	-25.6	-28.7	-32.0	-31.4	-30.7	-29.8	-28.9	-28.0	-26.8	-25.8	-25.2	-24.2	-23.0	-21.8	-20.5	-19.1	-17.2	-15.0
0.14	-17.4	-19.8	-22.3	-24.9	-28.0	-31.2	-30.6	-29.8	-28.9	-27.9	-27.0	-25.8	-24.7	-24.2	-23.3	-22.2	-21.1	-19.8	-18.4	-16.5	-14.3
0.13	-17.1	-19.4	-21.7	-24.2	-27.2	-30.4	-29.7	-28.9	-28.0	-27.0	-26.1	-24.8	-23.8	-23.3	-22.4	-21.4	-20.2	-19.0	-17.6	-15.7	-13.6
0.12	-17.0	-19.1	-21.2	-23.4	-26.3	-29.5	-28.8	-28.1	-27.1	-26.1	-25.2	-23.9	-22.9	-22.4	-21.6	-20.5	-19.3	-18.0	-16.6	-14.8	-12.8
0.11	-16.3	-18.4	-20.5	-22.6	-25.3	-28.3	-27.6	-26.7	-25.6	-24.6	-23.7	-22.5	-21.5	-21.0	-20.0	-18.8	-17.9	-16.9	-15.6	-13.8	-11.8
0.10	-15.5	-17.8	-19.9	-21.8	-24.3	-27.2	-26.2	-25.2	-24.0	-23.0	-22.1	-21.0	-20.0	-19.6	-18.6	-17.3	-16.6	-15.8	-14.6	-13.0	-11.1
0.09	-14.5	-17.1	-19.4	-20.9	-23.2	-25.9	-24.7	-23.5	-22.3	-21.3	-20.4	-19.4	-18.5	-18.1	-17.1	-15.9	-15.3	-14.7	-13.8	-12.3	-10.5
0.08	-13.5	-15.5	-17.4	-18.9	-20.9	-23.2	-22.3	-21.4	-20.4	-19.6	-18.8	-17.8	-17.1	-16.7	-15.8	-14.6	-14.0	-13.3	-12.5	-11.2	-9.8
0.07	-12.1	-13.5	-15.0	-16.5	-18.6	-21.1	-20.3	-19.3	-18.0	-17.2	-16.5	-15.8	-15.3	-15.0	-14.2	-13.3	-12.7	-12.0	-11.3	-10.1	-8.7
0.06	-10.4	-11.3	-12.4	-13.9	-16.4	-19.4	-18.4	-17.2	-15.2	-14.3	-13.9	-13.5	-13.2	-13.0	-12.5	-11.9	-11.3	-10.7	-10.2	-8.9	-7.2
0.05	-8.7	-9.8	-10.9	-12.0	-14.2	-17.0	-15.9	-14.7	-13.3	-12.3	-11.5	-11.0	-10.7	-10.8	-10.5	-9.9	-9.7	-9.3	-8.6	-7.3	-5.6
0.04	-7.0	-8.1	-9.2	-10.2	-12.1	-14.5	-13.3	-12.1	-10.9	-9.9	-9.0	-8.4	-8.0	-8.1	-7.9	-7.7	-7.8	-7.6	-7.0	-5.7	-4.0
0.03	-5.3	-6.2	-7.2	-8.4	-10.0	-11.8	-10.8	-9.4	-8.2	-7.2	-6.3	-5.7	-5.2	-5.0	-5.0	-5.3	-5.6	-5.6	-5.5	-4.2	-2.4
0.02	-3.7	-3.9	-4.4	-5.4	-7.1	-9.1	-7.9	-6.8	-5.8	-4.9	-4.0	-3.1	-2.7	-3.1	-3.1	-3.0	-3.5	-3.8	-3.8	-2.8	-1.4
0.01	-1.8	-1.8	-2.0	-2.5	-3.6	-4.6	-4.1	-3.4	-2.9	-2.4	-1.8	-1.3	-1.0	-1.4	-1.4	-1.2	-1.6	-1.8	-1.9	-1.4	-0.6
0.005	-0.8	-0.8	-0.9	-1.1	-1.6	-2.1	-1.8	-1.5	-1.3	-1.0	-0.8	-0.6	-0.5	-0.6	-0.6	-0.5	-0.7	-0.8	-0.8	-0.6	-0.3
0.001	0.0	0.0	0.0	0.0	0.0	0.0	0.0	0.0	0.0	0.0	0.0	0.0	0.0	0.0	0.0	0.0	0.0	0.0	0.0	0.0	0.0

Table A.5 Longitudinal wind speed, $\widehat{W}_x$, $Ro = 1E + 05$.

μ / $\hat{z}$	0	10	20	30	40	50	60	70	80	90	100	110	120	130	140	150	160	170	180	190	200
	$\widehat{W}_x$																				
0.15	30.5	35.0	39.7	44.8	48.6	51.9	54.6	57.3	60.0	62.2	64.3	65.8	67.1	68.0	68.9	69.7	70.0	70.3	70.6	70.9	71.1
0.14	30.5	35.0	39.7	44.8	48.6	51.9	54.6	57.3	60.0	62.2	64.3	65.8	67.1	67.9	68.7	69.5	69.6	69.8	70.0	70.3	70.6
0.13	30.5	35.0	39.7	44.8	48.6	51.9	54.6	57.3	60.0	62.2	64.3	65.7	66.9	67.6	68.3	69.0	69.0	69.2	69.5	69.7	70.0
0.12	30.5	35.0	39.7	44.8	48.6	51.9	54.6	57.3	60.0	62.2	64.3	65.6	66.6	67.1	67.6	68.2	68.4	68.6	68.9	69.1	69.4
0.11	30.5	35.0	39.7	44.8	48.6	51.9	54.6	57.3	60.0	62.2	64.3	65.4	66.2	66.5	67.0	67.8	67.9	68.0	68.2	68.4	68.7
0.10	30.5	35.0	39.7	44.8	48.6	51.9	54.6	57.3	60.0	62.1	64.0	64.9	65.6	65.9	66.5	67.2	67.3	67.4	67.4	67.6	67.9
0.09	30.5	35.0	39.7	44.8	48.6	51.9	54.6	57.3	59.9	61.8	63.4	64.3	65.0	65.3	65.9	66.7	66.7	66.7	66.6	66.8	67.1
0.08	30.5	35.0	39.7	44.8	48.6	51.9	54.4	56.7	58.8	60.5	62.0	63.1	63.9	64.3	64.9	65.5	65.6	65.6	65.6	65.7	65.7
0.07	30.5	35.0	39.7	44.6	48.4	51.2	53.5	55.6	57.5	59.1	60.6	61.7	62.6	62.9	63.5	64.2	64.2	64.2	64.2	64.2	64.3
0.06	30.4	34.8	39.5	44.6	47.7	49.9	51.9	54.0	56.0	57.7	59.2	60.2	61.0	61.1	61.7	62.6	62.4	62.3	62.4	62.5	62.7
0.05	28.4	32.4	36.8	41.6	45.1	47.8	49.9	51.9	54.0	55.7	57.2	58.3	59.1	59.2	59.8	60.6	60.4	60.1	59.9	59.7	59.6
0.04	26.4	30.2	34.4	39.1	42.5	45.4	47.5	49.4	51.2	52.5	53.6	54.7	55.4	55.3	55.8	58.6	56.5	56.4	56.3	56.2	56.2
0.03	24.4	28.2	32.3	38.7	39.8	42.3	44.3	45.9	47.0	47.9	48.5	49.4	50.0	49.7	50.1	50.9	51.1	51.3	51.6	51.8	52.0
0.02	22.3	26.2	30.0	33.4	34.7	34.9	35.3	35.5	35.6	36.8	38.5	39.8	40.8	41.4	42.1	43.0	43.2	43.5	43.8	44.0	44.3
0.01	17.6	20.0	22.3	24.3	24.7	24.4	24.3	24.2	24.2	25.0	26.4	27.4	28.3	28.9	29.6	30.2	30.5	30.8	31.1	31.4	31.6
0.005	14.2	15.4	16.6	17.7	18.0	18.0	18.1	18.3	18.4	18.9	19.7	20.3	20.8	24.3	21.7	22.2	22.5	22.7	23.0	23.3	23.6
0.001	11.5	11.8	12.1	12.4	12.6	12.9	13.2	13.5	13.8	14.0	14.3	14.6	14.9	15.2	15.5	15.7	16.0	16.3	16.6	16.9	17.1

Table A.6 Lateral wind speed, $\widehat{W}_y$, $Ro = 1E + 05$.

μ / $\hat{z}$	0	10	20	30	40	50	60	70	80	90	100	110	120	130	140	150	160	170	180	190	200
	$\widehat{W}_y$																				
0.15	-18.0	-20.4	-22.9	-25.6	-28.7	-32.0	-31.4	-30.7	-29.8	-28.9	-28.0	-26.8	-25.8	-25.2	-24.2	-23.0	-21.8	-20.5	-19.1	-17.2	-15.0
0.14	-17.4	-19.8	-22.3	-24.9	-28.0	-31.2	-30.6	-29.8	-28.9	-27.9	-27.0	-25.8	-24.7	-24.2	-23.3	-22.2	-21.1	-19.8	-18.4	-16.5	-14.3
0.13	-17.1	-19.4	-21.7	-24.2	-27.2	-30.4	-29.7	-28.9	-28.0	-27.0	-26.1	-24.8	-23.8	-23.2	-22.4	-21.4	-20.0	-19.0	-17.4	-15.7	-13.6
0.12	-17.0	-19.1	-21.2	-23.4	-26.3	-29.5	-28.8	-28.1	-27.1	-26.1	-25.2	-23.9	-22.9	-22.4	-21.6	-20.5	-19.3	-18.0	-16.6	-14.8	-12.8
0.11	-16.3	-18.4	-20.5	-22.6	-25.3	-28.3	-27.6	-26.7	-25.6	-24.6	-23.7	-22.5	-21.5	-21.0	-20.0	-18.8	-17.9	-16.9	-15.6	-13.8	-11.8
0.10	-15.5	-17.8	-19.9	-21.6	-24.3	-27.2	-26.2	-25.2	-24.0	-23.0	-22.1	-21.0	-20.0	-19.6	-18.6	-17.3	-16.6	-15.8	-14.6	-13.0	-11.1
0.09	-14.5	-17.1	-19.4	-20.9	-23.0	-25.9	-24.7	-23.5	-22.3	-21.3	-20.4	-19.4	-18.5	-18.1	-17.1	-15.9	-15.3	-14.7	-13.8	-12.3	-10.5
0.08	-13.5	-15.5	-17.4	-18.9	-20.9	-23.2	-22.3	-21.4	-20.4	-19.6	-18.8	-17.8	-17.1	-16.7	-15.8	-14.6	-14.0	-13.3	-12.5	-11.2	-9.8
0.07	-12.1	-13.5	-15.0	-16.5	-18.6	-21.1	-20.3	-19.3	-18.0	-17.2	-16.5	-15.8	-15.3	-15.0	-14.2	-13.3	-12.7	-12.0	-11.3	-10.1	-8.7
0.06	-10.4	-11.3	-12.4	-13.9	-16.4	-19.4	-18.4	-17.2	-15.2	-14.3	-13.9	-13.5	-13.2	-13.0	-12.5	-11.9	-11.3	-10.7	-10.2	-8.9	-7.2
0.05	-8.7	-9.8	-10.9	-12.0	-14.2	-17.0	-15.9	-14.7	-13.3	-12.3	-11.5	-11.0	-10.7	-10.8	-10.5	-9.9	-9.7	-9.3	-8.6	-7.3	-5.6
0.04	-7.0	-8.1	-9.2	-10.2	-12.1	-14.5	-13.3	-12.1	-10.9	-9.9	-9.0	-8.4	-8.0	-8.1	-7.9	-7.7	-7.8	-7.6	-7.0	-5.7	-4.0
0.03	-5.3	-6.2	-7.2	-8.4	-10.0	-11.8	-10.6	-9.4	-8.2	-7.2	-6.3	-5.7	-5.2	-5.0	-5.0	-5.3	-5.6	-5.8	-5.5	-4.2	-2.4
0.02	-3.7	-3.9	-4.4	-5.4	-7.1	-9.1	-7.9	-6.8	-5.8	-4.9	-4.0	-3.1	-2.7	-3.1	-3.1	-3.0	-3.5	-3.8	-3.8	-2.8	-1.4
0.01	-1.8	-1.8	-2.0	-2.5	-3.6	-4.8	-4.1	-3.4	-2.9	-2.4	-1.8	-1.3	-1.0	-1.4	-1.4	-1.2	-1.6	-1.8	-1.9	-1.4	-0.6
0.005	-0.8	-0.8	-0.9	-1.1	-1.6	-2.1	-1.8	-1.5	-1.3	-1.0	-0.8	-0.6	-0.5	-0.6	-0.6	-0.5	-0.7	-0.8	-0.8	-0.6	-0.3
0.001	0.0	0.0	0.0	0.0	0.0	0.0	0.0	0.0	0.0	0.0	0.0	0.0	0.0	0.0	0.0	0.0	0.0	0.0	0.0	0.0	0.0

Table A.7 Longitudinal wind speed, $\widehat{W}_x$, $Ro = 1E+04$.

μ	0	10	20	30	40	50	60	70	80	90	100	110	120	130	140	150	160	170	180	190	200
$\hat{z}$	$\widehat{W}_x$																				
0.15	24.8	29.2	33.9	39.0	42.9	46.2	48.8	51.5	54.2	56.5	58.6	60.0	61.3	62.2	63.1	64.0	64.3	64.5	64.8	65.1	65.4
0.14	24.8	29.2	33.9	39.0	42.9	46.2	48.8	51.5	54.2	56.5	58.6	60.0	61.3	62.1	62.9	63.7	63.8	64.0	64.3	64.6	64.8
0.13	24.8	29.2	33.9	39.0	42.9	46.2	48.8	51.5	54.2	56.5	58.6	60.0	61.2	61.8	62.5	63.2	63.3	63.4	63.7	64.0	64.3
0.12	24.8	29.2	33.9	39.0	42.9	46.2	48.8	51.5	54.2	56.5	58.6	59.9	60.9	61.3	61.9	62.5	62.6	62.8	63.1	63.4	63.7
0.11	24.8	29.2	33.9	39.0	42.9	46.2	48.8	51.5	54.2	56.5	58.6	59.6	60.4	60.7	61.3	62.0	62.1	62.2	62.4	62.6	62.9
0.10	24.8	29.2	33.9	39.0	42.9	46.2	48.8	51.5	54.2	56.4	58.2	59.2	59.9	60.1	60.7	61.5	61.5	61.6	61.7	61.9	62.2
0.09	24.8	29.2	33.9	39.0	42.9	46.2	48.8	51.5	54.2	56.1	57.6	58.5	59.2	59.6	60.2	60.9	60.9	60.9	60.9	61.1	61.3
0.08	24.8	29.2	33.9	39.0	42.9	46.2	48.6	51.0	53.0	54.7	56.2	57.3	58.2	58.6	59.2	59.8	59.9	59.9	59.9	59.9	60.0
0.07	24.8	29.2	33.9	39.0	42.6	45.5	47.7	49.8	51.7	53.3	54.8	56.0	56.8	57.2	57.7	58.4	58.4	58.4	58.4	58.5	58.5
0.06	24.6	29.1	33.8	38.8	42.0	44.1	46.2	48.2	50.3	52.0	53.4	54.5	55.2	55.4	56.0	56.9	56.7	56.5	56.6	56.8	65.9
0.05	22.6	26.7	31.0	35.9	39.3	42.1	44.1	46.2	48.3	50.0	51.4	52.6	53.4	53.5	54.0	54.8	54.6	54.4	54.1	54.0	53.9
0.04	20.6	24.5	28.6	33.3	36.8	39.6	41.7	43.7	45.4	46.8	47.9	49.0	49.6	49.6	50.1	50.8	50.8	50.7	50.5	50.4	50.4
0.03	18.6	22.5	26.5	30.9	34.1	36.6	38.5	40.2	41.3	42.1	42.8	43.7	44.2	43.9	44.4	45.1	45.4	45.6	45.8	46.0	46.3
0.02	16.6	20.5	24.2	27.7	29.0	29.2	29.5	29.8	29.9	31.0	32.7	34.0	35.1	35.6	36.4	37.2	37.5	37.8	38.0	38.3	38.5
0.01	11.8	14.3	16.5	18.5	19.0	18.6	18.6	18.5	18.4	19.3	20.6	21.7	22.5	23.2	23.6	24.5	24.8	25.0	25.3	25.6	25.9
0.005	8.4	9.7	10.9	11.9	12.3	12.3	12.4	12.5	12.6	13.2	13.9	14.5	15.1	15.5	16.0	16.4	16.7	17.0	17.3	17.5	17.8
0.001	5.8	6.0	6.3	6.6	6.9	7.2	7.4	7.7	8.0	8.3	8.6	8.8	9.1	9.4	9.7	10.0	10.3	10.5	10.8	11.1	11.4

Table A.8 Lateral wind speed, $\widehat{W}_y$, $Ro = 1E+04$.

μ	0	10	20	30	40	50	60	70	80	90	100	110	120	130	140	150	160	170	180	190	200
$\hat{z}$	$\widehat{W}_y$																				
0.15	-18.0	-20.4	-22.9	-25.6	-28.7	-32.0	-31.4	-30.7	-29.8	-28.9	-28.0	-26.8	-25.8	-25.2	-24.2	-23.0	-21.8	-20.5	-19.1	-17.2	-15.0
0.14	-17.4	-19.8	-22.3	-24.9	-28.0	-31.2	-30.6	-29.8	-28.9	-27.9	-27.0	-25.8	-24.7	-24.2	-23.3	-22.2	-21.1	-19.8	-18.4	-16.5	-14.3
0.13	-17.1	-19.4	-21.7	-24.2	-27.2	-30.4	-29.7	-28.9	-28.0	-27.0	-26.1	-24.8	-23.8	-23.3	-22.4	-21.4	-20.2	-19.0	-17.6	-15.7	-13.6
0.12	-17.0	-19.1	-21.2	-23.4	-26.3	-29.5	-26.8	-28.1	-27.1	-26.1	-25.2	-23.9	-22.9	-22.4	-21.6	-20.5	-19.3	-18.0	-16.6	-14.8	-12.8
0.11	-16.3	-18.4	-20.5	-22.6	-25.3	-28.3	-27.6	-26.7	-25.6	-24.6	-23.7	-22.5	-21.5	-21.0	-20.0	-18.6	-17.9	-16.9	-15.6	-13.8	-11.8
0.10	-15.5	-17.8	-19.9	-21.8	-24.3	-27.2	-26.2	-25.2	-24.0	-23.0	-22.1	-21.0	-20.0	-19.6	-18.6	-17.3	-16.6	-15.8	-14.6	-13.0	-11.1
0.09	-14.5	-17.1	-19.4	-20.9	-23.2	-25.9	-24.7	-23.5	-22.3	-21.3	-20.4	-19.4	-18.5	-18.1	-17.1	-15.9	-15.3	-14.7	-13.8	-12.3	-10.5
0.08	-13.5	-15.5	-17.4	-18.9	-20.9	-23.2	-22.3	-21.4	-20.4	-19.6	-18.8	-17.8	-17.1	-16.7	-15.8	-14.6	-14.0	-13.3	-12.5	-11.2	-9.8
0.07	-12.1	-13.5	-15.0	-16.5	-18.6	-21.1	-20.3	-19.3	-18.0	-17.2	-16.5	-15.8	-15.3	-15.0	-14.2	-13.3	-12.7	-12.0	-11.3	-10.1	-8.7
0.06	-10.4	-11.3	-12.4	-13.9	-16.4	-19.4	-18.4	-17.2	-15.2	-14.3	-13.9	-13.5	-13.2	-13.0	-12.5	-11.9	-11.3	-10.7	-10.2	-8.9	-7.2
0.05	-8.7	-9.8	-10.9	-12.0	-14.2	-17.0	-15.9	-14.7	-13.3	-12.3	-11.5	-11.0	-10.7	-10.6	-10.5	-9.9	-9.7	-9.3	-8.6	-7.3	-5.6
0.04	-7.0	-8.1	-9.2	-10.2	-12.1	-14.5	-13.3	-12.1	-10.9	-9.9	-9.0	-8.4	-8.0	-8.1	-7.9	-7.7	-7.8	-7.6	-7.0	-5.7	-4.0
0.03	-5.3	-6.2	-7.2	-8.4	-10.0	-11.8	-10.6	-9.4	-8.2	-7.2	-6.3	-5.7	-5.2	-5.0	-5.0	-5.3	-5.6	-5.8	-5.5	-4.2	-2.4
0.02	-3.7	-3.9	-4.4	-5.4	-7.1	-9.1	-7.9	-6.8	-5.8	-4.9	-4.0	-3.1	-2.7	-3.1	-3.1	-3.0	-3.5	-3.8	-3.8	-2.8	-1.4
0.01	-1.8	-1.8	-2.0	-2.5	-3.6	-4.8	-4.1	-3.4	-2.9	-2.4	-1.8	-1.3	-1.0	-1.4	-1.4	-1.2	-1.6	-1.8	-1.9	-1.4	-0.6
0.005	-0.8	-0.6	-0.9	-1.1	-1.6	-2.1	-1.8	-1.5	-1.3	-1.0	-0.8	-0.6	-0.5	-0.6	-0.6	-0.5	-0.7	-0.8	-0.8	-0.6	-0.3
0.001	0.0	0.0	0.0	0.0	0.0	0.0	0.0	0.0	0.0	0.0	0.0	0.0	0.0	0.0	0.0	0.0	0.0	0.0	0.0	0.0	0.0

Table A.9 Longitudinal wind speed, $\widehat{W}_x$, $Ro = 1E+03$.

μ	0	10	20	30	40	50	60	70	80	90	100	110	120	130	140	150	160	170	180	190	200
$\hat{z}$	$\widehat{W}_x$																				
0.15	19.0	23.5	28.2	33.2	37.1	40.4	43.1	45.8	48.4	50.7	52.8	54.3	55.6	56.5	57.3	58.2	57.5	58.8	59.1	59.3	59.6
0.14	19.0	23.5	28.2	33.2	37.1	40.4	43.1	45.8	48.4	50.7	52.8	54.3	55.5	56.3	57.1	58.0	58.1	58.2	58.5	58.8	59.1
0.13	19.0	23.5	28.2	33.2	37.1	40.4	43.1	45.8	48.4	50.7	52.8	54.2	55.4	56.1	56.7	57.4	57.5	57.7	58.0	58.2	58.5
0.12	19.0	23.5	28.2	33.2	37.1	40.4	43.1	45.8	48.4	50.7	52.8	54.1	55.1	55.6	56.1	56.7	56.9	57.1	57.3	57.6	57.9
0.11	19.0	23.5	28.2	33.2	37.1	40.4	43.1	45.8	48.4	50.7	52.8	53.9	54.7	55.0	55.5	56.2	56.4	56.5	56.7	56.9	57.2
0.10	19.0	23.5	28.2	33.2	37.1	40.4	43.1	45.8	48.4	50.6	52.5	53.4	54.1	54.4	55.0	55.7	55.8	55.9	55.9	56.1	56.4
0.09	19.0	23.5	28.2	33.2	37.1	40.4	43.1	45.7	48.4	50.3	51.9	52.7	53.5	53.8	54.4	55.2	55.2	55.1	55.1	55.3	55.6
0.08	19.0	23.5	28.2	33.2	37.1	40.4	42.9	45.2	47.2	48.9	50.4	51.5	52.4	52.8	53.4	54.0	54.1	54.1	54.1	54.2	54.2
0.07	19.0	23.5	28.2	33.2	36.8	39.7	42.0	44.1	46.0	47.6	49.1	50.2	51.1	51.4	52.0	52.7	52.7	52.7	52.7	52.7	52.8
0.06	18.9	23.3	28.0	33.1	36.2	38.4	40.4	42.4	44.5	46.2	47.7	48.7	49.5	49.6	50.2	51.1	50.9	50.8	50.9	51.0	51.1
0.05	16.9	20.9	25.2	30.1	33.6	36.3	38.4	40.4	42.5	44.2	45.7	46.3	47.6	47.7	48.3	49.1	48.8	48.6	48.4	48.2	48.1
0.04	14.9	18.7	22.9	27.5	31.0	33.9	36.0	37.9	39.7	41.0	42.1	43.2	43.9	43.8	44.3	45.1	45.0	44.9	44.8	44.7	44.6
0.03	12.8	16.7	20.8	25.2	28.3	30.8	32.8	34.4	35.5	36.3	37.0	37.9	38.4	38.2	38.6	39.4	39.6	39.8	40.1	40.3	40.5
0.02	10.8	14.7	18.5	21.9	23.2	23.4	23.8	24.0	24.1	25.3	26.9	28.3	29.3	29.9	30.6	31.5	31.7	32.0	32.3	32.5	32.8
0.01	6.0	8.5	10.8	12.8	13.2	12.9	12.8	12.7	12.6	13.5	14.9	15.9	16.8	17.4	18.1	18.7	19.0	19.3	19.6	19.8	20.1
0.005	2.7	3.9	5.1	6.1	6.5	6.5	6.6	6.7	6.9	7.4	8.2	8.8	9.3	9.8	10.2	10.7	10.9	11.2	11.5	11.8	12.1
0.001	0.0	0.3	0.6	0.8	1.1	1.4	1.7	2.0	2.2	2.5	2.8	3.1	3.4	3.7	3.9	4.2	4.5	4.8	5.1	5.3	5.6

Table A.10 Lateral wind speed, $\widehat{W}_y$, $Ro = 1E+03$.

μ	0	10	20	30	40	50	60	70	80	90	100	110	120	130	140	150	160	170	180	190	200
$\hat{z}$	$\widehat{W}_y$																				
0.15	-18.0	-20.4	-22.9	-25.6	-28.7	-32.0	-31.4	-30.7	-29.8	-28.9	-28.0	-26.8	-25.8	-25.2	-24.2	-23.0	-21.8	-20.5	-19.1	-17.2	-15.0
0.14	-17.4	-19.8	-22.3	-24.9	-28.0	-31.2	-30.6	-29.8	-28.9	-27.9	-27.0	-25.8	-24.7	-24.2	-23.3	-22.2	-21.1	-19.8	-18.4	-16.5	-14.3
0.13	-17.1	-19.4	-21.7	-24.2	-27.2	-30.4	-29.7	-28.9	-28.0	-27.0	-26.1	-24.8	-23.8	-23.3	-22.4	-21.4	-20.2	-19.0	-17.6	-15.7	-13.6
0.12	-17.0	-19.1	-21.2	-23.4	-26.3	-29.5	-28.8	-28.1	-27.1	-26.1	-25.2	-23.9	-22.9	-22.4	-21.6	-20.5	-19.3	-18.0	-16.6	-14.8	-12.8
0.11	-16.3	-18.4	-20.5	-22.4	-25.3	-28.3	-27.6	-26.7	-25.6	-24.6	-23.7	-22.5	-21.5	-21.0	-20.0	-18.6	-17.9	-16.9	-15.6	-13.8	-11.8
0.10	-15.5	-17.8	-19.9	-21.8	-24.3	-27.2	-26.2	-25.2	-24.0	-23.0	-22.1	-21.0	-20.0	-19.6	-18.6	-17.3	-16.6	-15.8	-14.6	-13.0	-11.1
0.09	-14.5	-17.1	-19.4	-20.9	-23.2	-25.9	-24.7	-23.5	-22.3	-21.3	-20.4	-19.4	-18.5	-18.1	-17.1	-15.9	-15.3	-14.7	-13.8	-12.3	-10.5
0.08	-13.5	-15.5	-17.4	-18.9	-20.9	-23.2	-22.3	-21.4	-20.4	-19.6	-18.8	-17.8	-17.1	-16.7	-15.6	-14.6	-14.0	-13.3	-12.5	-11.2	-9.8
0.07	-12.1	-13.5	-15.0	-16.5	-18.6	-21.1	-20.3	-19.3	-18.0	-17.2	-16.5	-15.8	-15.3	-15.0	-14.2	-13.3	-12.7	-12.0	-11.3	-10.1	-8.7
0.06	-10.4	-11.3	-12.4	-13.9	-16.4	-19.4	-18.4	-17.2	-15.2	-14.3	-13.9	-13.5	-13.2	-13.0	-12.5	-11.9	-11.3	-10.7	-10.2	-8.9	-7.2
0.05	-8.7	-9.6	-10.9	-12.0	-14.2	-17.0	-15.9	-14.7	-13.3	-12.3	-11.5	-11.0	-10.7	-10.6	-10.5	-9.9	-9.7	-9.3	-8.6	-7.3	-5.6
0.04	-7.0	-8.1	-9.2	-10.2	-12.1	-14.5	-13.3	-12.1	-10.9	-9.9	-9.0	-6.4	-8.0	-8.1	-7.9	-7.7	-7.8	-7.6	-7.0	-5.7	-4.0
0.03	-5.3	-6.2	-7.2	-8.4	-10.0	-11.6	-10.6	-9.4	-8.2	-7.2	-6.3	-5.7	-5.2	-5.0	-5.0	-5.3	-5.6	-5.8	-5.5	-4.2	-2.4
0.02	-3.7	-3.9	-4.4	-5.4	-7.1	-9.1	-7.9	-6.8	-5.8	-4.9	-4.0	-3.1	-2.7	-3.1	-3.1	-3.0	-3.5	-3.8	-3.8	-2.8	-1.4
0.01	-1.8	-1.8	-2.0	-2.5	-3.6	-4.8	-4.1	-3.4	-2.9	-2.4	-1.8	-1.3	-1.0	-1.4	-1.4	-4.2	-1.6	-1.8	-1.9	-1.4	-0.6
0.005	-0.8	-0.8	-0.9	-1.1	-1.6	-2.1	-1.8	-1.5	-1.3	-1.0	-0.8	-0.6	-0.5	-0.6	-0.6	-0.5	-0.7	-0.8	-0.8	-0.6	-0.3
0.001	0.0	0.0	0.0	0.0	0.0	0.0	0.0	0.0	0.0	0.0	0.0	0.0	0.0	0.0	0.0	0.0	0.0	0.0	0.0	0.0	0.0

APPENDIX B - COMPUTER LOOK-UP ROUTINE

This appendix contains a listing of the subroutines which use the tabulated data of Appendix A to generate stable boundary layer wind speeds for the input values of L, u_*, z_0, and f for each altitude of interest.

There are three subroutines listed here. The first subroutine, called STB, is the main subroutine. The input data are passed to STB, from which the other subroutines are called. STB calculates the Rossby number and selects the bracketing order of magnitudes to be consulted in the tabulated data. That is, if the Rossby number were to be calculated as $5E + 06$, the two sets of tabulated data for $Ro = 1E + 07$ and $Ro = 1E + 06$ would be selected as the tables from which the wind speeds would be interpolated. STB also calculates the stability parameter μ from the stability length parameter L.

The subordinate subroutine called INIT is then called from STB and reads all of the tabulated data into arrays.

The other subordinate subroutine, called WINDF, is also called from STB. This subroutine is called twice, once for each order or magnitude of the Rossby number. The x and y wind speed components are interpolated from the tables for the given altitude $\hat{z}$ and stability parameter μ. The results of the two WINDF calls is passed back to the main subroutine STB where the x and y wind speeds are linearly interpolated between the two Rossby numbers to obtain the values of interest.

Subroutine STB can be called any number of times in a loop to calculate wind speed components for a number of altitudes. In this manner, a stable boundary layer wind profile can be generated. Note that the tabulated data will only be read in once, and not every time the subroutine is called. This is controlled by checking the value of NST (a control variable that initiates the storage of the tabulated wind speeds) at the beginning of STB.

Following is a list of the variables used in the subroutine STB.

Z	Height (m)	INPUT
LSTAB	Stability length parameter, L (m)	INPUT
USTR	Surface friction velocity, u_* (m/s)	INPUT
F	Coriolis parameter, $f(s^{-1})$	INPUT
$Z0$	Surface roughness (m)	INPUT
NST	Control variable NST = 1 initiates the storage of the tabulated wind speeds	INPUT
WX	Wind speed in x-direction (m/s)	OUTPUT
WY	Wind speed in y-direction (m/s)	OUTPUT

```
      SUBROUTINE STB(Z,LSTAB,USTR,F,Z0,NST,WX,WY)
      COMMON/WIND/WDEL(17,22,2,5),IMU,IMUM,AMUU(22),ALFA,BETA
      REAL WXR(5),WYR(5),R(5),AMU,GAMMA
      IF(NST.NE.1)GO TO 100
      CALL INIT
      AMU=(0.4*USTR)/(F*LSTAB)
      ROSTR=USTR/(F*Z0)
      NST=2
      K=5
      IF(ROSTR.GE.1E+04) K=4
      IF(ROSTR.GE.1E+05) K=3
      IF(ROSTR.GE.1E+06) K=2
 100  CONTINUE
      DO 99 M=K-1,K
      CALL WINDF(AMU,Z,WX,WY,USTR,F,ROSTR,M)
      WXR(M)=WX
      WYR(M)=WY
  99  CONTINUE
      R(1)=1E+07
      R(2)=1E+06
      R(3)=1E+05
      R(4)=1E+04
      R(5)=1E+03
      GAMMA=(R(K-1)-ROSTR)/(R(K-1)-R(K))
      WX=WXR(K-1)-GAMMA*(WXR(K-1)-WXR(K))
      WY=WYR(K-1)-GAMMA*(WYR(K-1)-WYR(K))
      RETURN
      END

C****************************************

      SUBROUTINE INIT
      COMMON/WIND/WDEL(17,22,2,5),IMU,IMUM,AMUU(22),ALFA,BETA
 200  FORMAT(22F5.1)
 400  FORMAT(22F5.1)
C*************     FEED IN INITIAL DATA MU
      READ(5,200) (AMUU(I),I=1,22)
C*************     FEED IN DATA WDEL
      DO 3 M=1,5
      DO 3 K=1,2
      DO 3 I=1,17
      READ(5,400) (WDEL(I,J,K,M),J=1,22)
 3    CONTINUE
      ALFA=1
      RETURN
      END

********************************************

      SUBROUTINE WINDF(AMU,Z,WX,WY,USTR,F,ROSTR,M)
      COMMON/WIND/WDEL(17,22,2,5),IMU,IMUM,AMUU(22),ALFA,BETA
      REAL WXDEL1,WXDEL2,WYDEL1,WYDEL2
 4    IF(AMU.LT.AMUU(1).OR.AMU.GT.AMUU(22)) GO TO 8
      I=1
 9    I=I+1
      IF(AMU.GT.AMUU(I)) GO TO 9
      IMU=I
      IMUM=I-1
```

```
      ALFA=(AMUU(IMU)-AMU)/(AMUU(IMU)-AMUU(IMUM))
C************* COMPUTE ZBAR
      Z=Z*F/USTR
      IF(Z.LT.0.001) GO TO 15
      IF(Z.GT.0.15) GO TO 7
      J=1
      ZP(1)=0.001
      ZP(2)=0.005
      DO 20 N=1,15
      ZP(N)=FLOAT(N)/100
   20 CONTINUE
    5 J=J+1
      IF(Z.GT.ZP(J)) GO TO 5
      IZ=J
      IZM=J-1
      BETA=(ZP(IZ)-Z)/(ZP(IZ)-ZP(IZM))
C************** COMPUTE WX AND WY
      WXDEL1=-ALFA*(WDEL(IMU,IZ,1,M)-WDEL(IMUM,IZ,1,M))
     #+WDEL(IMU,IZ,1,M)
      WXDEL2=-ALFA*(WDEL(IMU,IZM,1,M)-WDEL(IMUM,IZM,1,M))
     #+WDEL(IMU,IZM,1,M)
      WYDEL1=-ALFA*(WDEL(IMU,IZ,2,M)-WDEL(IMUM,IZ,2,M))
     #+WDEL(IMU,IZ,2,M)
      WYDEL2=-ALFA*(WDEL(IMU,IZM,2,M)-WDEL(IMUM,IZM,2,M))
     #+WDEL(IMU,IZM,2,M)
      WX=WXDEL1-BETA*(WXDEL1-WXDEL2)
      WY=WYDEL1-BETA*(WYDEL1-WYDEL2)
      WX=WX*USTR
      WY=WY*USTR
      GO TO 1
 7    WRITE(6,700)
      GO TO 1
 15   WY=0
      WX=USTR*(ALOG(ROSTR*Z+1)+11.25*AMU*Z)/0.4
      GO TO 1
 8    WRITE(6,710)
 710  FORMAT(5X,'AMU IS OUT OF REGION')
 700  FORMAT(2X,'Z IS LARGER THAN 0.15')
 1    Z=Z*USTR/F
      RETURN
      END
```

APPENDIX C - DRAG AND DRIFT CALCULATIONS

Given

Round Fall Rate = 24.4 m/s (80 ft/sec).

Assume

Explosive canister is a sphere with the same weight and volume as the actual CATFAE round (r = approx. 1 ft diameter).

Calculation of Drag Coefficient

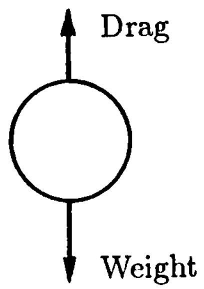

$$\sum F = M * a$$

at terminal velocity, acceleration is zero hence,

Drag = Weight = 1045 N.

$$C_D = \frac{Drag}{\frac{1}{2}\,\rho A\,V^2} = \frac{1045\ N}{\frac{1}{2}\,(1.22\ kg/m^3)\,(0.58 m^2)\,(24.4\ m/s)^2}$$

$$= 4.961$$

Calculation of Drift

With the approximate drag coefficient of the CATFAE round known, the drift of the round can be determined by imposing the wind profiles of Figure 3.4a on the round as it falls at its known rate. In performing this calculation, the wind profiles were broken into 22 vertical segments. The drag force to which the round is subjected was calculated for each piece of the profile using the following equation.

$$Drag = \frac{1}{2}\,\rho A\,u^2\,C_D$$

where

$$\rho = 1.22\ kg/m^3\ for\ air$$

$$A = 0.58m^2\ area\ of\ impingement$$

$$C_D = 5\ is\ the\ drag\ coefficient$$

$$u = velocity\ at\ particular\ profile\ segment.$$

With the drag force known, the acceleration imposed upon the round was determined by

$$F = m\ *\ a$$

$$a = F/m\ =\ Drag/m$$

and in turn, the horizontal displacement, or drift, of the round for each segment of the profile was found by

$$Drift = \frac{1}{2} a\ t^2$$

where

$$a = acceleration\ imposed\ by\ profile\ segment$$

$$t = time\ during\ which\ round\ fell\ through\ profile\ segment.$$

By summing the displacements for each profile segment, the total drift of the round due to the total profile was found. These drift distances are shown in Figure 3.4b for the two profiles of Figure 3.4a.

VITA

Alan E. Johnston was born in Nashville, Tennessee and raised in Knoxville. He received his B.S. degree in Aerospace Engineering from the University of Tennessee, Knoxville in 1986. Since 1983, he has been an employee of the National Aeronautics and Space Administration at the Marshall Space Flight Center in Huntsville, Alabama. From 1983 to 1986 he worked part time with NASA as a co- op student, then began full time employment in 1987. Mr. Johnston currently resides in Huntsville with his wife.